CRANFIELD UNIVERSITY

BY

MUBARAK AL-JABERI

THE VULNERABILITY OF LASER WARNING SYSTEMS AGAINST GUIDED WEAPONS BASED ON LOW POWER LASERS

THE DEPARTMENT OF AEROSPACE, POWER & SENSORS

PhD THESIS

CRANFIELD UNIVERSITY

COLLEGE OF MANAGEMENT & TECHNOLOGY
THE DEPARTMENT OF AEROSPACE, POWER & SENSORS

PhD THESIS

BY

MUBARAK AL-JABERI

THE VULNERABILITY OF LASER WARNING SYSTEMS AGAINST GUIDED WEAPONS BASED ON LOW POWER LASERS

SUPERVISOR: Dr. MARK RICHARDSON
HEAD OF ELECTRO-OPTICS GROUP

JAN 2006

DEDICATION

DEDICATED WITH GREAT LOVE, THOUGHTS AND PRAYERS TO MY FATHER AND MOTHER, WHO HAVE ALWAYS SUPPORTED ME DURING MY LIFE WITH THEIR ADVICE AND PRAYERS AND EVERYTHING THAT I NEED. MAY ALLAH BLESS THEM BOTH.

ALSO DEDICATED WITH LOVE AND GRATITUDE TO MY LOVELY WIFE, SONS AND DAUGHTER.

ACKNOWLEDGEMENTS

ABSTRACT

Laser assisted weapons, such as laser guided bombs, laser guided missiles and laser beam-riding missiles pose a significant threat to military assets in the modern battlefield. Laser beam-riding missiles are particularly hard to detect because they use low power lasers. Most laser warning systems produced so far can not detect laser beam-riding missiles because of their weak emissions which have signals less than 1% of laser range finder power[1]. They are even harder to defeat because current counter-measures are not designed to work against this threat.

The aim of this project is to examine the vulnerability of laser warning systems against guided weapons, to build an evaluation tool for laser warning sensors (LWS) and seekers, and try to find suitable counter-measures for laser beam-riding missiles that use low power lasers in their guidance systems. The project comes about because of the unexpected results obtained from extensive field trials carried out on various LWRs in the United Arab Emirates desert, where severe weather conditions may be experienced. The objective was to help find a solution for these systems to do their job in protecting the tanks and armoured vehicles crews from such a threat.

In order to approach the subject, a computer model has been developed to enable the assessment of all phases of a laser warning receiver and missile seeker. MATLAB & SIMULINK software have been used to build the model. During this process experimentation and field trials have been carried out to verify the reliability of the model.

This project will enable both the evaluation and design of any generic laser warning receiver or missile seeker and specific systems if various parameters are known. Moreover, this model will be used as a guide to the development of reliable countermeasures for laser beam-riding missiles.

---

[1] Prof. Richard Ogorkiewiez. Fundamentals of Armour Protection. Advances In Armoured Vehicles

LIST OF TERMS, SYMBOLS AND ABBREVIATIONS

AFC	Amplitude-Frequency Characteristic
AFV	Armored Fighting Vehicles
AOA	Angle of arrival
APD	Avalanche Photodiode
APS	Active Protection System
AT	Anti-tank
ATGM's	Anti Tank Guided Missiles
B_{Night}	Night sky spectral brightness
$B(\lambda)$	Spectral Background Brightness
CE	Chemical Energy
$C_n{}^2$	Index Structure Parameter
$C_T{}^2$	Temperature Structure Parameter
D	Diameter of the collector system
DIRCM	Directed infrared countermeasures systems
d_λ	Spectral bandwidth of the interference filter
ECM	Electronic Counter-Measures
ERA	Explosive Reactive Armour
f	Objective focal length
FSAP	Full Spectrum Active Protection
GUI	Graphical User Interface
$I_0(\lambda)$	Flux density of sunlight
$\bar{I}_D$	Average dark current
$\bar{i}_n^2$	Dispersion of the noise current
$\bar{i}_{shot.n}^2$	Shot noise
$\bar{i}_{therm}^2$	Thermal noise
k	Boltzmann constant
K	Amplification factor
k_{bf}	Transmission factor of bandpass filter
KE	Kinetic Energy

k$_{Clouds}$	Clouds reflection coefficient
ℓ	Size of sensitive area of photodetector
LWS	Laser Warning Sensor
M	multiplication factor
MBT's	Main Battle Tanks
MCD	Missile Countermeasures Device
NEP	Noise Equivalent Power
ρ	Reflection coefficient from surface
PIN	Positive-Intrinsic-Negative
$\overline{P}_A$	Average power of optical signal
P$_C$	Power collected at the input of the receiver
P_b	External Background noise power
P_r	Internal receiver noise power
P_Σ	Total average noise power
R$_F$	Feedback resistance
R$_L$	Load resistance
RPG	Rocket propelled grenade
SACLOS	Semi-Active Command to Line of Sight
S$_{beam}$	The sectional area of the laser beam at distance R
S$_D$	Area of input lens
$S_{in2}(t)$	Useful signal
S/N	Signal to Noise ratio
S$_{PD}$	The sectional area of the photodetector
SOJ	Stand-off jamming
$S_n(t)$	Noise signal
S_λ	Photodiode spectral sensitivity
t$_a$	Atmospheric attenuation
UAE	United Arab Emirates
$U_{out}(t)$	Amplification stage output voltage
$U_{phd}(t)$	Photodiode output voltage

U_{thresh}	Threshold voltage
X	Excess noise factor
σ	Atmospheric attenuation coefficient
μ	Coefficient describing the distribution of brightness
ψ	Solar angle

LIST OF ORIGINAL PAPERS, CONFERENCES & PRESENTATIONS

- 4 Parts Series (Journal of Battlefield Technology)

    ❖ Part I: Accepted
    ❖ Part II: Accepted
    ❖ Part III & Part IV: Final stage

- Conference Papers

    ❖ The title of the paper is (The Simulation of Laser-Based Guided Weapons Engagements)
    Conference name: Defence Security Symposium, SPIE Orlando, 7-21 April 2006

    Status: Accepted

    ❖ The Title: [Vulnerability of Laser Warning Systems against Guided Waepons Based on Low Power Lasers]
    Conference name: RESEARCH STUDENT SYMPOSIUM, 17th May 2005

- Conference Poster : RESEARCH STUDENT SYMPOSIUM, 17th May 2004

    Title of Poster: [Vulnerability of Laser Warning Systems against Guided Waepons Based on Low Power Lasers]

- Conferences

    ❖ Post Graduate Seminar, 18th November 2003
    ❖ Post Graduate Seminar, 31st March 2004
    ❖ Post Graduate Seminar, 25th November 2005

CONTENTS

List of Tables

List of Figures

Intentionally Blank

CHAPTER 1

Introduction

1.1 Background

Lasers are finding increased application in military weapon systems as a means of designating targets for guided missiles and as weapons themselves. Current laser warning systems provide laser detection, angle of arrival, wavelength discrimination and temporal characterization of the laser source. However, there is a need to improve their threshold detection level and false alarm rate for detection of low-intensity pulsed lasers associated with beam-riding type guided missiles. Laser warning systems must be improved to cope up with the new threat of low power laser beam-riding missiles.

This is not the only part to look after in order to enhance laser warning sensor (LWS) detection capability. Most of the conflict areas in the modern world have hot climates. Areas such as the middle-east have severe weather conditions which are now known to affect the performance of laser warning systems in a negative way. For example, every eight degrees increase in temperature doubles the noise that creates a big problem to the performance of any laser sensor[2]. A lot of well-known commercial organizations have participated in several trials of laser warning systems in the desert of the UAE where they could not perform according to their original specifications. Their specifications were prepared as a result of tests in their original countries where these systems worked properly. A considerable reduction in detection distance of 1 km has found in maximum range of these sensors to detect signal. They were supposed to detect the signal over a maximum range of 5.5 km but they couldn't do more than 4.5 km. Also, some of them had a lot of false alarms. These trials were conducted during summer, especially during the month of August where temperature and humidity are high, dust and solar irradiance is also at its peak. Tests results were consistent in the following year with a reduced performance of these sensors with respect to their detectability.

---

[2] Clarke, T.A. & Wang, X. An analysis of subpixel target location accuracy using Fourier Transform based models. SPIE Vol. 2598. pp. 77-88.

Aim of this project is to design and develop a mathematical model with improved detection performance. This model will be designed to simulate all weather conditions including temperature extremes experienced in the UAE. We will attempt to detect the weak optical signal at a specified maximum range of 5.5 km and optimize the parameters such as noise and background effect to improve the detection sensitivity of the sensor. Moreover, a seeker and counter-measure model will be added to the laser sensor model to create a complete system in order to evaluate the effect of change in weather conditions and other parameters which can affect the performance of the systems.

1.2 Present Study

This thesis is spread over nine chapters. Chapter one sets out the context of this work by discussing background knowledge. Deficiencies of the existing model and methodology to enhance their performance are highlighted. This work can not be well- understood without discussing issues related to the application of laser warning systems, vehicles survivability, vehicle protection systems, and the operational requirements. Chapter two presents these issues.

Chapter three covers the background theory to the laser sensor model. It focuses on the structure of the laser sensor detection model through building its mathematical model with all the elements such as laser source, atmospheric attenuation block, noises sources, photoreceiving optical system, amplification stage, threshold and solar background effects. In chapter four a mathematical model is developed and discussed using Matlab and Simulink codes. A graphical user interface (GUI) has also been built to facilitate the simulation of different atmospheric conditions. LOWTRAN VII code has been used to calculate the transmittance of five weather conditions chosen to simulate the extreme weather conditions of the UAE.

Model performance has been tested and verified against the required parameters and weather conditions in chapter five. Finally, simulation results are compared and verified with the experimental evidence and field trials.

In chapter 6, individual parameter sensitivity and an optimization of laser detection sensor model has been performed to increase the detection range. Moreover, the effect of atmospheric turbulence is also discussed and simulated.

Chapter 7 covers an important discussion on missile seekers. In laser beam-riding missiles, the seeker, which is basically a laser sensor, is located at the rear of the missile looking back to the firing post to get the guidance corrections. A seeker model has been developed to simulate the performance of the seeker and the effect of weather conditions on it.

A counter-measure model has been added to the seeker model to evaluate the ability of counter-measure device against the threat. Chapter 8 addresses this subject in more detail. Chapter 9 summarizes the work that has been done and gives recommendations for the future work.

CHAPTER 2

Application Bases of Laser Warning Systems

2.1 Vehicles Survivability Factors

The invention of Main Battle Tanks (MBT's) was a huge step to gain victory and to defeat the enemy. Tanks are the main strike assets at the disposal of land forces, and this has been confirmed and proven by a lot of conflicts all around the world where tanks played a big rule to achieve the goal. From that point of view, it was and still is, important for tank engineers to enhance tank survivability and their capabilities to stand against the lethal threats, especially from Anti-Tank Guided Missiles (ATGM's). The dramatic breakthroughs in the development of anti-tank warheads made Russian engineers think of an active protection system for their tanks and they started designing such protection aids during 1950s [1]. On the other hand, western countries didn't agree with this approach because of the damage that can happen to capability of the MBT itself, its crew, equipment and friendly forces nearby when the active protection explodes to destroy the incoming missile. As a result, these countries explored another way to protect their tanks and other capabilities that is called Soft Kill APS, explained later.

Let us discus some factors that affect the MBT's survivability. These are listed below:
a. Doctrine
b. Crew Training
c. Vehicle Design
d. Armour
e. Hard Kill Active Protection System (APS)
f. Soft Kill APS
g. Explosive Reactive Armour (ERA)

2.1.1 Doctrine

Vehicle protection has long been a priority to armies, but more recently due to a change in the scope and type of land conflicts, a much greater emphasis has been placed on this requirement. Vehicles are coming under threat from increasingly sophisticated weaponry which is able to exceed the ability of traditional armour. Therefore, armies are looking to improve the survivability of combat vehicles by applying both active and passive survivability enhancement measures. Armies are looking for a system protection scheme just like in Figure 1 covering a wide range of threats from different directions.
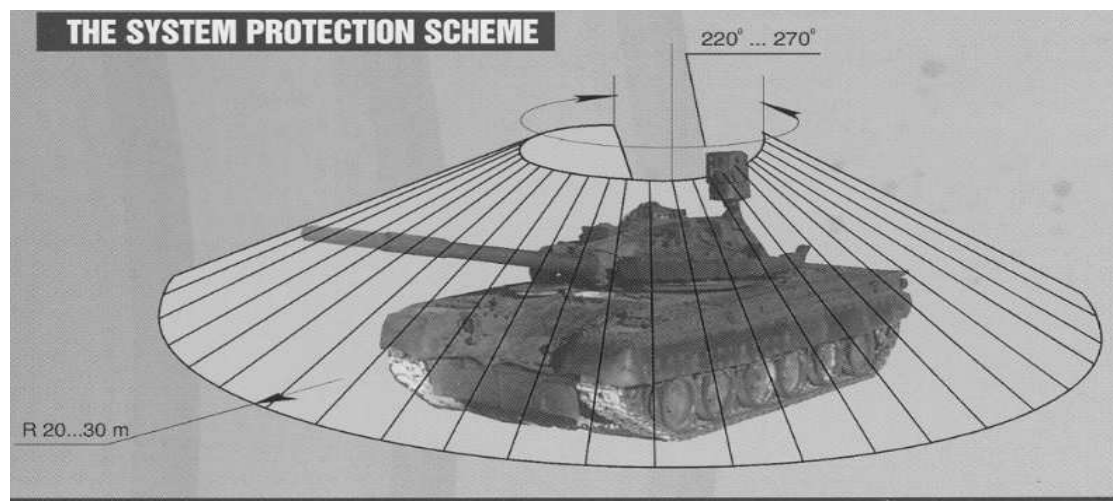
Figure 1 System protection scheme for MBT's

2.1.2 Crew Training

Members of tank crews function as an integrated team although each one has his primary duties. Their success depends on their effectiveness as one group in combat by working together to maintain and service their tank and equipment. Training is very important for all crew members, especially cross-training so they can operate in any position. Other important factors for crew success are effective leadership and high

motivation. Training should prepare crews to operate in hostile territory with the enemy from all directions.

2.1.3 Vehicle Design

When designing the tank there are three principle's of armored warfare that need to be taken in consideration: firepower, maneuverability, and protection.

Firepower: Tank design must provide the abilities to control the maximum distance targets that can be engaged, attack moving targets, destroy multiple targets in short time, and keep fighting even with sustained damage.

Manoeuvrability: Tank design must also take in consideration the required range of terrain that has to be covered, the size of obstacles such as trenches, ridges and water that can be overcome, and the distance that can be achieved before re-fuelling is required.

Protection: Another important factor in tank design is choosing the type of armour, the way of arranging them and the amount of protection each area gets.

Compromising between these three principles is very important in vehicle design. Increasing the firepower by using a larger gun can decrease maneuverability and hence decrease armour at the front of the turret, which means lower overall protection. It is also affected by other factors such as military strategies, budget, geography, political will and desire to sell the tank to other countries [2].

2.1.4 Armour

An armored vehicle such as a MBT is a basic requirement in modern armies. The vehicle and crew are vulnerable to various threats such as kinetic energy rounds fired form other tanks, anti-tank guided missiles(ATGMs) fired from infantry or aircraft, anti-tank mines, larger bombs and direct artillery hits. The MBT's can offer protection from artillery shrapnel and lighter anti-tank weapons but can't protect against all conceivable threats. They can be destroyed or disabled by different types of anti-tank weapons despite their heavy armor. Armoured units in the future will be smaller in size and will deploy a lower number of AFVs, which puts additional emphasis on survivability features [3].

2.1.5 Hard Kill Active Protection Systems (APS)

Russian APS were matured much earlier than the west's, as they were designed to counter the threat from the west's anti-tank systems such as TOW, Hellfire and HOT missiles fired from ground and helicopter platforms, as well as airborne launched anti-tank missiles such as the Maverick. Although the Russian systems were much heavier than their current western counterparts, they provided the counter-measures that could decimate the western threat. These heavy counter-measure systems were designed to protect the most important elements in the heavy armored divisions and were applied to platforms such as the T-55, T-72, T-80, T-90 tanks and BMP-3. The Drozd systems entered full scale development when Russia was no longer planning to confront NATO, but was deeply engaged in a war in Afghanistan and later in Chechnya, where these defensive counter-measures were required to protect much older T-55 tanks against Russian made RPGs and AT missiles. First was the Drozd, which protected the tank's forward arc. This system was later followed by the Arena-E system as shown in Figure 2, which introduced 360 degrees protection from side, front, and partially top attacks [4].

The US Army is considering to replace the 1990's technology of the Missile Counter-measures Device (MCD), with a Full Spectrum Active Protection (FSAP), a new system approach that will be balanced with the capabilities of future advanced armor technology. Such advanced active protection systems will be considered to provide the primary survivability component of future armored vehicles. The FSAP include missile engagement capabilities, to attack munitions intercept and defeat capability and kinetic energy threat engagement concept. As the system addresses both Kinetic Energy (KE) threats and Chemical Energy (CE) threats, it will utilize different counter-measure concepts to engage each threat. The CE counter-measures rely on technologically proven sensors and kill mechanisms [5].
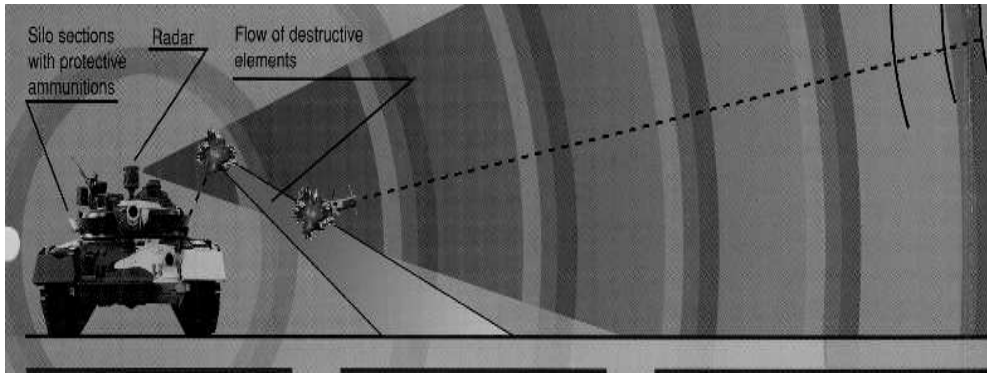
Figure 2 The functionality of Arina-E

2.1.6 Soft Kill APS

Soft-kill methods, similar to Electronic Counter-Measures (ECM) in aircraft, seduce and confuse an incoming missile, by using decoys, smoke and electro-optical signals, infrared or laser jamming.

A typical deployment of as IR jammer can be seen on the Russian T-90, which mounts the Shtora-1 APS shown in Figure 3, with Kontakt-5 ERA modules .The system protects the tank against guided missiles, using both the semi-active command to line of sight (SACLOS) guidance, by an IR source that mimics the flare on the back of missiles, as well as laser beam-riding and laser-homing weapons. It should be effective against missiles such as the TOW, HOT, AT-4, AT-5 and Sagger. The Russian system also has some capability to counter laser-guided munitions and ATGMs (Such as Hellfire, Kornet etc).
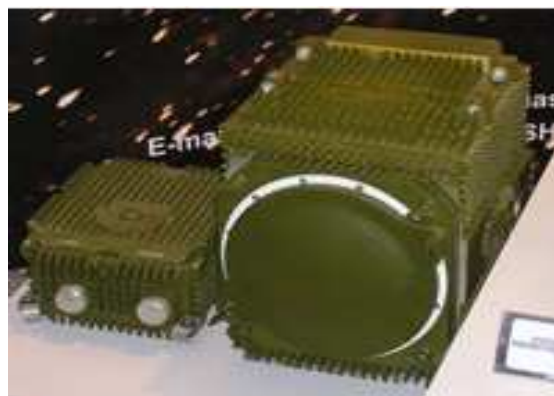
Figure 3 Shtora-1 laser warning device

Shtora-1 uses a laser warning device operating in the 0.65-1.6 micron range, comprising of an array of coarse and fine resolution sensors, mounted externally on the turret. Each of the rough (coarse) laser sensors covers a sector of 135 degrees, while the fine sensor covers a 45 degrees, with 3.75 degrees angle of arrival resolution, and 5 to 25 degrees elevation coverage. The system can automatically slew the turret and gun to the direction of the threat, to optimize the deployment of a thermal smoke screen or activation of active protection systems. The sensor detects laser illumination and alerts the crew and defensive systems. The warning display provides the commander and gunner with threat warning cueing, by sector (at a resolution of 5 degrees) and at a resolution of 3.75 degrees in the 90 deg. frontal arc. The display also provides jammer and counter-measures status indication. Counter-measures can employ 81mm thermal instant smoke grenades, which deploy an instant smoke screen at a range of 50-80 meters from the tank, within 1.5 - 3 seconds. The 20 meter wide, 15 meter high screen blocks visual, thermal and laser (0.4 - 14 micron) wave bands. The system also employs a pair of electro-optical jammers (see Figure 4), which "hijacks" the missile's command link by feeding the tracker with modulated signals that cause the missile to deviate from its course, and away from its intended target [6].

Figure 4 Shtor-1 employs a pair of electro-optical jammer

2.1.7 Explosive Reactive Armour (ERA)

ERA is a type of armour used primarily on tanks and personal carrier vehicles to lessen the damage from explosions caused by missile warhead, exploding shells, grenades, or

bombs. It consists of two rectangular metal plates, referred to as the reactive or dynamic elements, which sandwich an interlayer of high explosive [7].

This 'box' is set at high obliquity to the anticipated angle of attack by the HEAT jet, usually 60°, see Figure 5. ERA is placed where the threat is most expected like the front arc, the engine, and the sides.
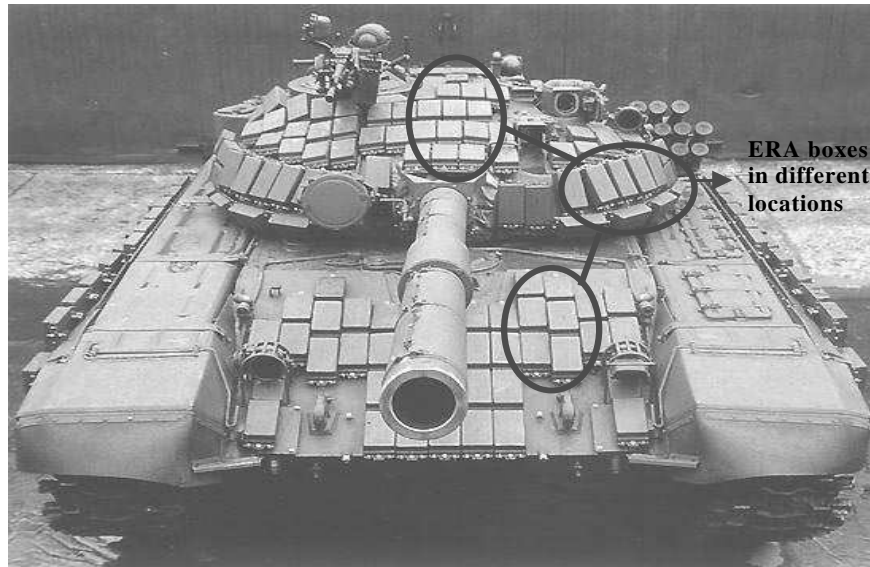
Figure 5 Explosive reactive armour

2.2 VEHICLES PROTECTION SYSTEM

As a rule, with the growth of power of antitank means, the protectability of tanks and fighting machines increases when:

- The thickness of armor increases
- Dynamic protection is added
- Vehicles' assembling improves (maximum effective armor thickness depending on direction)
- Improved armor is used

All these means are good. But weight, dimensions and cost of machines increase. Exotic steels, composites, ceramics are used today as an armor. However, further build-up of armor

protection leads to overweight tanks (for example, the weight of M1A1 makes 60 tones and the weight of M1A2 is about 70 tones) [8].

Integrated protection systems for the fighting vehicles permits to solve this problem. This system consists of three main parts [9]:
1. Laser Warning System
2. Counter-measures System
3. Control System

2.2.1 Laser Warning System

The laser warning system (LWS) is intended for detection of a laser irradiation. It develops the warning signal for counter-measures. The purpose of the LWS is to reduce the vulnerability to the numerous laser associated weapon threats on the modern battlefield, by providing the crew with an early warning that its vehicle or installation is being irradiated by a pulsed or modulated continuous laser light [10].

The crew can then take appropriate self-protective action such as deployment of a smoke or water-fog screen, vehicle manoeuvre or initiate counterfire. The laser warning system is designed for use on all kinds of land or seagoing combat or transport vehicles. It can also be integrated into protection systems of stationary installations, buildings etc. This system is capable of detecting a number of laser sources of various types threatening in a wide range of the IR and visual spectrum.

The laser warning system is a reliable, flexible, self-contained laser threat detection system suitable for integration into any protection system. The integration level may vary from stand-alone solutions that include complete threat indication and alarm capability to fully integrated solutions with alarm indications embedded onto display panels or screens of other systems implementing automatized activation of counter-actions.

The laser warning system consists of the following units:
- A few detector heads (Laser Detection Sensors)
- Indicator unit

Typical appearance of the system is given in Figure 6 [11].
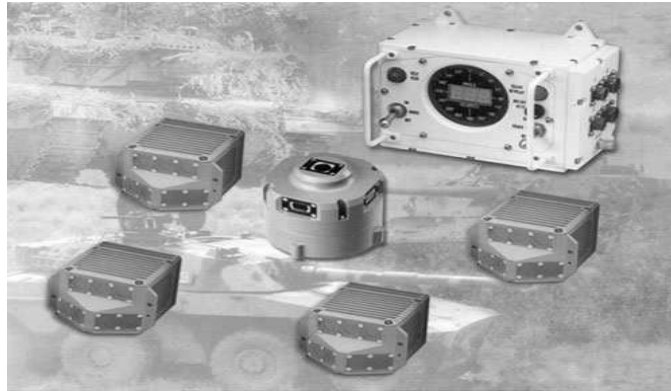
Figure 6 Laser warning system for combat vehicles (LWSCV) designed by Avitronics

All units are interconnected by a cable, through which signals from the detector heads are routed to the indicator unit. Beside visual threat identification an audible alarm can be produced as well. The detector head may have two detection subsystems, the direct and indirect detection modules [12]. The direct detection module senses the laser beams which directly hit the protected asset. The horizontal angle sector, from which the threat is coming, is identified and displayed along with other threat alarm indications. The other module, the indirect detection module, senses the target-off laser beam reflected to the detector head from the surrounding objects and surfaces. This rather unique feature of the laser warning system significantly contributes to better threat awareness introducing additional tactical possibilities with self-protective and counter-measures.

The indicator unit contains a panel with direction indications for the incoming laser threat. A digital display on the panel shows the detected angle in the preset angle unit.

2.2.2 Counter-measures System

The counter-measures system is intended for support of vehicles survivability. The system may include:

1. Jamming units
2. Smoke (or Aerosol) screen system
3. Vehicle manoeuvres
4. Fire suppression
5. Active protection

2.2.2.1   Jamming Units

The jamming unit is designed for protection of armoured fighting vehicles against attack by antitank guided missiles (ATGM), employing infra-red guidance [13]. Since active jammers (decoys) are non-expendable, they are able to provide permanent protection. The decoys employ infra-red emitters to "mimic" those used by most semi-automatic missile systems to facilitate missile tracking. In this way, the enemy fire control system is made to issue erroneous flight correction commands to the missile, causing it to deviate from its intended target.

The infra-red jammer has a few operational modes for different threats and can also be used in conjunction with an alarm detector. It is normally powered from an on-board 28 V DC power supply although different versions exist according to the power supply available on the vehicle.

In most anti-tank guided weapons, the missile is slaved to the gunner's line of sight and for this purpose the missile is fitted with a flare in the rear so that its position with respect to the target can be sensed from the launcher. As soon as the missile moves away from the target the deviation is detected and correction instructions are sent to the missile. When the target is fitted with an infra-red jamming system, the latter will substitute for the missile flare. The launcher then no longer measures the missile-to-target error but deviation of the jammer-to-target. The missile is no longer guided and quickly moves away from its course and drops without reaching its target.

There are usually two methods of operation. When the vehicle is stationary the jammer emits in a fixed direction, typically over the frontal arc and in line with the main armament. This method is used when it is known where the threat is coming from. The incoming missiles can be jammed as soon as possible.

When the vehicle is moving, the jammer emits while carrying out an optimized horizontal scan so as to increase considerably the protected area. This method is used in case of an indefinite threat.

2.2.2.2 Smoke (or Aerosol) Screen System

A smoke-screen is a release of smoke in order to mask the movements or location of military units such as infantry, tanks or ships. A smoke-screen enables the tank to perform evasive manoeuvres to counter the threat.

It is most commonly deployed in a canister, usually as a grenade. The grenade releases a very dense cloud of smoke designed to fill the surrounding area even in light wind. They have also been used by ships.

Whereas smoke-screens would originally have been used to hide movements from the enemy's line of sight modern technology means that they are now also available in new froms; they can screen in the infrared as well as visible spectrum of light to prevent detection by infrared sensors or viewers, and also available for vehicles is a superdense from used to prevent laser beams of enemy target designators, range finders, or laser beam-riding [14].

2.2.2.3 Vehicle Manoeuvres

The laser warning system is intended to activate an installed counter-measure systems if it is set up to work automatically or it may give a quick warning to the vehicle crew so they make the proper manoeuvre to get out of their original position. For this to happen, the detection time must be very short so that the crew can have the required time to take an evasive manoeuvre.

2.2.2.4 Fire Suppression

Suppressive fire is a military term for firing weapons at the enemy with the goal of forcing him to take cover and reduce his ability to return fire, such as when attacking an enemy position. Suppressive fire may be either aimed (at a specific enemy soldier, group of soldiers, or vehicle) or un-aimed (for example, at a building or tree-line where enemy soldiers are suspected to be hiding). To be effective, suppressive fire must be relatively continuous and high in volume [15].

Suppression of enemy fire is vital during troop movement especially in tactical situations such as an attack on an enemy position. Here is an example of a situation requiring the use of suppressive fire:

- The defenders hold a position, such as a building or trench line, perhaps reinforced with sandbags, landmines or other obstacles.
- The defenders have a clear field of fire, so the attacking force has very few places to take cover.
- The attacking force has a group of soldiers "lay down" suppressive fire on the defenders, in order to induce the defenders to take cover and minimize their return fire.
- Under the cover of suppressive fire, a second group of attacking troops advances towards the defender's position, then stops to lay down suppressive fire in their turn while the first group advances.
- The process repeats as needed, with each attacking group alternating roles (advancing or laying down suppressive fire) until they can attack the defenders at close quarters.

2.2.2.5 Active Protection

An active protection system is a system activated at very close range (but before the incoming missile hits the target) for the defence of the vehicle it is mounted on. There are two general types of active protection systems: hard kill, which physically damages or destroys the incoming missile, and the soft kill which uses some other method to prevent the missile from

hitting the vehicle. The TROPY APS, Drozd, Arena and Zaslon are hard kill systems, while Shtora is a soft kill system [16].

2.3 Laser Warning System Requirements

Laser Warning Systems for ground platforms are designed to deal effectively against laser threats of the present and future scenario. They should be able to [17]:

1. Detect Laser Threats
2. Identify type of incoming threat
3. Identify the direction of threat arrival
4. Reject reflected beam
5. Handle multiple threats
6. Communicate with other systems

2.3.1 Detect Laser Threats

LWS must be capable of detecting all types of lasers pulsed or continuous wave and discriminate them from the background and any other light source. Various types of lasers are [18]:

- Frequency doubled Nd:YAG
- Ruby laser
- GaAs lasers
- Nd:YAG, Nd:Glass
- Er:Glass
- Raman shifted Nd:YAG

2.3.2 Threat Type Identification

Identifying the impinging laser threat type is very important and that can be done by measuring its parameters and comparing them with an internal database which is designed to match different threat scenarios. Laser threats are:

- Laser Range Finder Systems

- Laser Designator Systems
- Laser Beam Rider Systems
- Unknown Laser Sources

2.3.3 Threat Direction of Arrival Identification

When designing a laser warning receiver (LWR), one of the most important issues to be considered is the threat direction of arrival. It is essential that it is determined in order to launch the counter-measure in the right direction.

2.3.4 Reflected Beam Rejection

Laser scattered from the atmosphere and reflected from the platform itself is one of the problems to overcome in order to reduce the false alarm rate. So, LWS must be able to get rid of laser reflections that hit the platform after the direct beam. Electronic filtering discriminates the glints and flashes to give an extremely low false alarm rate.

2.3.5 Multiple Threat Handling

One very important feature that a LWR must have is the capability to deal with multiple threats since there are a lot of lasers in the battlefield. The laser warning receiver is able to manage multiple threats, occurring with delay time, identifying direction of arrival and type

of each threat. The capability to reject reflected beams restricts the multiple threats handling.

2.3.6 Communication with other Systems

The LWR should be able to communicate with other systems within the vehicle for control and information delivery purpose. It is very important to have a high speed and secure communication system in order to launch counter-measures in-board or somewhere else, time is a critical issue.

2.4   Efficiency of the Laser Detection Sensors

Efficiency of a laser sensor is defined by the possibility of laser signal registration at maximum distance with the probability of correct detection not less then 0.9. Efficiency of the laser sensor can be evaluated according to the decrease of distance of signal source detection. This decrease is caused by the influence of different factors and changes (or non-optimality) of parameters. These factors include weather conditions, background situation and atmospheric turbulence.

We will make the evaluation of detection distance for a laser warning System. Laser beam-riding is a guidance method where the firing post guides the missile to hit the target. The missile has a detector at the rear looking back to get guidance information from the firing post which make it difficult to be detected by the laser warning systems. Figure 7 shows the geometry of the beam rider/laser warner.
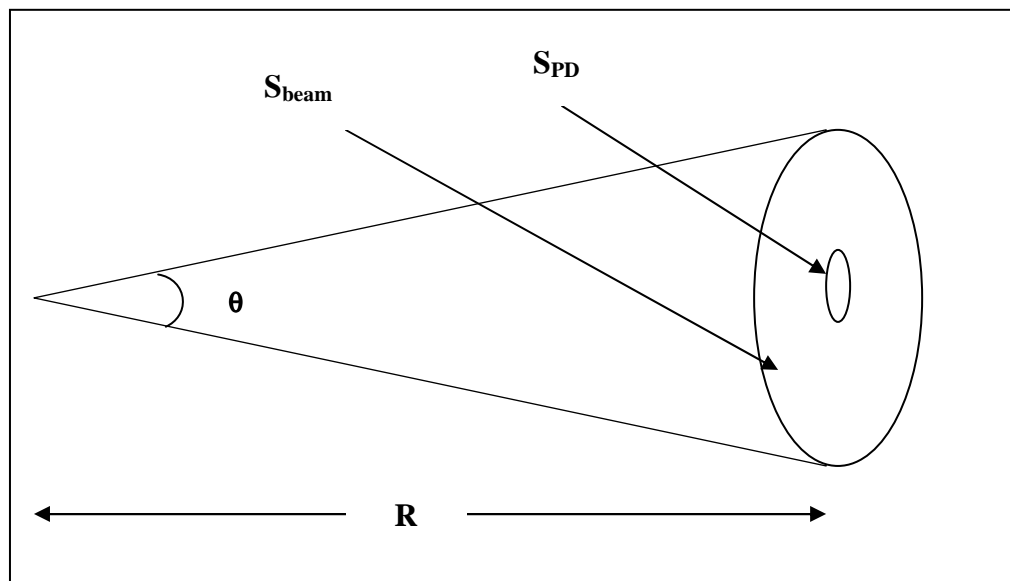
Figure 7 Beam rider/laser warner

The area of the sensing system is given by:

$$S_{PD} = \frac{\pi D^2}{4}$$

(2.1)

where D is the collecting system diameter.

$$S_{beam} = \frac{\pi \theta^2 R^2}{4} \qquad (2.2)$$

The power collected is given by:

$$P_C = P \frac{S_{PD} t_a}{S_{beam}}, \qquad (2.3)$$

where t_a is the atmospheric attenuation and can be approximated by,

$$t_a = \exp(-\sigma R), \qquad (2.4)$$

where σ is the atmospheric attenuation coefficient and maybe characterised as [19]:

a. $\sigma = 0.2$ km^{-1} on a good day
b. $\sigma = 0.7$ km^{-1} on a bad day

In order for a laser warning system to detect the incoming threat, the power collected is given by:

$$P_C = \frac{S}{N} NEP, \qquad (2.5)$$

where S/N is the signal to noise ratio (the lower S/N value the higher the likelihood of false alarm). NEP is the noise equivalent power of the detector used.

The required laser power may be written as:

$$P = \frac{S}{N} NEP \frac{S_{beam}}{S_{PD} t_a}, \qquad (2.6)$$

$$P = \frac{S}{N} NEP \frac{\theta^2 R^2}{D^2 t_a}, \qquad (2.7)$$

The detection distance may be written as [20],

$$R = \sqrt{\frac{PD^2 t_a}{(S/N) NEP \theta^2}}, \qquad (2.8)$$

Estimations of detection distance according to formula (2.8) are presented on Figure 8.
Input data:

P=25 mW; D=3 cm

$\sigma_1 = 0.2 km^{-1}$ (red)

$\sigma_2 = 0.45 km^{-1}$ (blue)

$\sigma_3 = 0.7 km^{-1}$ (black)

S/N=5

$\theta = 3 mrad$

NEP=P_{thr}
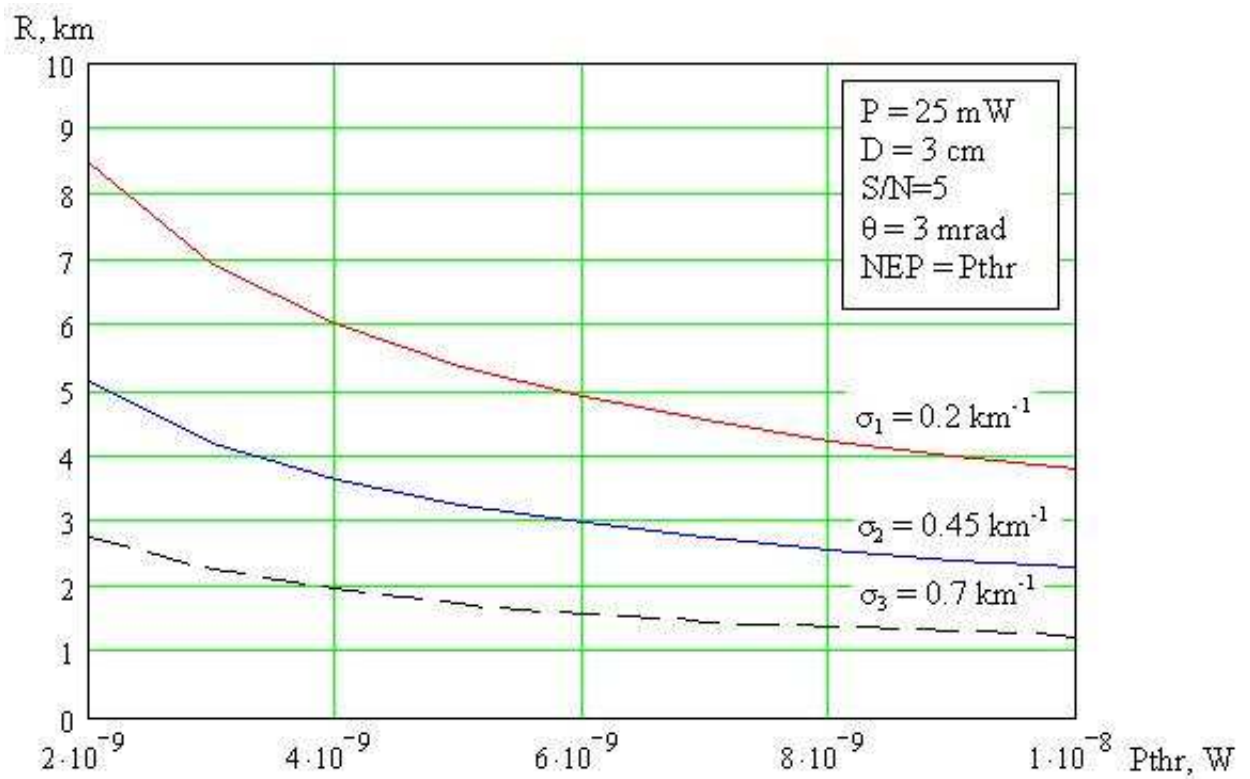
Figure 8 Dependence of detection range on threshold sensitivity of receiver

Analysis of results shows that detection distance of laser warning sensors essentially depends on atmospheric conditions and threshold sensitivity of receiving channel. When the atmospheric attenuation increases, the detection range decreased. For good conditions ($\sigma_1 = 0.2$ km^{-1}) and typical sensitivity of receiver ($P_{thr} = 5 \times 10^{-9}$ W) detection distance makes about 5.5 km. Under bad atmospheric conditions ($\sigma_3 = 0.7$ km^{-1}), detection distance can decrease to 1.8 km.

2.5   Conclusions

The survivability of tanks and armoured vehicles is one of the most difficult challenges for military technology. The cycle of counter-measures will never stop. The hard kill defensive aid has been proven as a successful system when it comes to protecting the crew and its capabilities. Soft kill is another system that should be considered as the future of counter-measure systems because of its relative simplicity and low cost compared to hard kill systems.

For increase of efficiency for laser warning sensors with increase detection range, it is necessary to improve the sensitivity of the receiving channel and reduce the influence of various factors which will be found as a result of research and development of the laser sensor model.

2.6   References

[1] Anti-Tank Guided Weapon, Hard-Kill Defensive Aids Suites. DTC (MA). Page 1-1.
[2] http://en.wikipedia.org/wiki/Tank#Design. 20/11/2005.
[3]http://www.defense-update.com/features/du-1-04/feature-armor-protection.htm. 5/9/2005.
[4] Prof. Richard Ogorkiewiez. Fundamentals of Armour Protection. Advances In Armoured
     Vehicles Survivability. Short Course 19-21 Sep. 2005.
[5] http://www.defense-update.com/features/du-1-04/Hard-kill.htm. 8/4/2005.
[6] http://www.defense-update.com/products/s/shtora-1.htm. 24/7/2005
[7] Prof. Richard Ogorkiewiez. Fundamentals of Armour Protection. Advances In Armoured
     Vehicles Survivability. Short Course 19-21 Sep. 2005.
[8] http://www.army-technology.com/projects/abrams/specs.html. 3/10/2005.
[9] Prof. Richard Ogorkiewiez. Fundamentals of Armour Protection. Advances In Armoured
     Vehicles Survivability. Short Course 19-21 Sep. 2005.
[10] http://www.defense-update.com/features/du-1-04/laser-warning-afv.htm. 7/11/2005.
[11] http://products.saab.se/PDBWeb/ShowProduct.aspx?ProductId=1303. 18/11/2005.
[12]http://products.saab.se/PDBWeb/ShowProduct.aspx?ProductId=1303&MoreInfo=true.
     9/9/2005.
[13] http://www.defense-update.com/features/du-1-04/soft-kill-west.htm. 2/12/2005
[14] http://en.wikipedia.org/wiki/Smoke_screen. 2/12/2005.
[15] http://en.wikipedia.org/wiki/Suppressing_fire. 12/12/2005.
[16] http://en.wikipedia.org/wiki/Active_protection_system. 15/12/2005
[17] Marconi Selenia Communications S.p.A. Functional Description, page 10.
[18] Rami Arili. "The Laser Adventure"
[19] Electro-Optical Systems Analysis-Part 1 by Dr Mark A. Richardson
[20] Equations 2-1 to 2-8 are taking from Electro-Optical Systems Analysis-Part 1 by Dr Mark A. Richardson

CHAPTER 3

Development of the Laser Detection Sensor Model

3.1 Introduction

The laser warning sensor engagement model introduced here is capable of simulating all aspects of a laser beam-riding missile engagement and laser warning receiver scenario. It simulates all the factors that may affect the laser beam propagation through the atmosphere until it hits the target (missile seeker or LWR).

The model is designed to simulate the effect of various weather conditions on the performance of laser warning receivers and laser missile seekers in typical desert environments and is the first Laser Warning Sensor (LWS) model capable of simulating the weather conditions of United Arab Emirates (UAE) using Matlab & Simulink software and the LOWTRAN VII atmospheric computer code. Moreover, the model is designed to simulate the effects of any solar interaction on the warning system and generate the background clutter as might be expected of the UAE desert. Finally, it demonstrates the capablility of detecting weak optical signals at the maximum ranges of anti-tank missiles in the severe weather conditions in the desert.

3.1.1 Basic Methodology

The model is written as a combination of Simulink blocks and Matlab code in a modular fashion. The basic methodology can be seen in Figure 9, which depicts the whole system from the laser source where the signal is generated, through to the receiver that represents the laser warning receiver and/or the laser missile seeker.

Such a system is needed to take into account the functional efficiency of the laser detection sensor. These factors include:

- Parameters of laser radiation source;
- Parameters of atmosphere;
- Parameters of the photodetector.
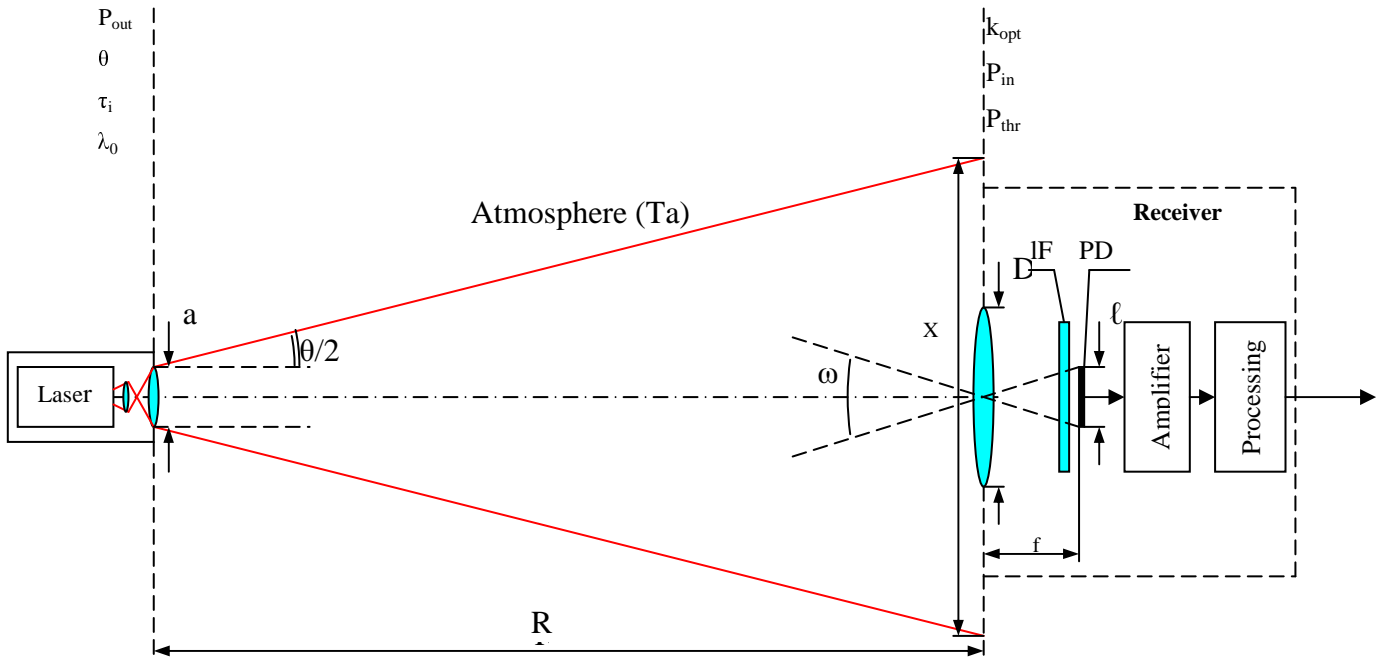
Figure 9 Illustration of LWS system

In this figure we explain various expressions below:

P_{out}—output power of laser irradiator;

τ_i—impulse length;

θ—angle of divergence of laser irradiator;

λ_0—wavelength of irradiation;

a—diameter of transmitter aperture;

R—distance from irradiator to receiver;

P_{in}—power of laser irradiation on receiver input;

x—size of laser beam in receiving objective plane;

D—diameter of receiving aperture;

ℓ—size of photodetector sensing area;

f—focal length of receiving objective;

ω—field of view of receiver;

P_{thr}—threshold power;

k_{opt}—loss coefficient on optical elements;

T_{abs}—atmospheric absorption attenuation;

T_{sct}—atmospheric scattering attenuation;

Δf—bandwidth;

T—temperature;

$\Delta\lambda$—optical bandpass filter; and

PD—photodetector.

43

On the basis of accounting for all the above factors, the mathematical model has been developed for a fully functioning laser sensor. This model is shown in Figure 10.
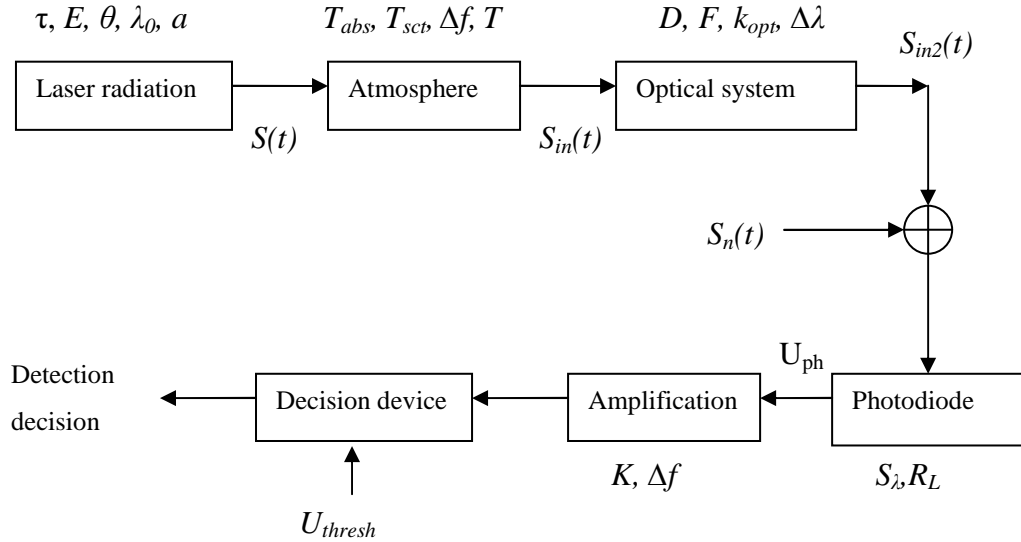
Figure 10 Laser sensor functioning mathematical model

It should be noted that this model has an objective of detecting the threat laser at turn-on when it has a wide beam angle for missile seeker capture. This is the most demanding scenario as the lowest laser intensity is present at the sensor at this time.

3.1.2 Basic Elements of The Model

The laser sensor model has following basic elements:

1. Laser Radiation, whose parameters define the required sensitivity of the receiving channel of Laser Sensor, and also its frequency and spectral characteristics.

2. Atmosphere that causes the attenuation of laser radiation connected to its absorption and scattering, and also distortion of laser radiation on account of atmospheric turbulence.

3. Optical System which focuses radiation the a sensitive area of the photodetector, and also carries out both spatial and spectral filtration of optical signal.

4. The adder is carrying out the process of mixing the useful signal with the with noise signal.

5. Photodiode, carrying out function of transformation of optical signal in electric signal.

6. The amplifier stage intended for maintenance of the required gain factor of electric signal.

7. Decision device, intended for signal shaping on its output in case of excess of useful signal amplitude of some threshold level.

Each element of the model has the parameters that allow it to carry out mathematical transformations of the signal.

3.2   Elements of Mathematical Model

3.2.1   Laser source Gaussian pulse

Many optical systems, exhibit pulse outputs with a temporal variation that is closely approximated by a Gaussian distribution [1]. Hence that variation in the optical output power ($P_o(t)$) with time may be described as:

$$P_0(t) = \frac{1}{\sqrt{2\pi}} e^{-\left(\frac{t^2}{2\sigma^2}\right)},$$
(3.1)

where, σ and σ^2 are the standard deviation and variance of the Gaussian distribution respectively.

In our model of Figure 3.2, the output signal from the laser source s(t) will be as follows:

$$s(t) = P_{out} \exp\{-t^2/2\sigma^2\},$$
(3.2)

where

$$P_{out} = \frac{E}{\tau},$$
(3.3)

and E is the energy of the pulse and τ is the pulse width and t is the current time.

Equation 3.2 is the base of the first subsystem in the sensor model and describes the radiation (emission) source, parameters of which we set (power – from mW to MW, pulse duration, tens of nanoseconds, Gauss pulse shape).

The received signal is described by Gaussian shape because this shape is characteristic for any laser emitters working in a multimode operation. An assumption has been made that the power of a laser pulse has distribution in time under the Gaussian law. The laser pulse is modeled by using of Simulink library to form the required signal with Gaussian distribution. The Gaussian distribution amplitude is equal one, average of distribution equal zero and root-mean-square value (standard deviation) equal 19 nanoseconds. Such standard deviation provides full time of a laser pulse equal 35 nanoseconds. After that a signal we multiply on value of the set power (25 mW). So, at the output of the block 1 of the laser sensor model, the signal has the following characteristics:

     - Amplitude (power): 0,025 W;

     - Pulse duration at level 0,5 (FHWM): 30 nanoseconds

It is appropriate to mention here that in this block it is possible to model other types of laser signals.

3.2.2 Laser signal passed through the atmosphere

Laser signal passed through the atmosphere (taking into account influence of turbulence and thermal distortions) is described by expression:

$$s_{in}(t) = s(t) \cdot T_A(\lambda) \cdot K_A(\lambda) \qquad (3.4)$$

where $s_{in}(t)$ is the signal at the input of the optical system (Figure 10), $T_A(\lambda)$ represents the atmospheric transmission for the laser path, and $K_A(\lambda)$ is the factor describing turbulent distortions of amplitude of an optical signal:

$$K_A(\lambda) = \exp(-\sigma_I) \qquad (3.5)$$

where $\sigma_I^2 = < [LnI - < LnI >]^2 >$ is the dispersion of logarithm emission intensity I for heavy fluctuations [V.I.Tatarskiy][2]:

$$\sigma_I^2 = 1 - (1 + 6\sigma_0^2)^{-1/6}, \tag{3.6}$$

and [3],

$$\sigma_0^2 = 1.23 C_n^2 k^{7/6} R^{11/6}, \tag{3.7}$$

where σ_0^2 represents the dispersion of logarithm emission intensity for slack fluctuations
C_n^2 is the structural constant of atmosphere refraction coefficient
$k = 2\pi/\lambda$ is the wave number
λ is the wavelength
R is the distance to the emission source

The effect of turbulence (scintillation) has been modelled as a deterministic process based upon the theories of V.I.Tatarskiy [2] and Kolmororov-Obukhov [3]. However, scintillation is a random (statistical) process which may not be well suited to such a treatment. An attenuation approach based upon the fraction of pulses (say 90%) above a certain threshold may be more appropriate.

$T_A(\lambda)$ is described by the following expression [4] :

$$T_A(\lambda) = T_A^{absor}(\lambda) \cdot T_A^{scatter}(\lambda) \tag{3.8}$$

Atmospheric transmission is an important factor to be considered and it consists of two components, absorption and scattering. In addition, the atmospheric attenuation is not uniform and it is a function of wavelength. We will consider the absorption first. The atmospheric absorption attenuation can be calculated using the following equation [4]:

$$T_A^{absor}(\lambda) = \exp(-\alpha_{absor}(\lambda) \cdot R) \tag{3.9}$$

where $\qquad \alpha_{\text{absor}}(\lambda) = \alpha_{absor.H_2O}(\lambda) + \alpha_{absor.CO_2}(\lambda) + \alpha_{absor.O_3}(\lambda)$ $\qquad$ (3.10)

for $\lambda = 1.06$ µm, which is one of the most important wavelengths to cover in our study,

$$\alpha_{H_2O} \gg \alpha_{CO_2}; \alpha_{O_3} \qquad (3.11)$$

The radiation absorption coefficient of water vapor in the atmosphere on a horizontal path is given by [5] :

$$\alpha_{absor.H_2O}(\lambda) = f(\omega_0; E_E; T; H) \qquad (3.12)$$

where, ω_0 is the quantity of precipitable water (H_2O) (mm) over a distance of 1 km.

E_E - aqueous pressure, Pa ($7 \cdot 10^{-3} \ldots 1.2 \cdot 10^{-2}$ Pa)

T- atmospheric temperature, K ($300 \ldots 330$ K) degree Kelvin

H- relative air humidity (in percentage)

Secondly, the atmospheric scattering attenuation can be calculated and is given by:

$$T_A^{\text{scatter}}(\lambda) = \exp(-\alpha_{scatter}(\lambda) \cdot R) \qquad (3.13)$$

For laser radiation scattering we need to consider the following three cases:

a) Clear atmosphere ($R_m \geq 10$ km) [6]:

$$\alpha_{\text{scatter}}(\lambda) = \frac{3.91}{R_m}\left(\frac{\lambda}{0.55}\right)^{-0.585\cdot\sqrt[3]{R_m}} \qquad (3.14)$$

where:

R_m is meteorological range (km) and λ is wavelength of irradiation (µm)

b) Haze conditions:

$\alpha_{scatter}(\lambda) = f(d, N)$ represents haze conditions. The parameter d is the radius of particles and N is the density of particles.

c) Fog conditions: $\alpha_{scatter}(\lambda) = f(d, N)$

48

The second subsystem of the model will be designed to describe the influence of the atmosphere on the laser beam according to equation (3.4). This subsystem is constructed from elementary blocks of Simulink and calculation of the atmospheric coefficients for absorption and scattering are done using LOWTRAN VII code.

LOWTRAN is the name of a series of computer codes beginning with LOWTRAN 2(first available in 1972) and ending with the most recent version LOWTRAN 7 (first available in 1989). LOWTRAN calculates the transmittance and/or radiance for a specified path through the atmosphere based in the LOWTRAN band model discussed previously, molecular continuum absorption, molecular scattering , and aerosol absorption and scattering models. Radiance calculation includes atmospheric self-emission, solar and/or lunar radiance single scattered into the path, direct solar irradiance through a slant path to space, and multiple scattered solar and/or self-emission radiance into the path. The model covers the spectral range from 0 to 50,000 cm^{-1} at a resolution of 20 cm^{-1} . The band model spectral parameters exist every 5 cm^{-1}.

 The atmosphere is represented as 32 layers from 0 to 100,000 km altitude. Layer thickness is 1 km upto 25 km, 5 km from 25 to 50 km (the top of the stratosphere), and the last two layers are 20 and 30 km thick, respectively. Detailed structure just above the land or sea is not represented by this model and thus model predictions can be inaccurate if nonstandard conditions exist. Attenuation and refractive effects are calculated for each layer and summed along the path. The physical characteristics of each layer are determined by inputs and predetermined standard models of various regions and seasons (Appendix A). The option to specify a particular atmosphere also exists. The atmosphere is assumed to be in thermal equilibrium; the code should not be used above 100 km or at and above the ionosphere.

LOWTRAN had been validated against field measurements and is widely used for many broadband system performance studies. The single scattering model used by Lowtran has limited applicability under high attenuation conditions where multiple scattering can be important. For most of this work, Lowtran was considered adequate. However, and the design of the atmospheric attenuation block permits the simple replacement of the source data file

with that from more advanced atmospheric models should it be deemed more applicable for the high attenuation conditions.

In this chapter, five weather conditions have been considered. These weather conditions have been chosen to simulate the weather conditions in the United Arab Emirates desert and the desert weather conditions in general. LOWTRAN software has been run for these five weather conditions each one separately. The output data from LOWTRAN (Transmission and Solar Irradiance) will be used to calculate the atmospheric attenuation at a specific wavelength by a MATLAB program using equation (3.8).

3.2.3 Optical System

As seen in Figure 9, the signal at the entrance of the photodiode is given by:

$$s_{in2}(t) = s_{in}(t)\frac{S_D}{S_{beam}}$$
(3.15)

where,

$$S_D = \frac{\pi \cdot D^2}{4}$$
(3.16)

S_D is the area of received aperture and D is its diameter.

$$S_{beam} = \frac{\pi \cdot [a + (\theta + \theta_A) \cdot R]^2}{4}$$
(3.17)

Where S_{beam} is the sectional area of the laser beam at distance R from the laser source, a is the diameter of the transmitting objective, θ the divergence of the laser beam (typically between 2 to 5mrad) and θ_A is the divergence caused by turbulence that can be evaluated using the following equation [6]:

$$\theta_A \approx \frac{\lambda}{r_0}$$
(3.18)

where λ is the emission wavelength and r_0 is the length of wave coherence[7]:

$$r_0 = (0.54 \cdot Cn^2 \cdot k^2 \cdot R)^{-3/5}$$
(3.19)

where,

$C_n{}^2$ – structural constant of refractive index

k = 2π/λ – wavenumber

λ - wavelength

R – distance passed by laser beam

The third subsystem of the model describes the effect of the receiving optical system on the signal coming from the threat according to equation (3.15).

3.2.4 Noise Power

A very important issue for analysis is noise. We have two sources of noise: external noise and internal noise. The external noise is due to the weather conditions, type of background, solar irradiance etc. The internal noise is due to electronic factors such as, thermal noise, shot noise etc.

The noise input power to the photodetector is given by:

$$S_n(t) = P_\Sigma \cdot n(t) \tag{3.20}$$

where P_Σ is the total average noise power;

$$P_\Sigma = P_b + P_r \tag{3.21}$$

P_b - external Background noise power;

P_r - internal receiver noise power.

Generally, the probability density of P_Σ is considered as Gaussian:

$$p(n(t)) = \frac{1}{\sigma_n \sqrt{2\pi}} \exp\{-(n-\mu_n)^2 / 2\sigma_n^2\} \tag{3.22}$$

thus, n(t) is Gaussian, stationary, white noise with its parameters $\sigma^2{}_n = 1, \mu_n = 0$.

3.2.4.1 External Background Noise

P_b is the external background noise power and is given by:

$$P_b = \int_{\lambda_1}^{\lambda_2} B(\lambda) \cdot \omega \cdot S_D \cdot K_{opt} \cdot d\lambda,$$

(3.23)

where ω is the field of view of the receiver. From the scenario geometry (Figure 9) the field of view of the receiver is given by:

$$\omega = \frac{\pi \cdot \ell^2}{4 \cdot f^2},$$

(3.24)

Where ℓ - size of sensitive area of photodetector (typically 0.2 to 1 mm)

f - objective focal length

S_D is the input lens area

K_{opt} is the transmission coefficient of the optical system (typically 0.4 to 0.6)

dλ is the spectral bandwidth of the interference filter

$B(\lambda)$ is the spectral Background brightness

This model is appropriate for a narrow field of view but may not represent accurately the situation for the relatively wide fields of view used in some practical laser warning receivers. In particular, the near and far points of the background and their contributions to the overall background irradiance may not be represented reliably.

Sources of solar background can be seen in Figure 11. It is one of the most significant sources of noise the model should be capable of dealing with, particularly with respect to conditions expected in the UAE.
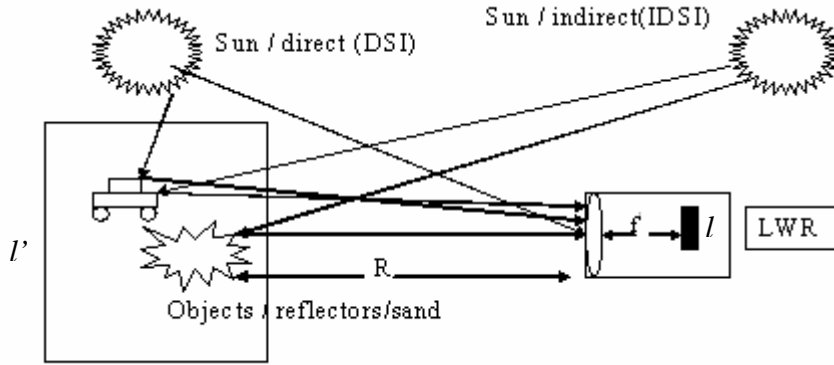
Figure 11 Sources of Solar Background

Four cases will be considered, namely: direct solar illumination, diffuse reflection of typical surfaces (such as desert sand), diffuse reflection of cloud surfaces and night sky radiation.

Three samples of UAE desert sand have been tested to generate their diffuse reflectivities over the wavelength range of interest and any of these values can be used as the background in the model.

$B(\lambda)$ is composed of four terms as follows:

$$B(\lambda) = \sum_{i=1}^{4} B_i(\lambda) = \mu \cdot I_0(\lambda) \cdot \frac{\cos(\psi)}{\pi} + \mu \cdot I_0(\lambda) \cdot \frac{\cos(\psi)}{\pi} \cdot \rho + \mu \cdot I_0(\lambda) \cdot k_{Clouds} + B_{Night} \qquad (3.25)$$

In this formula:

- The first term - direct solar illumination
- Second term – diffuse surface reflection
- Third term – diffuse cloud reflection
- Fourth term - night sky radiation.

The parameters included in the equation are:

- ρ is the reflection coefficient from the surface (typical value of $\rho = 0.02$ to 0.3)
- k_{Clouds} — reflection coefficient from clouds (typical value of $k_{Clouds} = 0.001$ to 0.2)

- B_{Night} — spectral brightness of night sky ($B_{Night} = 10^{-10}$ W/cm^2·μm·srad)

- μ - the coefficient describing the distribution of brightness depending on the solar angle (ψ) in the sky and the observation angle.

- $I_0(\lambda)$ is the flux density of sunlight and can be seen in Figure 12 [5]. However, the model takes its values for $I_0(\lambda)$ from the LOWTRAN VII atmospheric computer code.

I_0, W/(cm^2·μm)
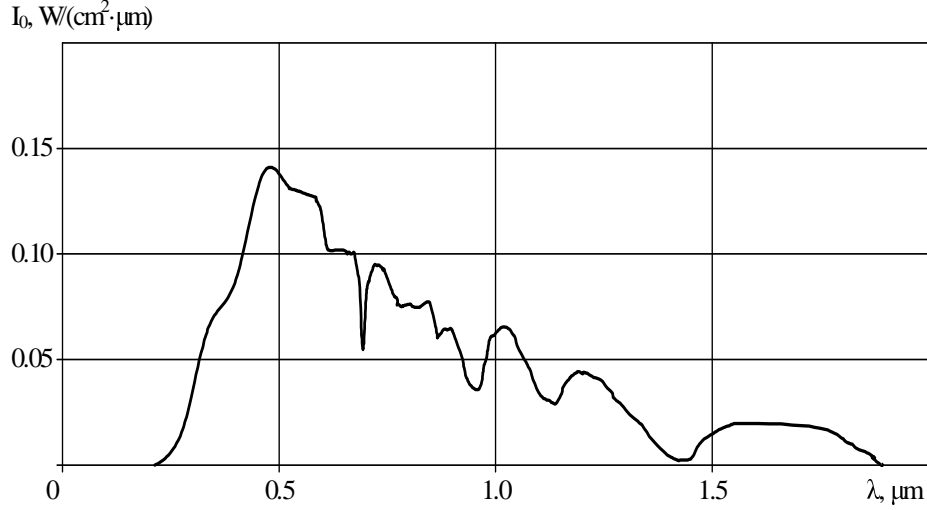
Figure 12 Solar Spectral Irradiance

3.2.4.2 Internal Noise of System

P_r - internal receiver noise power of the receiver and can be calculated as[7]:

$$P_r = \frac{\sqrt{\bar{i}_n^2}}{S_\lambda}$$
(3.26)

Where, $\bar{i}_n^2$ is dispersion of the noise current and S_λ represents the spectral sensitivity of the photodetector, A/W.

The dispersion of the noise current consists of several current noises, the largest of which are the thermal ($\bar{i}_{therm.n}^2$) and shot ($\bar{i}_{shot.n}^2$) noises [8]:

$$\bar{i}_n^2 = \bar{i}_{therm.n}^2 + \bar{i}_{shot.n}^2 + \bar{i}_{other.n}^2$$
(3.27)

54

$$(\bar{i}^2_{therm.n}; \bar{i}^2_{shot.n} >> \bar{i}^2_{other.n}) \tag{3.28}$$

Where the thermal noise of the receiver is given by [9]:

$$\bar{i}^2_{therm.n} = \frac{4 \cdot k \cdot T \cdot \Delta f}{R_L}, \tag{3.29}$$

where k is Boltzmann constant, T represents the environmental temperature (typically 300 to 330K), R_L is load resistance of photodetector (typically 10^4 to 10^5 ohm) and the receiver electronic bandwidth is given by:

$$\Delta f \approx \frac{1}{\tau}, \tag{3.30}$$

where τ is the pulse width.

The photodetector (APD) shot noise can be given by [10]:

$$\bar{i}^2_{shot.n} = 2 \cdot e \cdot \Delta f \cdot M^A \cdot X \cdot (\bar{I}_D + S_\lambda \cdot \overline{P_A} + S_\lambda \cdot \overline{P_b}), \tag{3.31}$$

where,

e - electron charge

Δf - electronic bandwidth

M – multiplication factor(10…100)

A - excess noise index

X - excess noise factor

$\bar{I}_D$ - average dark current ($\bar{I}_D = 0.5...5$ nA)

$\overline{P_A}$ - average power of optical signal

$\overline{P_b}$ - average power of Background

S_λ - spectral sensitivity of photodetector

After the third subsystem there is an 'adder' that sums the useful signal from the laser source with the noise signals. The noise source is described by a Gaussian distribution. Furthermore, the blend of an optical signal and noise goes on as an input to the photodetector, which transforms the optical signal into an electrical signal.

3.2.5 Photodiode Output

The photodetector is responsible of converting the received signal to a useful electrical signal that can be then transferred to the processing circuitry. The following equation is used to evaluate the behaviour of the photodiode:

$$U_{phd}(t) = S_\lambda [S_{in2}(t) + S_n(t)]R_L ,$$ (3.32)

Where,

$U_{phd}(t)$ - photodiode output voltage

S_λ – photodiode spectral sensitivity

$S_{in2}(t)$ - useful signal

$S_n(t)$ - noise signal

R_L – load resistance

Since we are looking to detect a weak optical signal at long ranges, we need to choose a photodiode with a high responsitivity. We are covering a wide optical bandwidth from $0.4\,\mu m$ to $1.7\,\mu m$ which will therefore require more than one photodiode.

The selection of a photodiode (APD or PIN) is defined by the requirements of the parameters of the receiving channel. If high sensitivity is required an APD is the best choice (due to its 50 to 200 times greater responsivity). If a low noise level is required a PIN photodiode would be a good choice. For detection of low power lasers at maximum range it would appear that an APD is the most appropriate choice due to its high sensitivity. This choice is justified by examining PIN vs APD signal to noise ratio in Chapter 4. The properties required from a photodiode (and that of the associated amplifier) are:

1. High responsivity (A/W)
2. Good linearity
3. Wide bandwidth
4. Low noise

3.2.6 Amplification Stage

The output voltage from the amplification stage may be described by:

$$U_{out}(t) = K \cdot U_{phd}(t),$$ (3.33)

where,

$U_{out}(t)$ - amplification stage output voltage

K - factor of amplification

$U_{phd}(t)$ - photodiode output voltage

The amplification path is modelled on 2 cascade circuits. The pulse width for the optical signal in the model is 30 ns which makes the typical bandwidth requirement 33MHz. Frequency filters for both amplifiers are built from standard blocks of Simulink libraries «Analog Filter Design ». In conjunction, they limit the region of amplification to between 0.9 MHz (low-frequency noise cut-off) to 33 MHz (corresponding to the signal pulse width). Butterworth filters have been utilised because of the required uniform shape of the amplitude-frequency characteristic (AFC), the simplicity in use of cut-off frequency definition and the filter order defines the slope of the AFC.

In practice, typical timing comparators, which are used as the decision device in an LWR, require an input signal of the order of 100 mV. As the noise equivalent power (NEP) of typical photodiodes are ~10 pA/Hz that yields a minimum perceived voltage of approximately 1.5 mV. Therefore the overall gain factor of the amplification section should be of the order of 70…80 (100mV/1.5mV).

The 1st amplifier (prime amplifier) is represented in the model as an ideal amplifier with fixed amplification factor (equal to 4) which is connected in series with a highpass filter (Butterworth filter of 2nd order with a cut-on frequency of 0.9 MHz) and a high voltage limiter block to prevent saturation in the amplifier cascade.

The 2nd amplifier is implemented in series with the first amplifier with a fixed amplification factor (equal to 20), a voltage limiter block, and a lowpass filter (Butterworth filter of 2nd order with cutoff frequency of 33 Mhz).

3.2.7 Threshold Voltage & Decision Making

The Threshold voltage is given by,

$$U_{thresh} = P_r \cdot S_\lambda \cdot R_l \cdot K \cdot q(D,F),$$ (3.34)

Where,

P_r - receiver noise power

S_λ - spectral sensitivity of photodetector

R_l - load resistance of photodetector

K - factor of amplification

$q(D,F)$- signal/noise ratio, which provides the required values of probability of correct detection (D) and a false alarm (F). Typical q(D,F)=5…10.

If the condition:

$$U_{out}(t) > U_{thresh}$$ (3.35)

is satisfied, the signal is detected.
If the above condition is not satisfied,

$$U_{out}(t) \leq U_{thresh}$$ (3.36)

the signal is not detected.

3.3 Conclusions

In this chapter, we introduced the theory behind laser sensor model and the mathematical equations needed to create this model. Each part of the laser sensor has been explained and discussed in detail. It is the base for building the model using MATLAB and

Simulink libraries with the help of LOWTRAN VII atmospheric computer code. Laser source of radiation, Atmosphere, optical system, photodiode, amplification stage, and decision device are the components for the laser sensor model setup.

For the effect of solar background, we collected three samples of the UAE desert sand. These samples will be subject of an experiment to read the reflectivity of each one of them. We now implement the theoretical model and observe results for or test data. There are still some gaps to be filled and the most important one is the effect of atmospheric turbulence on the laser beam trip to the target that will be introduced later on in this thesis.

We expect the model to run as designed and our aim is to detect the weak optical signal at 5.5 km (which is the maximum range for antitank missiles) or more since the maximum detected range we measured in the real trials was 4.5 km.

3.4   References

[1] Optical Fiber Communications Principles and Practice.   John M. Senior. Page 544.

[2] Tatarski, V., Wave Propagation in Turbulent Medium, New York: McGraw-Hill, 1961.

[3] Introduction to Infrared and electro-optical systems, Ronald G. Friggers, Paul Cox, Timothy Edwards, Page 140.

[4] Introduction to Infrared and Electro-Optical Systems, Ronald G. Driggers, Paul Cox, and Timothy Edwards, Artech House,1999, p.407.

[5] Optical Detection Theory for Laser Application, George R. Osche, Page 201.

[6] Woodman D. P., Limitations in Using Atmospheric Models for Laser Transmission Estimates, Appl. Opitcs, 13, 1974, pp. 2193-2195

[7] Journal of Battlefield Technology, Vol 8, No1, March 2005. Kellaway & Richardson, Laser Analysis-Part 3. Page 30.

[8] Optical Detection Theory for Laser Application, George R. Osche, Page 200.

[9] Introduction to Infrared and electro-optical systems, Ronald G. Friggers, Paul Cox, Timothy Edwards, Page 203.

[10] Introduction to Infrared and Electro-Optical Systems, Ronald G. Driggers, Paul Cox, and Timothy Edwards, Artech House,1999, p.241.

[11] Optical Detection Theory for Laser Application, George R. Osche, Page 138.

[12] Optical Detection Theory for Laser Applications, George R. Osche, Page 140.

CHAPTER 4

Testing of Laser Sensor Model

4.1 Introduction

The previous chapter presented the theory of a laser warning sensor and its components. We now build the model and run it. With the help of MATLAB and Simulink, the theoretical model can be divided into blocks representing the real world scenarios of laser sensors where the sensor is subject for wide range of factors that affect its performance.

In this chapter, we present the model calculated data, experiments of measuring the reflectivity of desert sand samples, using LOWTRAN VII atmospheric computer code to calculate data for five weather conditions, the MATLAB code to read data and inject them to the Simulink blocks. We will also discuss results of the model, analyze outputs of the model, verify outputs, and draw some conclusions based on our results.

4.2 Laser Detection Sensor Model

The laser detection sensor model has been developed on the basis of the mathematical equations described in chapter 3. The model is composed of a set of subsystem blocks incorporating an algorithm representing the functionality of that block in the laser detection sensor process. These subsystem blocks are shown depicted in Figure 13.

Each block has an input panel to insert and correct the initial parameters to realize the internal mathematical transformations of the algorithm and also investigate its functionalities. The model also provides an opportunity for visualization of all the output signals of each block with help of the in-built *oscilloscope*. The result of the model is fixed as a header: "DETECTED" or "NOT DETECTED".
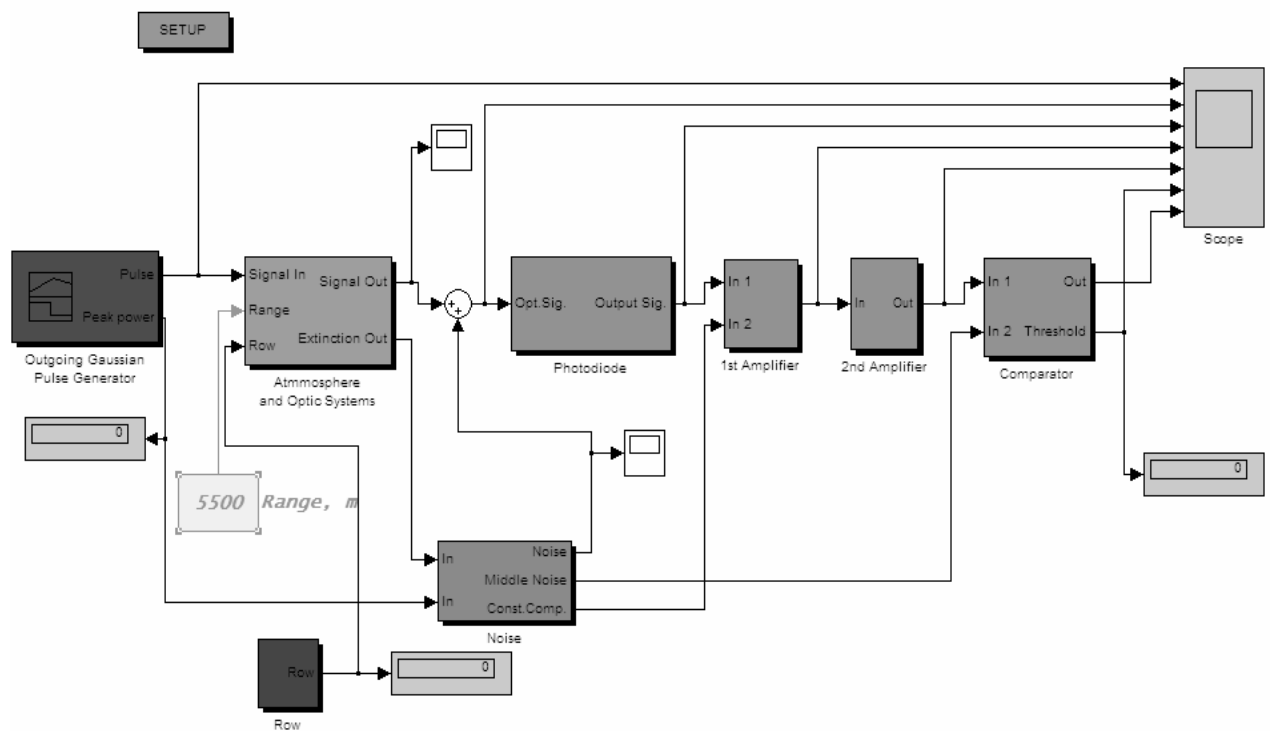
Figure 13 Laser Sensor Model

The structure of model includes the following blocks:

1. Outgoing Gaussian Pulse Generator
2. Atmosphere and Optic System
3. Noise
4. Photodiode
5. 1st Amplifier
6. 2nd Amplifier
7. Comparator
8. Setup
9. Range
10. Scope

The block "Outgoing Gaussian Pulse Generator" represents the subsystem modelling the formation of the laser signal as a Gaussian Pulse of the required duration and amplitude, and also the periodicity of the pulses with the set duration and the period of recurrence. The given subsystem is realized on the basis of standard elementary blocks from the Simulink library. The internal block "Clock" forms the continuous modelling time and this reference is adhered to from the start of the model.

The block "Atmosphere and Optic System" represents the subsystem modelling the effect of attenuation and distortion of the laser radiation at it passes through a turbulent atmosphere and the optical channel. Once again the subsystem is realized on the basis of standard elementary blocks of Simulink library and uses data derived from the off-line calculations of the LOWTRAN VII atmospheric computer code [1].

The "Noise" block represents the subsystem in which the noise signal is formed, resulting in an input for the photodetector. This consists of the shot noise and dark current of the photodetector, the shot noise of the background radiation and thermal noise of the electronics.

The "Photodiode " block represents the subsystem in which transformation of an optical signal to an electric signal is carried out.

The "1st Amplifier" subsystem carries out the transformation of the photodiode output current pulses to pulses of voltage and amplifies the signals up to the required value. In the model it is realised as consecutive switching on/off of the block of the ideal amplifier, the higher frequency filter and the peak terminator (which simulates process of saturation of the amplifier).

The "2nd Amplifier" subsystem is working as an ideal amplifier with a fixed gain and the limited bandpass. It is again realized as consecutive switching on/off of the block of the ideal amplifier, the low frequency filter and the block of the peak terminator modelling the process of saturation in the intensifying cascade. The bandpass of the intensifying cascade has been chosen from the value of the width of laser signal. The gain of amplification has been designed on the basis of satisfying the condition of maintaining the required size of signal amplitude for confident operation of the comparator.

The "Comparator" block represents the subsystem that forms an output pulse only in the case of the input signal amplitude exceeding a threshold level. It has two inputs, one is the useful signal, and the other is the threshold voltage. In the circuit of threshold voltage formation, there is a block to input the value of the signal/noise ratio that provides the required value to achieve the correct detection probability and false alarm rate.

The "Setup" block represents the Graphical User Interface which opens dialog windows for the input and corrections of the initial data. The "Range" block is intended for the input of values of the distance from the source of the laser radiation to laser sensor. The "Scope" block enables the visual display of the signals which are generated by each of the separate elements of the model.

4.3   Graphical User Interface (GUI)

A GUI designed in Matlab facilitates the user to run the model easily. Figure 14 shows the GUI layout.
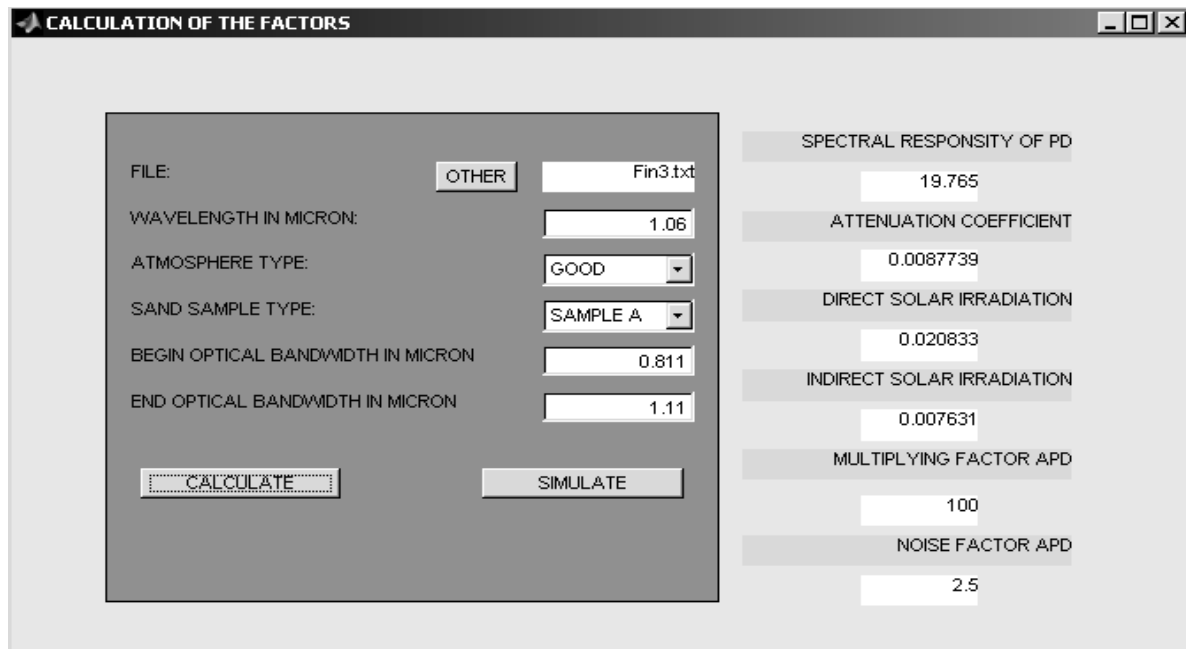
Figure 14 GUI for laser sensor model

It is clear from the figure that the user has the capability to change the source file by clicking on the "OTHER" button which opens the files folder containing the input data.

The GUI contains the following inputs:

1.   Wavelength In Micron: The user enters the wavelength of the threat laser

2. Atmosphere Type: The user has an option to select the weather condition from five possibilities.

3. Sand Samples: As mentioned before we are using three sand samples from United Arab Emirates desert and here the user has an option to choose one of them.

4. Begin Optical Bandwidth: The lower wavelength limit (in microns) of the complete optical system (including any filters).

5. End Optical Bandwidth: The upper wavelength limit (in microns) of the optical system (including any filters).

After inputting this initial data the "Calculate" button is clicked. This then calculates the following data (for input into the appropriate Simulink block):

- Spectral responsivity of the photodiode
- Attenuation coefficient
- Direct solar irradiation
- Indirect solar irradiation
- Multiplying factor of APD
- Noise factor of APD

After this the model is then run by clicking the "Simulate" button.

4.4 ATMOSPHERIC DATA

The choice of the atmosphere type used is based on information on the current weather conditions. The following five weather types have been modelled: Good, Typical-I, Typical-II, Bad-I, and Bad-II. These conditions are related to the type of weather typical in the UAE during the four seasons of the year. The attenuation of the laser radiation for different weather conditions is calculated with the LOWTRAN VII atmospheric computer code.Dependence of atmospheric transmittance on wavelength for five types of weather conditions are shown in Appendix A.

4.5 SAND DATA

The choice of the background sand type as a reflecting surface is carried out on the basis of the information on the location of laser sensor and results of measurements of the reflection of various samples of UAE sand. Results have shown there to be three basic types of sand and their measured values are shown in Appendix B. The measured values of reflection gain are used for calculation of brightness of non directed sunlight getting into an input of the photodiode.

4.6 PHOTODIODE DATA

The detector is an essential component for our system and is one of the crucial elements which dictate the overall system performance. Its function is to convert the received optical signal into an electrical signal, which is then amplified before further processing. Therefore when considering signal attenuation along the path, the system performance is determined at the detector. The following criteria define the important performance and compatibility requirements for detectors [2]:

- High sensitivity at the operating wavelength. The quantum efficiency should be high to produce a maximum electrical signal for a given amount of optical power.
- High fidelity. To faithfully reproduce the received signal waveform electrically.
- Short response time to obtain a suitable bandwidth.
- Minimum noise. Typically the lower the dark current the better is the detector.
- High internal gain with low noise circuitry.
- High reliability. Capable of continuous stable operation for many years.
- Relatively low cost.

From the above and the requirement for as long a range detection as possible (see chapter 3) APDs are chosen as the most appropriate detector. Three Photodiodes have been chosen to cover the wavelength of interest (typically 0.4-1.7 μm) [3]:

- Si APD S2382 (Hamamatsu); maximum spectral response at λ_{max}=0.8μm.
- Si APD S8890 (Hamamatsu); maximum spectral response at λ_{max}=0.94μm.
- InGaAs APD C30644E (EG*G); maximum spectral response at λ_{max}=1.55μm.

Figure 15 shows the Responsivity (spectral response) of these three APD's.
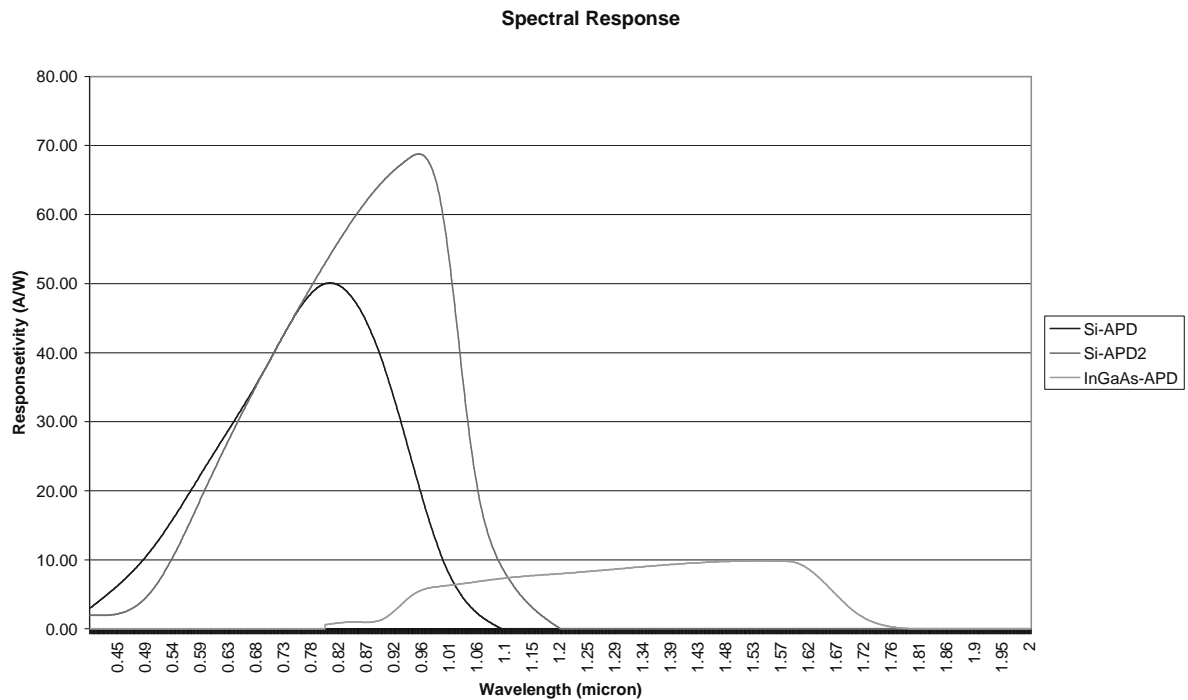
Spectral Response

Figure 15 Spectral response

In the MATLAB program, all the spectral ranges from 0.4μm up to 1.7μm are divided into 3 intervals for each type of the photodiodes. An automatic selection criterion of photodiode depending on a laser source wavelength has been added. If the wavelength of interest (λ) which the user enter, comes in one of the following intervals, the spectral response of the photodiode covering that specific area will be taken, Appendix I contains APD's specifications.

In the model an automatic selection criteria for the photodiode has been implemented depending on the laser source wavelength. The spectral coverage of each choice is as defined below:

- $\Delta\lambda_1$=0.4…0.81μm - Si APD S2382
- $\Delta\lambda_2$=0.811…1.11μm - Si APD S8890
- $\Delta\lambda_3$=1.111…1.7μm - InGaAs APD C30644E

The model also contains values for the gain or Multiplying Factor (M) and Noise Factor (X) for the APDs. Typical values are M=100, X=2.5.

As mentioned in Chapter 3, we need to do a justification using the laser sensor model to prove that APD is more appropriate for detecting laser threat at far ranges. The results are shown in Tables 1 & 2.

Photodiode parameters in the laser sensor model (for λ=1.06μm)	APD	PIN
Spectral sensitivity, A/W	19.765	0.1976
Multiplication factor(M)	100	1
Excess noise factor(X)	2.5	1

Table 1 APD & PIN parameters in LWS

Type photodiode	Wave length, μm	Spectral range, μm	Atmospheric conditions				
			Good km	Typ-1 km	Typ-2 km	Bad-1 km	Bad-2 km
APD	1.06	0.811-1.11	5.5	5.3	4.2	2.2	2.1
PIN	1.06	0.811-1.11	4.5	4.3	3.3	1.5	1.4

Table 2 Maximal detection range of the laser sensor with APD and PIN photodiodes

From the model it is clear that the performance of the APD photodiode in detecting weak optical signals at long ranges is much better than the performance of PIN photodiode and that is due to the high sensitivity of the APD which has an internal gain feature.

4.7 OTHER DATA

Other inputs (Direct solar irradiance, Indirect solar irradiance as discussed in Part – I) are called by the MATLAB code. A typical set of input data can be seen in Table 3.

Setup	
Wavelength in micron	1.06
Atmosphere type	Good
Sand sample type	Sample A
Begin optical bandwidth in micron	0.811
End optical bandwidth in micron	1.11
Generator	
Gauss pulse mean, s	35×10^{-9}
Gauss pulse standard deviation, s	13×10^{-9}
Pulse peak power, W	25×10^{-3}
Atmosphere and optical system	
Absorption coefficient	From LOWTRAN
Scattering coefficient	From LOWTRAN
Diameter input lens, mm	30
Diameter output lens, mm	30
Divergence, mrad	3
Squared structural constant of refraction coefficient, $m^{-2/3}$	52×10^{-17}
Noise	
Optical system loss factor	0.5
PD sensitive area diameter, mm	0.5
Input optic lens diameter, mm	30
Focal distance, mm	40
Boltzmann constant, $J \cdot K^{-1}$	1.38×10^{-23}
Temperature, K	328
Bandwidth, Hz	33×10^{6}
Load Resistance, Ohm	10^{5}
Electron charge, Cl	1.6×10^{-19}
Dark current, A	0.5×10^{-9}
Background noise	
Coefficient Distribution of brightness	0.172
Angle between Sun and Optical axis, degree	40

Dispersion coefficient of clouds	0.001
Spectral brightness of night sky, $W/cm^2 \cdot \mu m \cdot srad$	10×10^{-10}
Photodiode	
Spectral Sensitivity, A/W	From Lookup Table
1st Amplifier	
Gain	4
Derivator characteristic time, s	900×10^{-9}
Internal resistance, Ohm	10^3
2nd Amplifier	
Gain	20
Passband edge frequency, Hz	30×10^6
Comparator	
Integrator characteristic time, s	100×10^{-9}
Tuning coefficient	1

Table 3 Input Data

4.8 Model Functionality Testing

Runs with the model have been conducted with various weather conditions and atmosphere turbulence levels and also for various values of device parameters. Figure 16 shows the oscilloscope output signals for various model blocks for the initial data of Table 3 and a range of 5500m to the laser source:
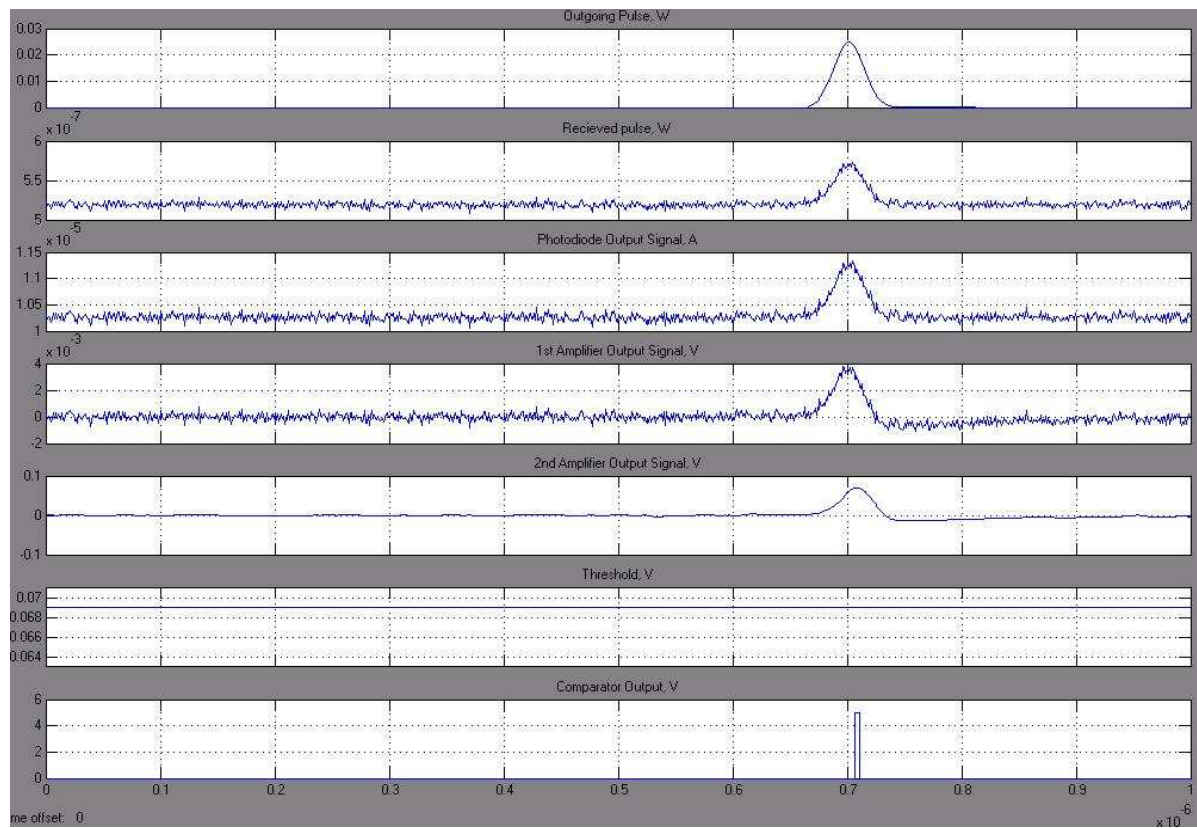
Figure 16 Output signals of model blocks for the initial data resulted in Table 4.1 and at range 5500m

Results of mathematical calculations for the same conditions are submitted in Appendix D. The comparative analysis of the amplitudes of useful signal and noise on the oscilloscope shows that the model is functioning as expected. It is clear that we have a detection at the used parameters.

The results of evaluation of the maximal detection range of laser radiation threat at various atmospheric conditions and various spectral ranges are given in Table 4. It is clear that the detection range increased with higher wavelengths.

APD type	Wave length, μm	Spectral range, μm	Atmospheric conditions				
			Good, km	Typ-1, km	Typ-2, km	Bad-1, km	Bad-2, km
Si APD S2382, Hamamatsu	0.63	0.4-0.81	4.3	4.1	3.0	2.1	1.9
Si APD S8890, Hamamatsu	1.06	0.811-1.11	5.5	5.3	4.2	2.2	2.1
InGaAs APD C30644E, EG&G	1.54	1.111-1.7	7.2	7.1	5.7	2.5	2.4

Table 4 Maximum detection range of laser source with various spectral ranges and atmospheres

The results of the maximum detection range of the laser source under various atmospheric conditions and various background sand types is given in Table 5.

Sand Sample	Atmospheric conditions				
	Good, km	Typ-1, km	Typ-2, km	Bad-1, km	Bad-2, km
Sand A	5.5	5.3	4.2	2.2	2.1
Sand B	5.9	5.7	4.4	2.2	2.1
Sand C	5.8	5.6	4.3	2.2	2.1

Table 5 Maximum detection range of a laser source with various background sand types and atmospheres

The analysis of the output results shows that the type of sand as a reflecting surface for indirect sun radiation has an influences on the detection range under good atmospheric conditions only. Under bad atmospheric conditions the other factors are dominate. In Chapter 6 the research into various factors that influence the overall performance of the laser sensor is carried out and recommendations on optimization of its parameters are formulated.

4.9   Conclusions

A laser sensor model has been built and tested for different cases and weather conditions. The outputs of the model demonstrate it is behaving as predicted. The model is flexible and general enough to encompase all expected variations and can easily be updated with new or different data files.

The analysis of output results testifies that the detection range essentially depends on atmospheric conditions, the performances of the receiving channel and the photo detector type. For the given characteristics of the laser sensor the maximal range of detection does not exceed 5.5km. With deterioration of atmospheric conditions the range of detection is essentially reduced and in the range from Good up to Bad-2, it reduces by a factor of almost 2.

Moreover, the analysis of results show that the type of sand as a reflecting surface for indirect solar irradiation has an influence on the detection range under good atmospheric conditions only and under bad atmospheric conditions other factors are became dominating.

In chapter 6, a study of the influence various factors on an overall performance of the Laser Sensor will be carried out and recommendations on optimization of its parameters are formulated. We will compare the model results to laboratory based experiments and the results from some field trials, with real systems, in the UAE. This will demonstrate the validity of the model which will hence enable realistic predictions for optimisation of LWRs and countermeasure analysis to be carried out.

4.10   References

[1] Introduction To Infrared and Electro-Optical   Systems. Ronald G. Driggers, Paul Cox, and Timothy Edwards. Page 145.

[2] Optical Fiber Communications Principles and Practice. John M. Senior. Page 326-327.

[3] http://sales.hamamatsu.com/en/products/solid-state-division.php. 4/9/2004.

[4]   Introduction To Infrared and Electro-Optical Systems. Ronald G. Driggers, Paul Cox, and Timothy Edwards. Page 3.

CHAPTER 5

Experimental Verifications & Field Trials Verifications of Laser Sensor Model

5.1 Introduction

It is important in this stage to find a way to verify the functionality of the laser sensor model. The basic way to do that is to build it and test it for the same parameters of the laser sensor model and then compare the results coming from both of them. In this chapter, the model circuit has been built and tested. The results for the sensor have been compared to the calculation, simulation and field trials results and show a good correspondence.

5.2 Research of Signal Amplitude

The experimental setup was developed to check if the model is adequate for the real physical functioning of a laser sensor. The purpose of the experimental research is to define the degree of conformity between the values of signal voltage and noise (measured at the output of photoreceiving device) and the values received during the model's operation with the same basic data.

Methods of experimental research consist of:

- Successive measurements of noise and signal voltage amplitude for different distances from the laser source and for different levels of background radiation
- Comparison between the output results of the experiment and the simulation results.

The experimental setup is shown in Figure 17. It consists of the following elements that simulate:

- Laser source
- Optical channel where the laser beam propagates
- Photoreceiving device with amplification stage as a sensor

The laser source is a He-Ne-laser with a power of 1 mW with an optical mechanical chopper that models the radiated pulse. The optical channel contains a set of attenuator filters in order to simulate the distance changes between laser source and sensor. Also, it has optical

elements in order to imitate atmospheric attenuation and far distances. Radiation from the background simulator is put into the optical channel through a beamsplitter cube. The photoreceiving device is made on the basis of the PIN-photodiode with one-cascade amplification stage, see Appendix D.

5.2.1 Basic Methodology

The working steps for the experimental research setup are:

1. Develop the mathematical model of the experimental setup. It should describe adequately the space transformation and attenuation of the laser beam in the optical channel.

2. Define the dependence between the transmission values of optical attenuator filters and values of the corresponding distances from laser source to photoreceiving device.
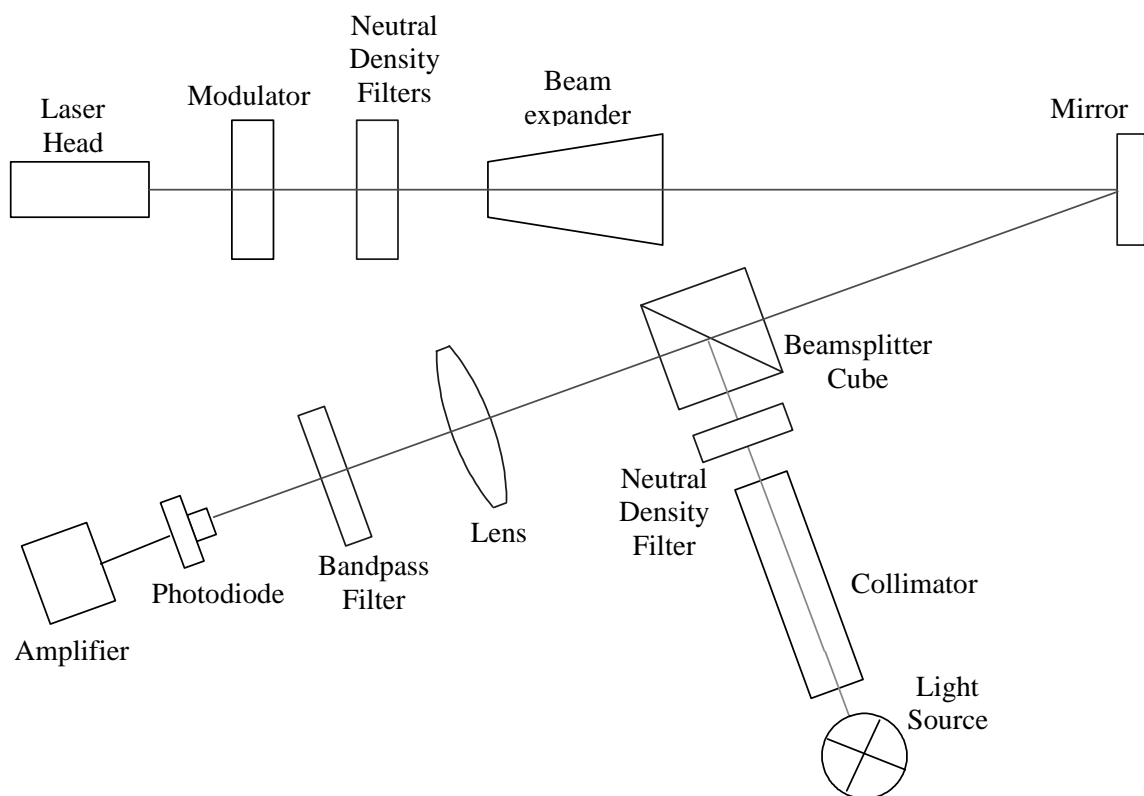
Figure 17 The Scheme of LWS Experimental Setup

Figures 18 & 19 show pictures of the lab experiment set up. More pictures can be found in Appendix J.
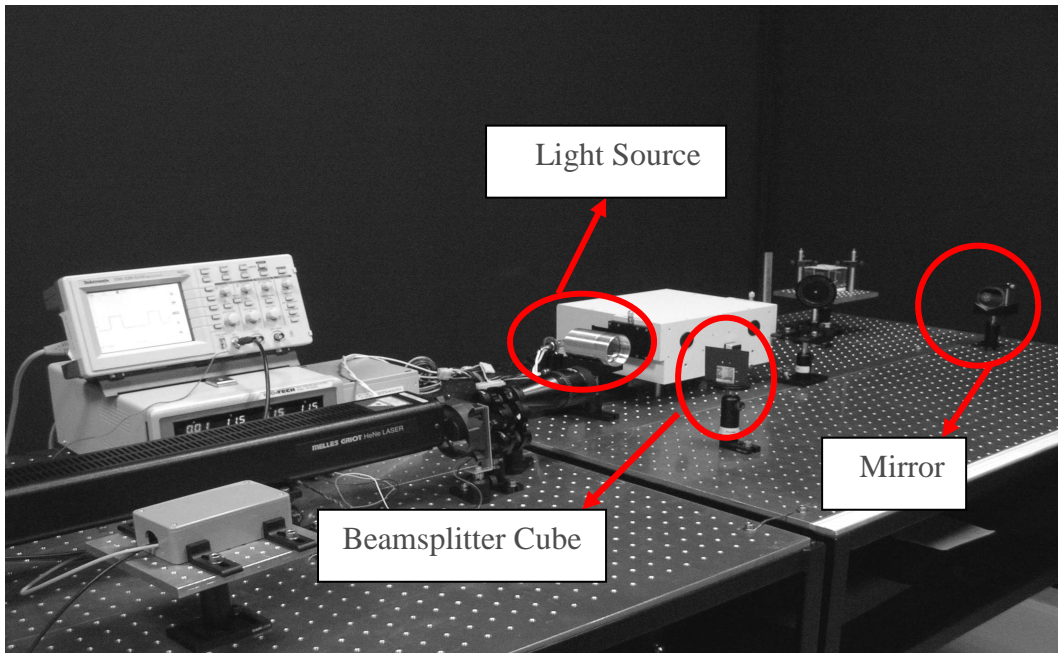
Figure 18 Lab experiment set up picture
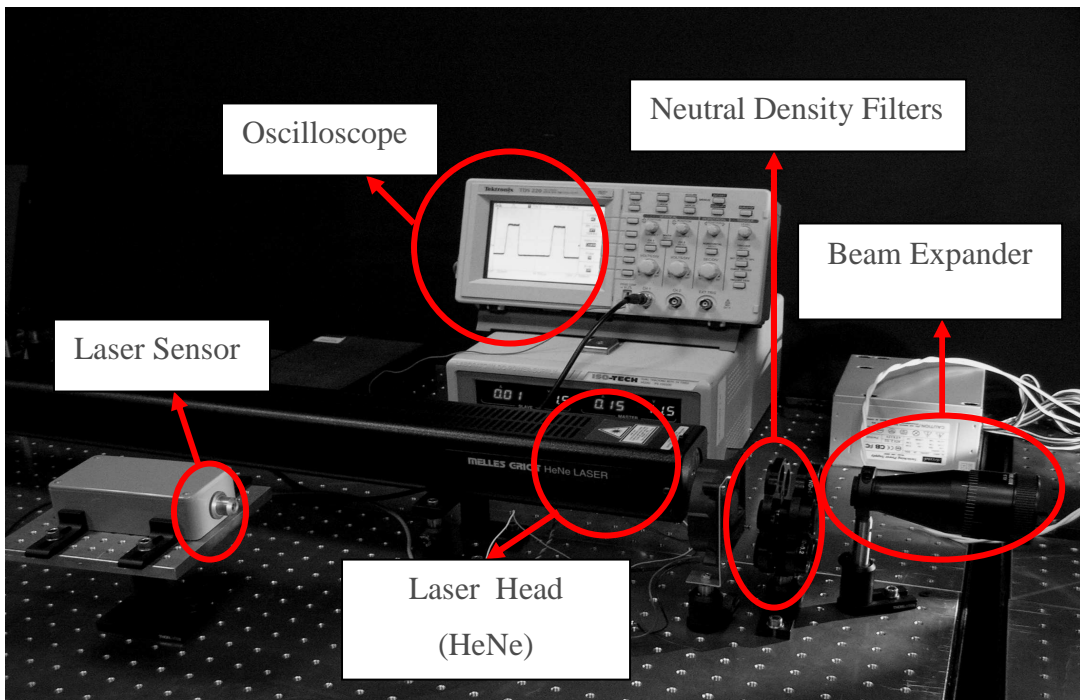
Figure 19 Lab experiment set up picture

Characteristics of elements in experimental setup are given in Table 6.

Laser head	He-Ne Laser
	1 mW
Modulator	Pulse length - 750 μs
	Pulse time - 2700 μs
Neutral density filters for signal	Variable
Beam expander	Beam divergence on output - 4.3 mrad
BE-10X	Output beam diameter - 15 mm
	Expansion - 10x
Mirror	D=50.8 mm
PF20-03-G01	Reflectivity > 0.9
High intensity light source OSL 1	High output 150W lamp
Collimator OS6	Light divergence on output - 33 mrad
	Diameter output lens - 50.8 mm
Neutral density filters for background noise	Variable
Beamsplitter cube	Size - 25.4 mm
BS014	Split ratio - 50:50
Lens	Diameter of aperture - 8 mm
	Focal length - 40 mm
Bandpass filter	Transmission on 633 nm - 0.6
Ealing Corp. # 35-3904	Bandwidth FWHM - 10 nm
PIN Photodiode	Sensitivity on 633 nm - 0.4 A/W
OSD1-5T	
Amplifier	Feedback resistance - 10^6 Ohm

Table 6 Characteristics of experimental setup's elements

5.3 Mathematical Model of Experimental Setup

A mathematical model of the experimental setup is developed for correct comparison of results. It takes into consideration the influence of all its elements. The mathematical model is described by the following expression:

$$U_{amp} = P_{las}\, k_{nf}\, k_{exp}\, \frac{a^2}{\frac{\pi(\theta R_{cub} + b)^2}{4}}\, k_{cub}\, \frac{\frac{\pi D^2}{4}}{(a + \theta R_{opt})^2}\, k_{bf}\, \varepsilon_\lambda\, R_F \qquad (5.1)$$

where,

U_{amp} - amplitude signal voltage

$P_{las} = 1$ mW - continuous output power of laser source

k_{nf} - transmission factor of neutral density filters (variable)

$k_{exp} = 0.9$ - transmission factor of beam expander

$a = 25.4$ mm - dimension of beamsplitter cube edge

$\theta = 4.3$ mrad - beam divergence in beam expander output

$R_{cub} = 191$ cm - distance from the beam expander to the beamsplitter cube

$b = 15$ mm - diameter of laser beam in beam expander output

$k_{cub} = 0.5$ - transmission factor of beamsplitter cube

$D = 8$ mm - diameter of receiving lens

$R_{opt} = 70$ cm - distance from the beamsplitter cube to the receiving lens

$k_{bf} = 0.6$ - transmission factor of bandpass filter

$\varepsilon_\lambda = 0.4$ A/W - spectral sensitivity of photodiode

$R_F = 10^6$ Ohm - feedback resistance

Amplitude signal voltage at the amplifier's output is measured with the help of the given mathematical model. It is measured against the transmission of optical neutral density filters (Figure 21). Results of calculation of $U_{amp} = f(k_{nf})$, are shown in Figure 20.
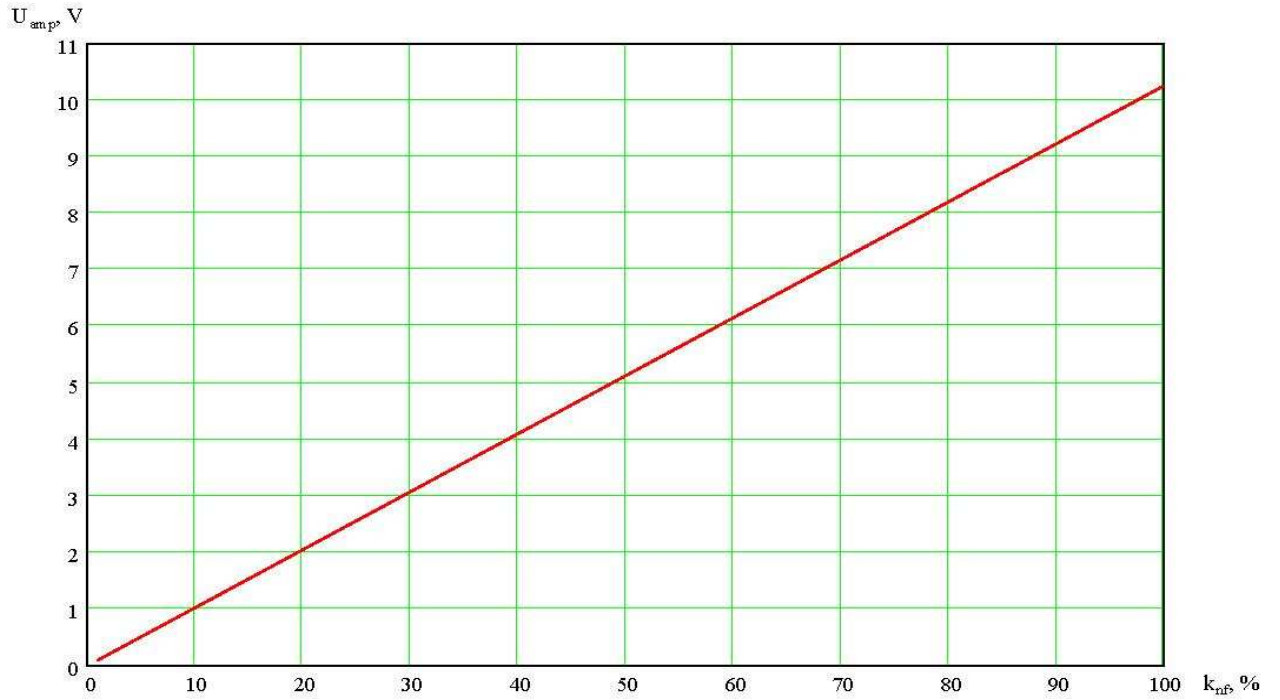
Figure 20 Amplifier output against transmission of optical filters

Dependence of the signal amplitude voltage on distance is described by the following expression, where the effect of the atmosphere is added:

$$U_{amp}(R) = P_{las} \, k_{exp} \, \frac{a^2}{\frac{\pi(\theta R_{cub} + b)^2}{4}} \, k_{cub} \, T_a \, \frac{\frac{\pi D^2}{4}}{(a + \theta R)^2} \, k_{bf} \, \varepsilon_\lambda \, R_F \tag{5.2}$$

where,

$T_a = 1$ is transmission factor of the atmosphere, R represents distance to the laser source. Results of calculation of $U_{amp} = f(R)$ are shown in Figure 21.

Figure 21 Amplifier output against range

5.3.1 Calibration Curve Where Transmission of Attenuator Filters Vs. Range

Connection between the transmissions of the optical neutral density filters and the distance to the laser source is evaluated according to the following formula:

$$k_{nf}(R) = \frac{P_{in}(R)}{P_{in.exp}} \quad , \tag{5.3}$$

where $P_{in}(R)$ is power at the input of the optical system photodetector and is given by:

$$P_{in}(R) = P_{las}\, k_{exp}\, \frac{a^2}{\frac{\pi(\theta R_{cub} + b)^2}{4}}\, k_{cub}\, T_a\, \frac{\frac{\pi D^2}{4}}{(a + \theta R)^2}\, k_{bf} \tag{5.4}$$

$P_{in.exp}$ is power at the input of the optical system photodetector of the experimental setup for some distance and can be written as:

79

$$P_{in.exp} = P_{las} \, k_{exp} \, \frac{a^2}{\frac{\pi(\theta R_{cub} + b)^2}{4}} \, k_{cub} \, T_a \, \frac{\frac{\pi D^2}{4}}{(a + \theta \cdot 0.7)^2} \, k_{bf} = 2.56 \; x10^{-5} \, W \qquad (5.5)$$

Calculation results of $k_{nf} = f(R)$ are given in Figure 22. It is the calibration curve. It permits to choose the transmission of attenuator filter correspond to the range of the laser threat source.

Figure 22 Calibration curve where transmission of attenuator filters vs. range

The values of optical neutral filters and their corresponding distances in the experimental setup are given in the Table 7. It is clear that the maximum transmission can be found at a distance of 0.79 m of the laser source.

k_{nf} (transmission), %	R, m
97.4	0.79
82.5	1.36
65	2.29
50.7	3.37
24.4	7.47
20.7	8.62
16	10.61
10	14.98
6.3	20.42
4.5	25.24
2.4	36.74
1.03	59.19

Table 7 Values of the optical neutral filters and their corresponding distances in the experimental setup

The value of the output power is estimated according to the formula:

$$P_{out} = P_{las} k_{exp} \frac{a^2}{\frac{\pi(\theta R_{cub} + b)^2}{4}} k_{cub} = 0.686 \; x10^{-3} \, \text{W} \tag{5.6}$$

5.4 Experimental Results

Results for different values of transmission of optical neutral filters are given in Table 8. They are experimentally measured for the signal voltage amplitude at the amplifier's output without the presence of the solar background radiation imitator.

k_{nf}(transmission), %	U_{amp}, V
97.4	9.6
82.5	8.1
65	6.4
50.7	5
24.4	2.4
20.7	2
16	1.5
10	1.1
6.3	0.6
4.5	0.44
2.4	0.23
1.03	0.11

Table 8 Experimental results, transmission versus the amplifier output

The higher the transmission (low attenuation), the bigger is the output voltage at the amplifier output port. These experimental results confirm the results we got from the model simulation.

5.5 Research of The Model

The following stage is carried out using the laser sensor model. Basic or input data are given in the Table 9. They are made to evaluate the laser sensor model with the same input data used to create the experiment.

Generator	
Pulse period, s	$2700 \cdot 10^{-6}$
Pulse width, %	27.778
Pulse peak power, W	$0.686 \cdot 10^{-3}$
Atmosphere and optical system	
Diameter input lens, mm	8
Diameter output lens, mm	25.4
Divergence, mrad	4.3
Bandpass filter transmission	0.6
Noise	
Optical system loss factor	0.5
PD crystal diameter, mm	1
Spectral responsivity of PD, A/W	0.4
Input lens diameter, mm	8
Focal length, mm	40
Boltzmann constant, $J \cdot K^{-1}$	$1.38 \cdot 10^{-23}$
Temperature, K	300
Bandwidth, Hz	$20 \cdot 10^{3}$
Load Resistance, Ohm	10^{6}
Electron charge, Cl	$1.6 \cdot 10^{-19}$
Dark current, A	$0.5 \cdot 10^{-9}$
Photodiode	
Spectral responsivity of PD, A/W	0.4
Gain	1
Amplifier	
Feedback resistance, Ohm	10^{6}
Bandwidth, Hz	$10.6 \cdot 10^{3}$
Gain	1
Comparator	
Spectral resposivity of PD, A/W	0.4
Feedback resistance, Ohm	10^{6}
Signal/Noise	5
Bandpass filter	
Transmission bandwidth on 0.5, μm	0.628-0.638

Table 9 Experimental input data to LWS model

5.6 Model Results (Without Background Light Source)

Simulation results of LWS model of signals amplitudes (when there is no source of background radiation) are given in the Table 10.

T, %	R, m	Received pulse, μW	PD output signal, μA	Amplifier output signal, mV
97.4	0.79	24.9	9.98	9980
82.5	1.36	21.2	8.47	8470
65	2.29	16.6	6.66	6650
50.7	3.37	13	5.2	5200
24.4	7.47	6.25	2.5	2500
20.7	8.62	5.3	2.12	2120
16	10.61	4.1	1.64	1640
10	14.98	2.56	1.02	1020
6.3	20.42	1.61	0.64	645
4.5	25.24	1.15	0.46	461
2.4	36.74	0.61	0.24	245
1.03	59.19	0.26	0.1	105

Table 10 Simulation results of model signal amplitudes (when there is no source of background radiation)

Evaluations of signal and noise for the distance of 36.74 m, which corresponds to transmission of attenuator filters 2.4%, are given as an example (Appendix F).

General results of experimental measurements, calculations and evaluation of signal amplitude in the model are given at Figure 23.
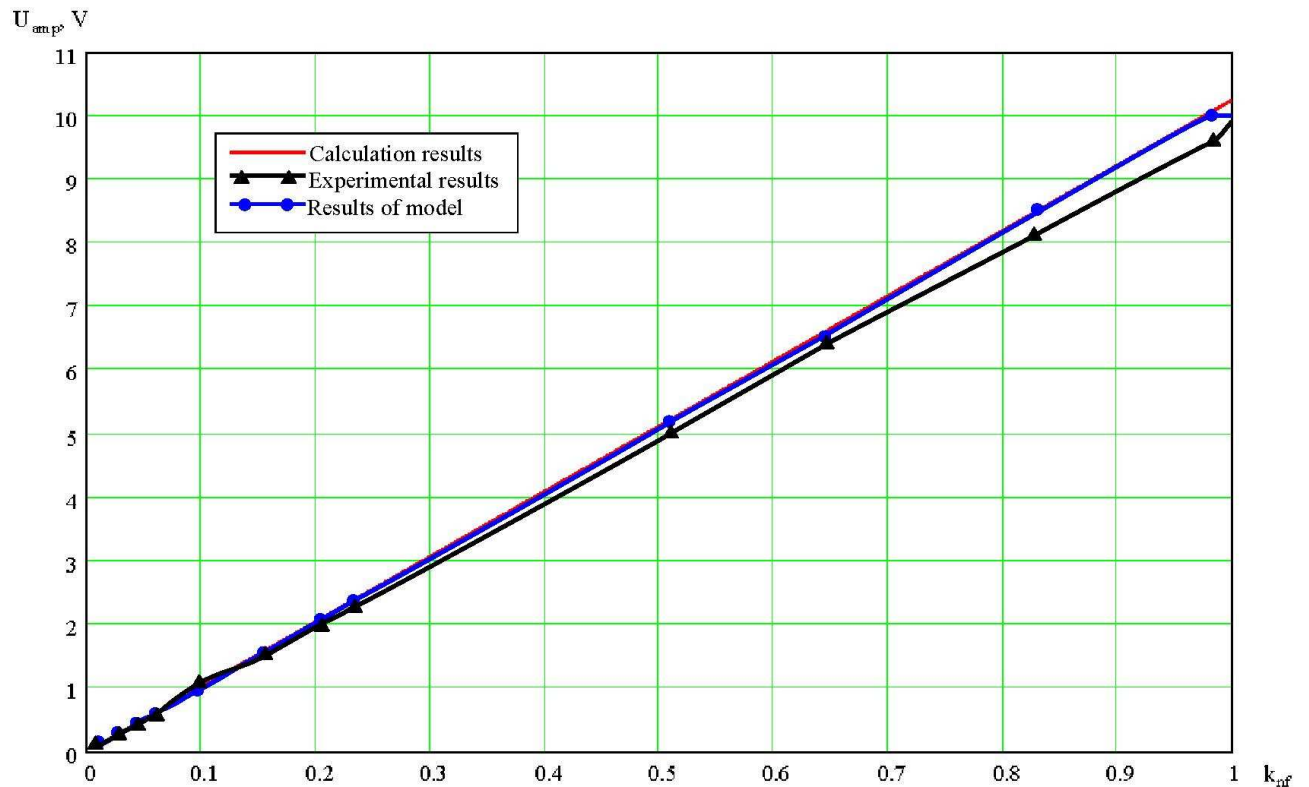
Figure 23 Calculated, experimental and model results without light source

The output results reveal good correspondence between the developed model and the functioning of the sensor's experimental prototype. Reasonable differences between experimental and model results can be explained by nonlinear operation mode of amplifier at high signal amplitudes.

5.7 Research of Noise (Adding Light Source)

The main objectives of experimental analysis of noise are:
- To make a detailed estimation of the effects of noise voltage constituents on sensor's characteristics
- To define the degree of conformity between experimental and model results

Noise components of a laser sensor with PIN-photodiode as a detector are [1]:
- Shot noise of dark current, which is caused by thermal generation of free current carriers, when there is no optical signal.
- Shot noise of the signal, which is caused by statistical fluctuations of optical signal (photon noise).

85

- Shot noise of the background radiation, which is caused by statistical fluctuations of background radiation.
- Thermal noise of electronic channel, which is caused by the excitation of thermal current carriers.

Calculated values of these noise constituents in the experimental setup showed that when the amplifier had a narrow band (Δf =20 kHz), the amplitudes of noise voltage have rather small values (Appendix G). This makes it difficult to register on the oscilloscope.

When the background radiation is rather powerful, the noise voltage has a constant component. Fluctuations, which have a Gaussian distribution, are imposed on this component. If there is a noise voltage component, the dynamic range of photoreceiving devices decreases, and sometimes (when the brightness of background radiation is high) the signal even disappears because of saturation of the amplifier. This effect is used to analyze the influence of external background radiation on the output parameters of photoreceiving device. The saturation effect was simulated by adding the amplitude limiter to the model. The voltage of the limiter was 10 V.

Constant component of noise voltage is calculated with the help of the following formula:

$$U_c = \overline{P}_b \varepsilon_\lambda R_F \tag{5.7}$$

where,

U_c – noise voltage of constant component

P_b - power of background

ε_λ - spectral sensitivity of PD

R_F - feedback resistance

$$\overline{P}_b = B\Delta\lambda_{bf} S_{os} \omega k_{opt} T_{nf} \tag{5.8}$$

where,

B - brightness of background(brightness of light source)

$\Delta\lambda_{bf}$ - optical filter bandpass

$S_D = \dfrac{\pi D^2}{4}$ - area of receiving objective

$\omega = \dfrac{\pi l^2}{4 f^2}$ - sensor field of view $\hspace{3cm}$ (5.9)

l - diameter of sensitive area of PD

f - focal length of receiving objective

k_{opt} - transmission factor of receiving optical system

T_{nf} - transmission factor of neutral filter

A high intensity light source with an output power of 150W (T=320K) is used as imitator of background radiation (specification of light source in Appendix F). The radiation of the source is put through the transparent cube (beamsplitter) into the field of photoreceiving device's vision. The power of the background (equation 5-8) was regulated by changes of transmission of attenuation filters and by measurements of size of photoreceiving device's field of view (equation 5-9). This size depends on the diameter of the photodiode active region and the focal length of receiving lens.

Fundamental experimental research included measurements of noise voltage component and signal amplitude for different powers of background radiation and different fields of view of the receiving optical system. The distance from the photoreceiving device to transparent cube (beamsplitter) is chosen in such a way, that the linear dimensions of optical system's field of view don't exceed the linear dimensions of the cube.

The following devices are used during experiments: two photodiodes with diameters of their active region 1mm and 5mm; two receiving lens with focal lengths 40mm and 100mm.

The following calculation results of the model are given in the Table 11:

1) Results of noise voltage constant component for different values of photoreceiving device's field of vision.

2) Results for different transmissions of attenuation filters.

T_{nf}, %	U_c, V (d=1mm, f=100mm)	U_c, V (d=1mm, f=40mm)	U_c, V (d=5mm, f=100mm)	U_c, V (d=5mm, f=40mm)
100	0.5	3.125	saturation	saturation
82.5	0.413	2.578	saturation	saturation
65	0.325	2.031	8.125	saturation
50.7	0.254	1.584	6.338	saturation
24.4	0.122	0.763	3.05	saturation
10	0.05	0.313	1.25	7.813
4.5	0.023	0.141	0.563	3.516
1.03	0.005	0.032	0.129	0.805

Table 11 Model (calculations) results of dependence of constant component noise voltage from changes of background brightness (T_{nf}) at various fields of view of receiving optical system (d, f)

According to this table there is a saturation effect of the photodiode with diameter of active region 5 mm (value of noise voltage constant component exceeds 10 volts). Also, for the receiving optical system with focal length 40 mm there is a saturation effect at a larger range of background powers when the illumination from the light source is high.

Table 12 presents results for signal amplitudes with different values of photoreceiving device's field of view. It also lists results for different powers of residual radiation.

T_{nf}, %	U_{amp}, V (d=1mm, f=100mm)	U_{amp}, V (d=1mm, f=40mm)	U_{amp}, V (d=5mm, f=100mm)	U_{amp}, V (d=5mm, f=40mm)
100	9.5	6.875	0	0
82.5	9.587	7.422	0	0
65	9.675	7.969	1.875	0
50.7	9.746	8.416	3.662	0
24.4	9.878	9.237	6.95	0
10	9.95	9.687	8.75	2.187
4.5	9.977	9.859	9.437	6.484
1.03	9.995	9.968	9.871	9.195

Table 12 Results of calculations of dependence of a signal amplitude voltage from changes of background brightness (T_{nf}) at various fields of view of receiving optical system (d, f)

These results show that the signal amplitude decreases when the field of view decrease (level of accepted field decreases) because of the amplifier's saturation effect. Also, signal disappears in a large range of background powers when the active region of photodiode is 5mm.

Experimental results in Table 13 represent the dependence between noise voltage constant component and changes of background powers and optical system's field of view.

T_{nf}, %	U_c, V (d=1mm, f=100mm)	U_c, V (d=1mm, f=40mm)	U_c, V (d=5mm, f=100mm)	U_c, V (d=5mm, f=40mm)
100	0.48	3	10	10
82.5	0.4	2.5	10	10
65	0.3	2	8	10
50.7	0.24	1.5	6.2	10
24.4	0.12	0.7	3	10
10	0.048	0.29	1.1	7.5
4.5	0.022	0.14	0.5	3.3
1.03	0.005	0.03	0.1	0.7

Table 13 Experimental results of dependence of noise voltage constant component from change of background brightness (T_{nf}) at various fields of view of receiving optical system (d, f)

From the table, we can observe that in some range of background powers the values of noise voltage constant component reach 10 volts when the dimensions of photodiode active region are 5 mm. That corresponds to the maximum value of amplifier's saturation voltage.

Table 14 presents the research results of dependence between signal amplitude and changes of background powers and receiving optical system's field of view.

T_{nf}, %	U_{amp}, V (d=1mm, f=100mm)	U_{amp}, V (d=1mm, f=40mm)	U_{amp}, V (d=5mm, f=100mm)	U_{amp}, V (d=5mm, f=40mm)
100	9.5	7	0	0
82.5	9.6	7.5	0	0
65	9.7	8	2	0
50.7	9.75	8.4	3.8	0
24.4	9.8	9.3	7	0
10	9.8	9.7	8.9	2.5
4.5	9.8	9.8	9.5	6.7
1.03	9.8	9.8	9.8	9.3

Table 14 Experimental results of dependence of signal amplitude from change of background brightness (T_{nf}) at various fields of view of receiving optical system (d, f)

Analysis of results shows that there is no signal at the output when there are high background power values and d=5. That is because of the amplifier's saturation effect.

Figures 24 to 27 show the experimental results of calculations and model simulations. They were made for noise voltage constant component when there were different values of diameter of photodiode active region and focal lengths of receiving optical system.

Results for using a photodiode with a sensitive area diameter of d=1mm and focal length f=100mm are shown in Figure 24. Experimental, simulation, and calculations results curves are given a clear picture that our hardware confirmed the results we got by the laser sensor model simulation results. The small differences are due to the amplifier nonlinearity effects.
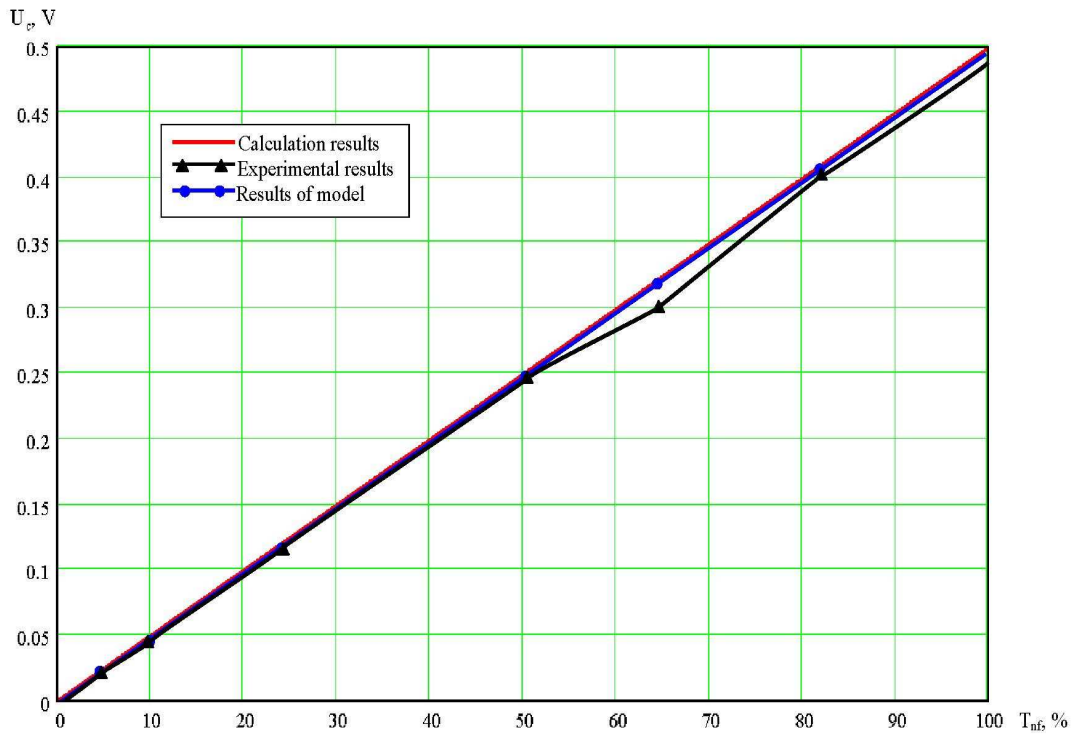
Figure 24 Experimental, calculations and model results for d=1mm f=100mm

Results for d=1mm f=40mm on Figure 25.
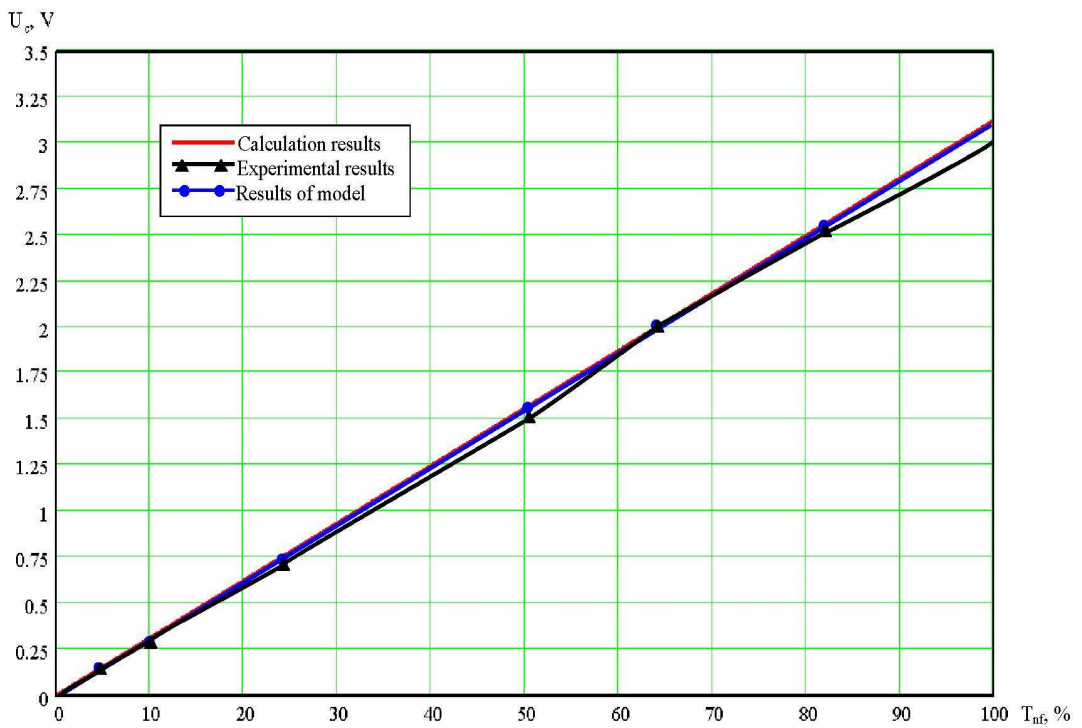
Figure 25 Experimental, calculations and model results for d=1mm f=40mm

In Figures 26 and 27, we are using a photodiode with a sensitive area of 5 mm and here we notice the saturation effect of the amplifier we are using in our hardware.
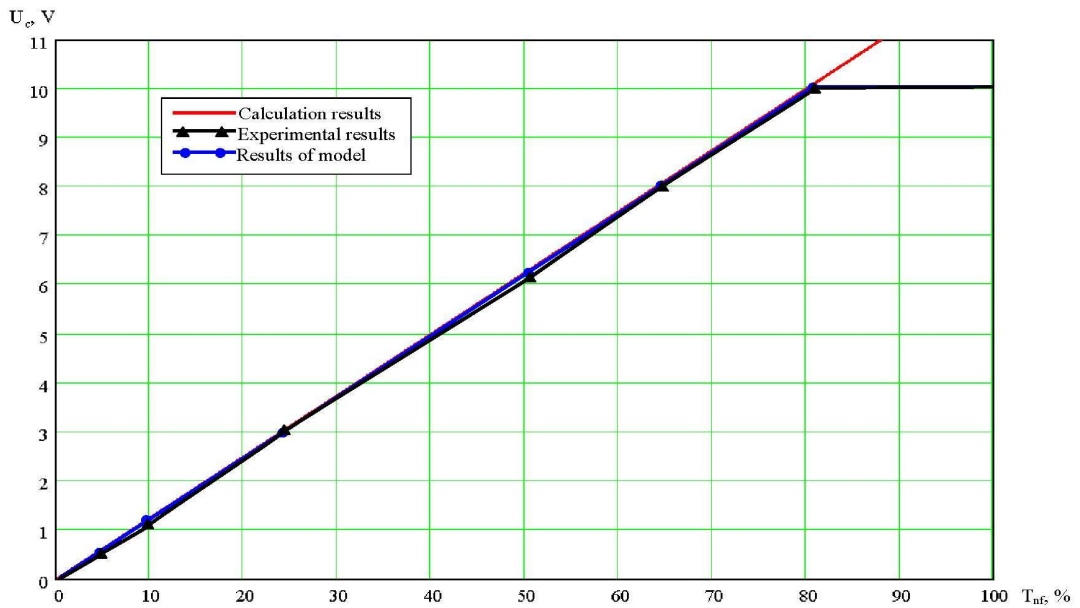
Figure 26 Experimental, calculations and model results for d=5mm f=100mm

By using the same size of sensitive area but decreasing the focal length to 40 mm we notice bigger differences between the model and experimental results and this is due to less noise coming into the input of our hardware. Results for d=5mm f=40mm on Figure 27.
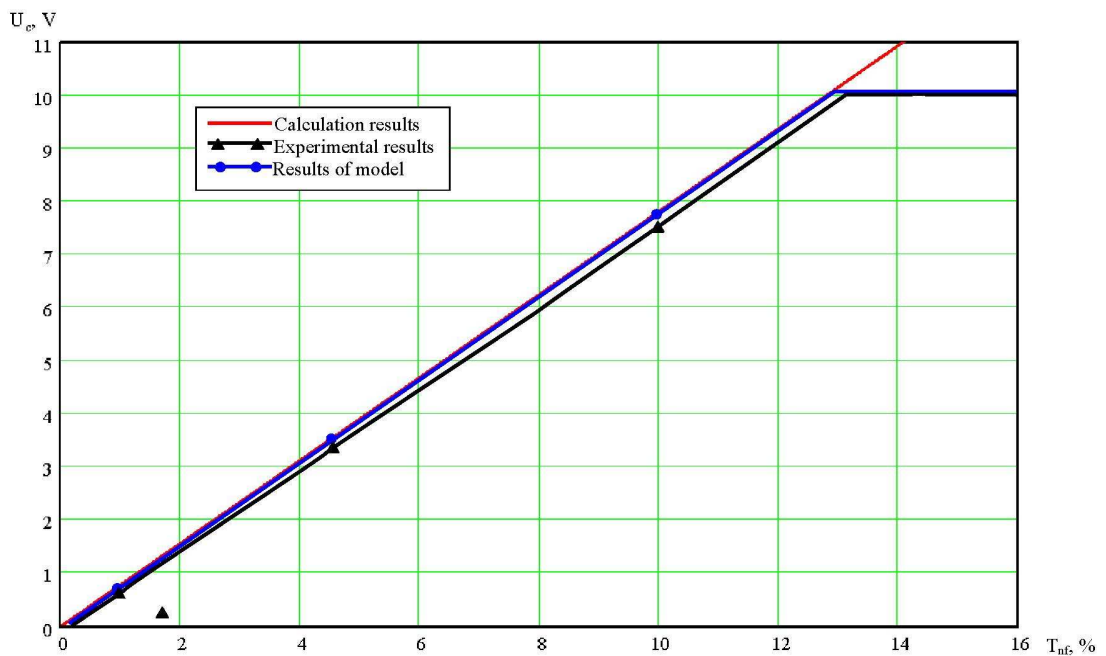
Figure 27 Experimental, calculations and model results for d=5mm f=40mm

Analysis of diagrams shows a good correspondence between experimental, calculations and model results. Figure 28 shows experimental and model results for signal amplitude for different values and dimensions of photodiode active region and focal distances of receiving optical system.
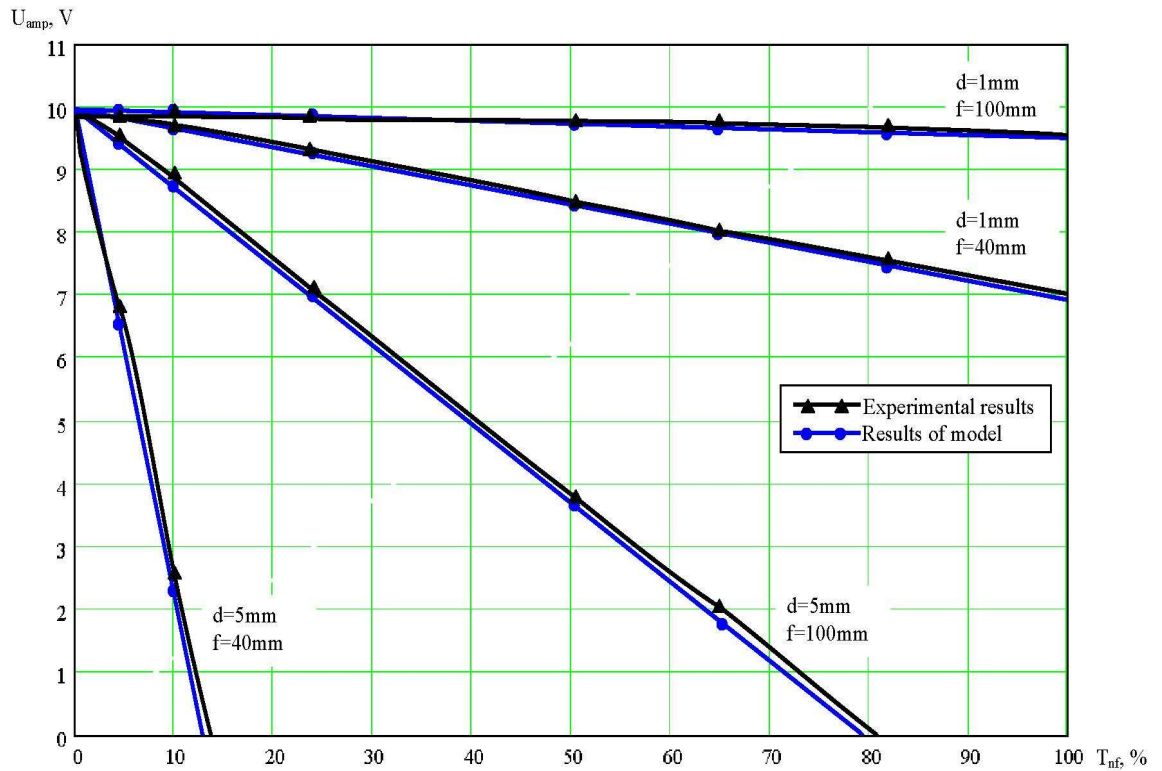
Figure 28 Comparison between experimental and model results at different photodiode sensitive areas & different focal lengths

Analysis of results showed that signal amplitude decreased with an increase in diameter of photodiode active region. It also decreased with decrease in focal length of receiving optical lens. With the increase in the diameter of the photodiode sensitive area (5 mm) and reduction of the focal length of (40 mm) the size of a field of view grows. Therefore, in order to decrease the influence of the background on the output parameters of the photoreceiving device, the receiving optical systems should be chosen in such a way, that they would have the smallest useable field of view which still enables the realization of the device's other required performance characteristics.

5.8 Field Trials

As stated in Chapter 1, some field trials have been carried out in the desert of UAE. Several well-known companies have been competing to win a huge contract for laser warning systems for the UAE army. For confidential reasons, it is not possible to reveal the names of these companies so we will use alphabetic letters to address them.

As was shown in a Chapter 2, the protection systems of tanks or other armoured fighting vehicles against attacks by anti-tank missiles with laser guidance systems consists of:

- Laser warning system
- Control unit
- Counter-measures

The studies of laser warning systems and work conducted showed that their efficiency essentially depends both on the parameters of the laser sensors and on external conditions (weather condition, degree of atmospheric turbulence, temperature, humidity, etc.).

The UAE land forces commander decided to test several laser warning systems produced by four well-known companies in the conditions of the UAE and this is the procedure that is followed to accept new systems in the land forces. They need to be sure that these systems will perform as specified in the severe weather conditions of the desert. These systems were tested in the period of 2001-2003 in hot summer time which is most characteristic of the weathers conditions of UAE.

The field trials were conducted as a verification of the laser warning systems and their maximal detection range of the laser sources in the hot climatic desert conditions. For this, four laser warning receivers by different companies-producers with similar parameters were chosen and as sources different types of laser rangefinders were used. Laser warning systems and rangefinders (lasers sources) were placed on different fighting vehicles. The distance (maximal detection range) between them was constantly measured during the field trials.

The method of the field trials constructed of measuring the maximal range, at which a laser warning receiver detected a signal from a laser rangefinder, laser designator and laser beam-riding guidance systems. Measurements were conducted for all types of weather conditions of the UAE.. Weather conditions were broken into 5 categories: Good; Typical-1; Typical-2; Bad-1; Bad-2. The characteristics of each of these categories in detail were described in Chapter 4. The field trials were conducted on a military ground for all types of weathers conditions. For each trial, maximal range was registered, at which the laser warning receivers could detect laser source yet in the set spectral range. For all four types of laser warning systems the trials were conducted on a wavelength source of 1.06 µm. The maximal field detection range of the four laser warning system companies (A, B, C, D) are given in Table 15.

Companies	Range, m				
	Good	Typ-1	Typ-2	Bad-1	Bad-2
A	4500	4100	3300	2100	1950
B	4300	4000	3200	2000	1900
C	3900	3800	2950	1950	1890
D	3800	3500	2500	1830	1700

Table 15 Field trials results

The analysis of the results showed that weather conditions substantially influenced the performance of the laser warning systems. Weather conditions determine the degree of transmission of the laser radiation in the atmosphere at the explored wavelength. As the weather conditions change from Good to Bad-2, the atmospheric transmission coefficient at a wavelength of 1.06 µm changes from 0.9 to 0.01 [LOWTRAN]. The substantial weakening of laser radiation can be explained by its distribution in the atmosphere and, as a result, reduced detection range of the laser sources.

It is obvious from Table 15 that company A has the best indexes for detection range of the lasers sources. In the same weather conditions and laser source power, the advantage of company A system over other systems, obviously, conditioned by the best sensitivity of laser sensors and electronic components. The results of field trials carried out in summertime (May -

August) in conditions of United Arab Emirates desert by various companies - manufacturers (A, B, C, D) during 2001-2003.

5.9 Comparison (Calculated-Simulation-Experimental-Field Trials)

The main purpose of this chapter is to verify the adequacy of the experimental results, results of the laser sensor model, and compare them with the results of the field trials of real laser warning systems. Building an experimental setting included all basic elements of the typical laser sensor and atmospheric channel with a light source as an imitator of the solar background. For the process, calibration curves and tables have been developed to imitate the change of range between the laser sensor and source. In addition, connecting the values of range with the characteristics of neutral optical filters that affect the optical signal on its way to the sensor was considered in the experimental setup.

The developed model of the laser sensor described all the mathematical transformations of the optical signal from a laser source to the receiving device. Thus the parameters of the model's elements corresponded to the parameters of the experimental elements. Amplitudes of output signals of the recording device of the experimental setup were compared to amplitudes of outputs signals on the oscilloscope of the laser sensor model.

For the imitation of the external background, a powerful incandescent lamp was used with a controllable brightness. The results of the output signal's amplitudes measurements showed that with the increase of the background brightness and sensor field of view the noise level increases in the receiving channel. This results in worsening of the sensor's sensitivity and, accordingly, reduces the detection distance of the laser source.

The analysis of the received results (Figures 23-28) showed the good coincidence of information of the experimental setup and model. It goes to show that the developed model of a laser sensor adequately describes the physical processes that is going on in the elements of the experimental setting.

The next step was to compare the model's results and field trials. In this case, the parameters of the model elements must correspond to typical characteristics of real laser

warning receivers. Such parameters of model elements are described in Chapter 4. The results of the model's testing for five types of weathers conditions were given in Chapter 4. The comparative analysis of results for the model and field trials showed that in both cases the tendency of dependence of detection range on weather conditions is clear in both of them. With worsening of the weather conditions the detection ranges decline. However the results of the laser sensor model are better than results of the field trials. In Good weather conditions, the maximal detection range in the model is 5500 m for a wavelength of 1.06 µm, and in the field trials it is only 4500 m by company A. The differences are due to the following reasons:

- Nonoptimal choice of the photodetector type with maximal sensitivity at a wavelength 1.06 µm;
- Nonoptimal choice of optical filter spectral band;
- Low efficiency of temperature-compensated circuits in the hot climate conditions of UAE;
- Nonoptimal choice of bandwidth of the receiving channel which results in an increasing noise level;
- The increase of field of view results in increasing of level of the received background radiation in a bright sunny day;
- Decreasing of dynamic range of the receiving channel in conditions of large background radiation;
- Decreasing of multiplication factor in photodetectors with the internal amplification because of temperature influence.

It is clear that there is the possibility to increasing the efficiency of a laser warning systems by realization of the following measures:

- Choice of modern small level noise element base
- Optimization of laser sensor parameters
- Increase of receiving channel sensitivity
- Reduction of noise level
- Use of thermo-compensation chains

The trends experienced in the field trials are faithfully mirrored by the model and given sufficient detail about the value of the parameters in the real systems then surprising accuracy in model prediction can result.

5.10   Conclusions

The simulated laser sensor was built as hardware and tested for various cases. Many parameters have been evaluated to see if we can match the output coming from laser sensor model simulation. The experimental work is divided into two parts, first without a light source and second when adding the light source to see the effect of solar background on the output results just like in the simulation.

First, a mathematical model of the experimental setup was introduced and discussed. It was important to define the dependence between value of transmission of optical attenuator filters, used to carry out the test, and values of the corresponding distances from the laser source to the photoreceiving device. Then, and after creating the calibration curve, we read the output for various cases without the light source and run the simulation model for the same setup. The results show that there are small differences between the two outputs and that can be explained as a result of the nonlinear operation of the amplifier.

The same process has been repeated but with the light source to imitate the solar background. Comparison of experimental results with the model shows rather good correspondence. Now it is time to build the seeker model.

5.11   References

[1]Introduction To Infrared and Electro-Optical Systems. Ronald G. Driggers, Paul Cox, and Timothy Edwards. Page 145.

CHAPTER 6

Development of Requirements for Laser Sensor Parameters

6.1 Introduction

Building the laser sensor model, test it and verifying its performance was a step in order to reach the following point. The model is a tool to study, investigate, and develop new systems to overcome the problems which threaten their existence in some parts of the world with a very bad weather conditions.

Improving the performance of the laser sensor model is an important task in this study. In this chapter, we will go deeper in understanding each parameter of the sensor model in order to find the optimum values that give us the best performance. Moreover, as mentioned in conclusion of Chapter 3, this chapter will cover the atmospheric attenuation and how it affects the sensitivity of the laser sensor model.

6.2 Estimation of Sensor Threshold Sensitivity

6.2.1 Noise Current Components

The threshold sensitivity of a photoreceiving device is characterized by the value of minimally registered power (energy) of laser radiation as an input to the photodetector sensitive area. The value of minimally registered radiation power is defined by the noise level of the photoreceiving device and evaluated by the following ratio [1]:

$$P_{thr} = \frac{\sqrt{\bar{i}_n^2}}{\varepsilon_\lambda}$$

(6.1)

where, P_{thr} is the threshold (minimal) power of laser radiation at the input of the photodetector, leading a signal, equivalent to a background level, $\bar{i}_n^2$ represents the dispersion of noise current and ε_λ is the spectral sensitivity of the photodetector [2].

The noise of a photodetector device can be caused by both internal, and external sources. The external noise sources is refer to background radiation. Internal noise sources refer to dark current of the photodetector, fluctuation of signal parameters, random process of photodetector's charge carriers and amplification of electronic path [3]. Depending on photodetector type and measurement conditions various noise sources can be dominant.

Most photodetectors use avalanche photodiodes (APD) with sensitivity some orders above PIN-photodiodes [4]. However for APD's the reference is the larger noise level called APD excess noise. The basic components of noise of the photoreceiving devices using APD's, are [5]:

- Shot noise of dark current caused by thermal generation of current carriers in the absence of an optical signal ($\bar{i}_d^2$)
- Shot noise of signal caused by statistical fluctuations of optical radiation ($\bar{i}_s^2$)
- Shot noise of background radiation caused by statistical fluctuations of background ($\bar{i}_b^2$)
- Thermal noise of the electronic path caused by thermal carrier excitation of current ($\bar{i}_{therm}^2$).

Other components of the noise current, such as flicker noise, radiating noise are smaller in value, than those above. As all components of noise are statistically independent, the total dispersion of noise current of a photodetector device will be defined by the following ratio:

$$\bar{i}_n^2 = \bar{i}_d^2 + \bar{i}_s^2 + \bar{i}_b^2 + \bar{i}_{therm}^2 \qquad (6.2)$$

The shot noise dispersion of dark current of an APD is defined by expression [6]:

100

$$\bar{i}_d^2 = 2e\Delta f \bar{I}_d M^A X \qquad (6.3)$$

where,

e - electron charge

Δf - bandwidth of receiving channel

$\bar{I}_d$ - mean of dark current

M - multiplication coefficient of APD

A – excess noise index

X - excess noise factor, dependent on M.

Dispersion of signal shot noise is defined by expression [7]:

$$\bar{i}_s^2 = 2e\Delta f M^A X \varepsilon_\lambda \bar{P}_{in} \qquad (6.4)$$

Where, $\bar{P}_{in}$ is the average power of the received optical signal and ε_λ is spectral sensitivity of the APD at the laser radiation wavelength.

The average power of the received optical signal can be found from the formula (without taking into account turbulence):

$$\bar{P}_{in} = \frac{P_{out} T_A D^2}{\theta^2 R^2} \qquad (6.5)$$

Where,

R - range to the laser source

P_{out} - power of ranging laser radiation

D - diameter of receiving objective

$T_A = \exp(-\alpha \cdot R)$ - coefficient of atmosphere transparency

α - attenuation coefficient of laser radiation at the given wavelength

θ - divergence of laser beam

Using Mathcad and expression (6.5), it is useful to explore the dependency of the power level of the received optical signal on range to the laser source at various values of receiving objective diameter. The results are presented on Figure 29. Values of the parameters which enter into the equation were chosen analogous to the sensor model.
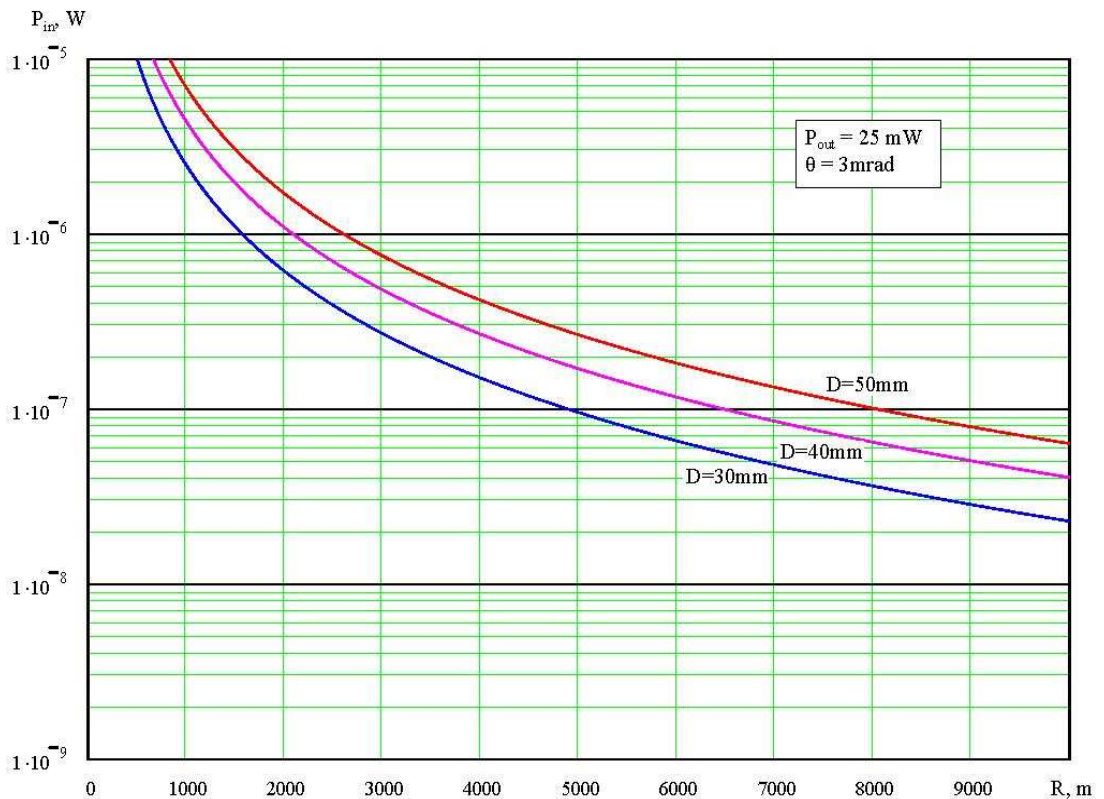
Figure 29 Dependence of received signal power on range to a laser source

Analysis of results shows that with increase of distance up to laser source, power of the received signal is essentially reduced. At R=5500m, D=3cm, P_{in}=7.88x10^{-8} W. The value of dispersion of background radiation shot noise is defined by expression [8]:

$$\bar{i_b}^2 = 2e\Delta f\overline{P_b}\varepsilon_\lambda M^A X \qquad (6.6)$$

where $\overline{P_b}$ is the average power of background radiation.

Sources of background radiation are the Sun, planets, clouds, atmosphere and surface of the Earth. Background radiation power is calculated using the following equation (equation 3.23) [9]:

102

$$\overline{P}_b = B_\lambda S_D \omega \Delta \lambda K_{opt} \qquad (6.7)$$

where B_λ is brightness of a cloudless sky. It is defined by the following expression [10]:

$$B_\lambda = \mu_0 I_0 \frac{\cos \psi}{\pi}, \qquad (6.8)$$

where, μ_0 is coefficient that characterizes the distribution of brightness of the firmament, I_0 is the flux density of sunlight on the upper bound of the atmosphere and Ψ is zenith angle of the Sun. The factor S_D in equation 6.7 represents the area of the receiving objective and is given by:

$$S_D = \frac{\pi D^2}{4}, \qquad (6.9)$$

Factor ω, in equation 6.7, represents the field of view of the photoreceiving device. It is defined by the following expression:

$$\omega = \frac{\pi l^2}{4 f^2}, \qquad (6.10)$$

Where l is the diameter of the sensing area of the photodetector and f is focal length of the receiving objective. The factor $\Delta \lambda$ and K_{opt} of equation 6.7 are the bandwidth of the interference filter and the transmission coefficient of the optical system (typically 0.4 to 0.6) respectively.

Using Mathcad, some work has been carried out studying the dependence of background radiation average power from parameters of the laser sensor. Results are presented in Figure 30.
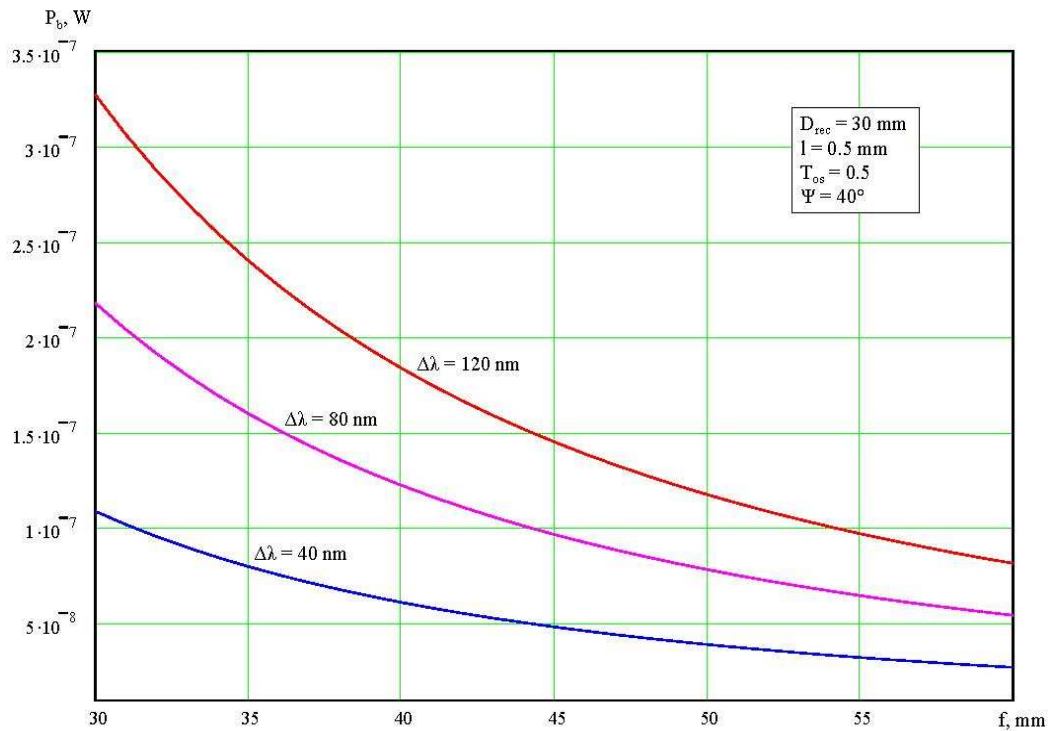
Figure 30 Dependence of background radiation average power on focal length of receiving objective

Analysis of results testifies that for effective reduction of background radiation level entering the photoreceiving device, it is necessary to reduce its field of view by increasing the focal length of the receiving objective and reduction of the dimension of the sensing area of photodetector. At the same time, it is essential to reduce the bandwidth of interference filter. For example, at a focal length f=40mm and bandwidth $\Delta\lambda$ =40nm, the background power, P_b is $6.15 \cdot 10^{-8}$ W .

The dispersion of thermal noise of the electronic path is calculated from the ratio [11]:

$$\overline{i}^{\,2}_{therm} = \frac{4\ kT\ \Delta f}{R_L}\ , \tag{6.11}$$

where, k=1.38·10[-23] J/K is Boltzmann constant, T is temperature in Kelvin, Δf represents bandwidth of the receiving path and R_L is load resistance of the photodetector.

6.2.2 Threshold sensitivity

Thus, in view of equations (6.1-6.11) we get to the final expression for the calculation of threshold sensitivity of the receiving channel of a laser sensor with an avalanche photodiode:

$$P_{thr} = \frac{\sqrt{2e\Delta f M^A X (\bar{I}_d + \bar{P}_{in}\varepsilon_\lambda + \bar{P}_b\varepsilon_\lambda) + 4kT\Delta f / R_L}}{\varepsilon_\lambda} , \qquad 6.12)$$

According to expression (6.12), the dependence of the threshold power on spectral sensitivity of the photodiode at various values of receiving channel bandwidth can be observed. Results of these observations are presented in Figure 31. The values of parameters that have been used are following:

M=100

К=2,5

A=1

$\bar{I}_d$ =0,5nA

$\bar{P}_{in}$ =7,88x10^{-8}W

$\bar{P}_b$ =6.15x10^{-8}W

T=300К

R_L=10^{5}Ohm

ε_λ=20…50A/W

Δf=33MHz, 60MHz, 120MHz.
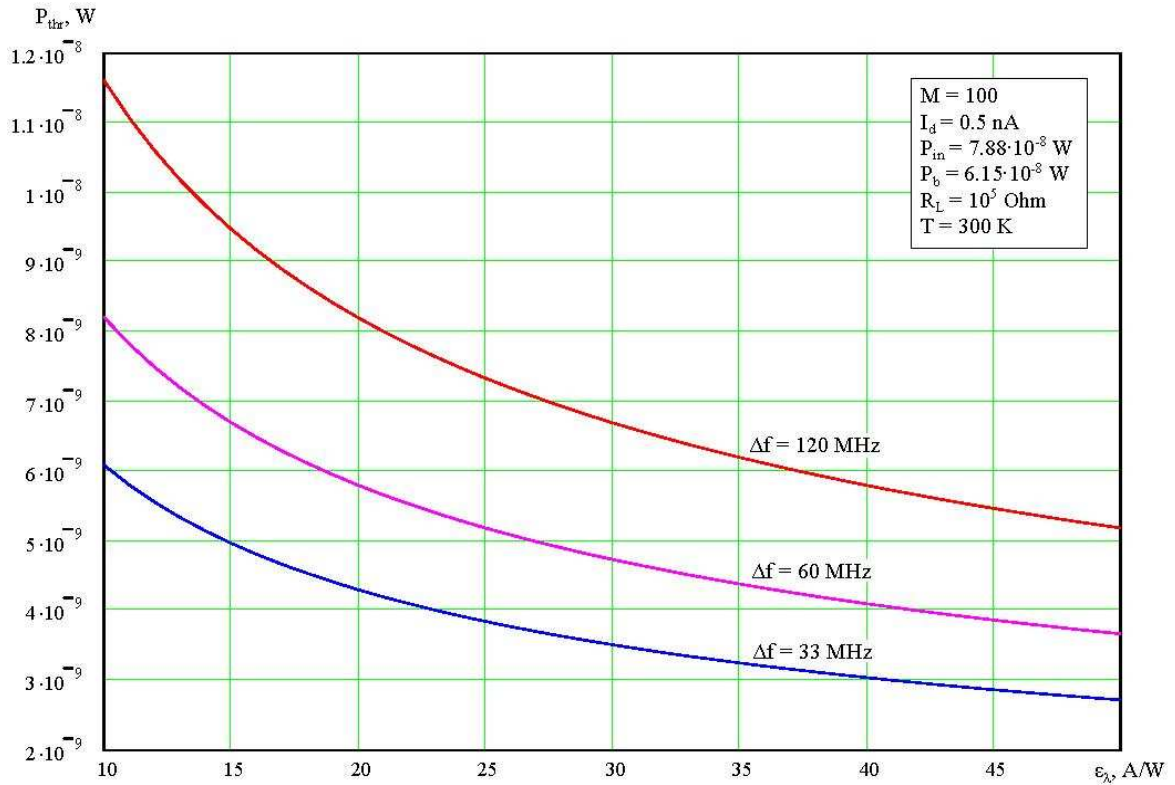
Figure 31 Dependence of threshold power on spectral sensitivity of the avalanche photodiode

Analysis of results of modeling shows that the value of threshold power can be lowered essentially by reducing of all noise components, optimization of pass bandwidth of receiving channel and the choice of the photodiode with maximal sensitivity wavelength of transmitting device of laser source. At spectral sensitivity 50 A/W and a pass bandwidth 33MHz threshold power for typical requirements makes of 2.72×10^{-9} W.

6.3   Study of the Influence of Atmosphere Turbulence on Laser Radiation

6.3.1   Atmospheric Turbulence

The effects on transmission of laser radiation through the atmosphere can be divided into two groups. The first group includes effects that cause a change of total radiation intensity. The second group includes affects that causes a change of spatial characteristics of the laser beam and redistribution of intensity in its cross section [12].

106

Among the effects relating to first group, it is necessary to allocate the effects of absorption and scattering of laser radiation on molecules and aerosols in the atmosphere resulting in its attenuation. These two processes are usually grouped together under the topic of extinction. Quantitatively these effects are characterized by an atmospheric transparency coefficient $T_A(\lambda)$, which is calculated by the discrete block of the mathematical model, laser sensor, with the help of LOWTRAN VII atmospheric computer code:

$$T_A(\lambda) = \exp^{-(\alpha_A + \alpha_D)R}, \tag{6.13}$$

where α_A and α_D are coefficients of absorption and dispersion respectively. R is distance from laser source to the sensor.

Among the effects relating to second group mentioned above, it is necessary to allocate expansion of a laser beam, distortion of laser beam, fluctuations of arrival angle and fluctuation of intensity. All of these are caused by atmospheric turbulence that causes fluctuations of temperature, humidity and density of the air, and consequently, its refraction index. Areas of local change of refraction coefficient (optical heterogeneity) can have extent from a few millimeters up to hundreds of meters [13].

Conditions of strong turbulence in the bottom atmospheric layers include heterogeneity of various scales and various structures. Therefore the study of the influence of turbulence on transmission of laser radiation includes the so-called structural functions entered by A.N. Kolmogorov. So, for medium spatial structural function of refraction index looks like [14]:

$$D_n(r) = [n(r_2) - n(r_1)]^2 = \Delta n^2(r), \tag{6.14}$$

where $D_n(r)$ is spatial structural function and $r = r_2 - r_1$ is distance between researched points. For locally isotropic and homogeneous turbulence it is fair to use the law of two thirds of Kolmogorov-Obukhov . The Kolmogorov-Obukhov law states that differences in indices and temperatures are proportional to the two-thirds power [15]:

$$D_n(r) = C_n^2 r^{2/3}, \tag{6.15}$$

where C_n^2 is structural constant of refraction index, $l_0 < r < L_0$, $l_0 = 1...2$ mm - internal scale of turbulence; $L_0 = 5...10$ m - external scale of turbulence [16]. Structural constant of refraction index ranges from $10^{-15} m^{-2/3}$ for weak turbulence to $10^{-13} m^{-2/3}$ for strong turbulence [17].

6.3.2 Turbulent expansion of a laser beam

Atmospheric turbulence results in fluctuation of phase as longitudinally, and also across the laser beam therefore it is reduced time and spatial coherence of radiation. At horizontal transmission of plane waves a phase coherence ratio on a section of beam can be estimated by the value r_0, known as the coherence dimension [18]:

$$r_0 = (0.54 C_n^2 k^2 R)^{-3/5} \tag{6.16}$$

where $k = 2\pi/\lambda$ is the wave number and R is the distance to the laser source.

The coherence dimension of a wave presents the minimal distance between two nearest beams in laser beam that appears uncorrelated because of transmission turbulent heterogeneities in an atmosphere with various refraction index, i.e. phase difference of their wave fronts exceeds 2π.

We have also studied the dependence of dimension coherence of the laser beam from traversed distances for different wavelengths (λ_1=0.63μm; λ_2=1.06μm; λ_3=1.54μm) and turbulence type (weak: $C_n^2 \approx 52 \cdot 10^{-17}$ $m^{-2/3}$; medium - $C_n^2 = 75 \cdot 10^{-16}$ $m^{-2/3}$; strong - $C_n^2 = 10 \cdot 10^{-14}$ $m^{-2/3}$). Results of these evaluations are presented in Figure 32, for weak turbulence, where as Figure 33 and Figure 34 present evaluations for medium turbulence and strong turbulence respectively.
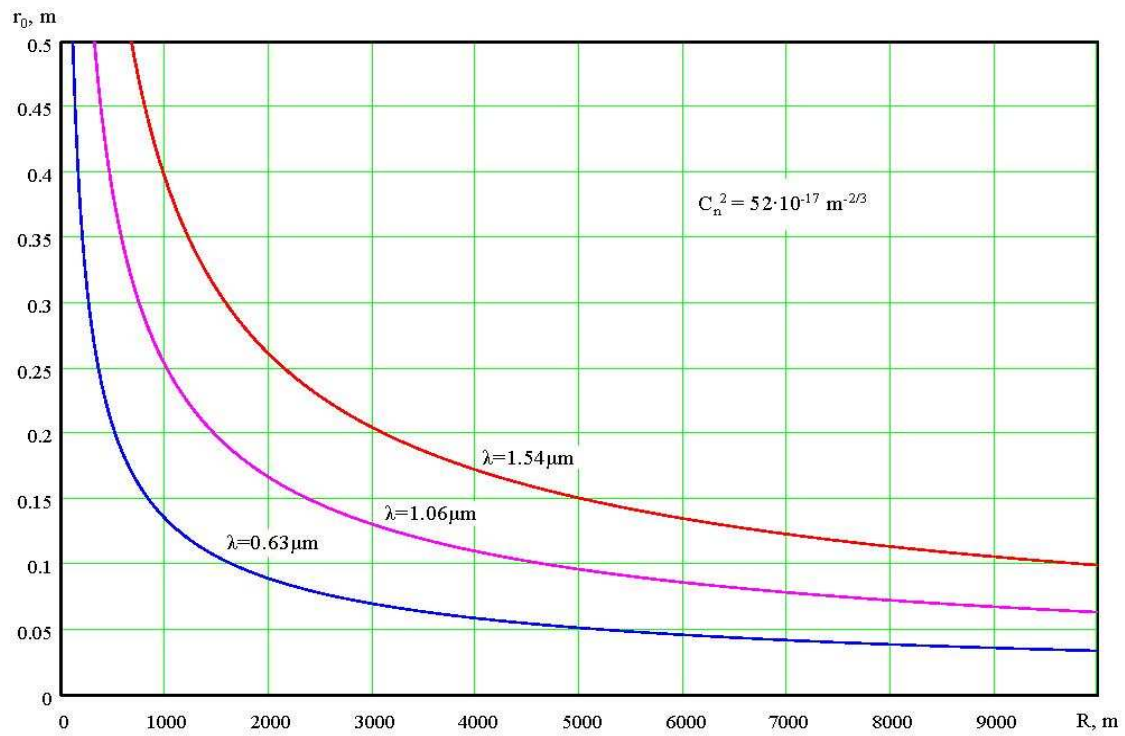
Figure 32 Dimension coherence r_0 vs range for weak turbulence at different wavelengths
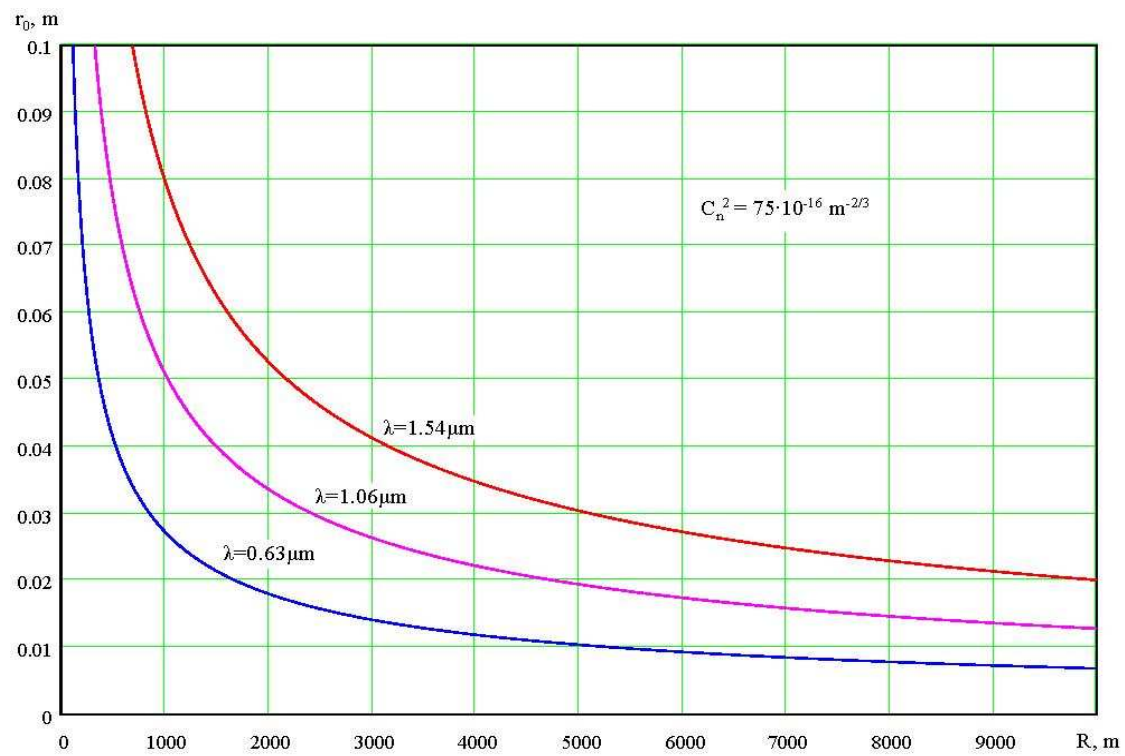
Figure 33 Dimension coherence r_0 vs range for medium turbulence at different wavelengths
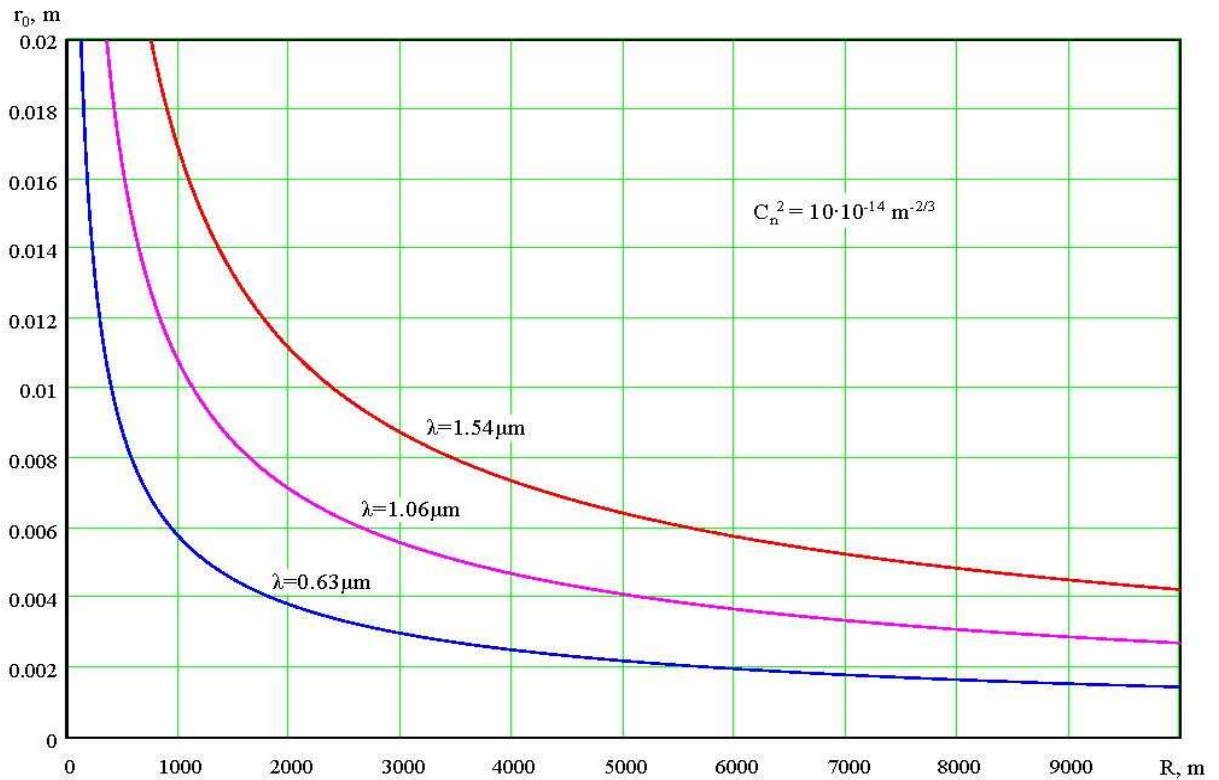
Figure 34 Dimension coherence r_0 vs range for strong turbulence at different wavelengths

Analysis of these curves shows that the dimension of coherence of an optical wave is essentially reduced when we increase the traversed distance in a turbulent atmosphere and deterioration of a turbulence number, and grows with the increase of radiation wavelength. For a distance of 5500m, wavelength $\lambda=1.06\mu m$ and strong turbulence $C_n^2 \approx 10\cdot10^{-14}$ m$^{-2/3}$ the dimension of coherence makes $r_0=3.88$mm. It results in a decrease of coherence and an essential distortion of the laser beam which is shown in expansion of the beam and redistribution of energy in its section. In this case there is an additional divergence of the laser radiation, caused by the influence of a turbulent atmosphere [19]:

$$\theta_A \approx \frac{\lambda}{r_0} \tag{6.17}$$

where θ_A is divergence caused by atmospheric turbulence, λ is wavelength of radiation and r_0 is dimension of coherence wave.

Then the expansion of the laser beam diameter (d) collimated laser beam on distance R from a source can be estimated by the following expression:

$$d = \sqrt{a^2 + (\theta + \theta_A)^2 R^2}$$ (6.18)

where,

a - beam diameter at the output of laser source

θ - radiation divergence of laser source

θ_A - radiation divergence caused by turbulence

R - distance to the laser source

Using Mathcad, we have also studied the dependence of laser beam diameter expansion on the change of range to the laser source for three different dimensions of coherence wave to a corresponding three conditions of turbulence. The following data are used: a=25mm, θ_P=3mrad, λ=1.06μm. The results are shown in Figure 35.
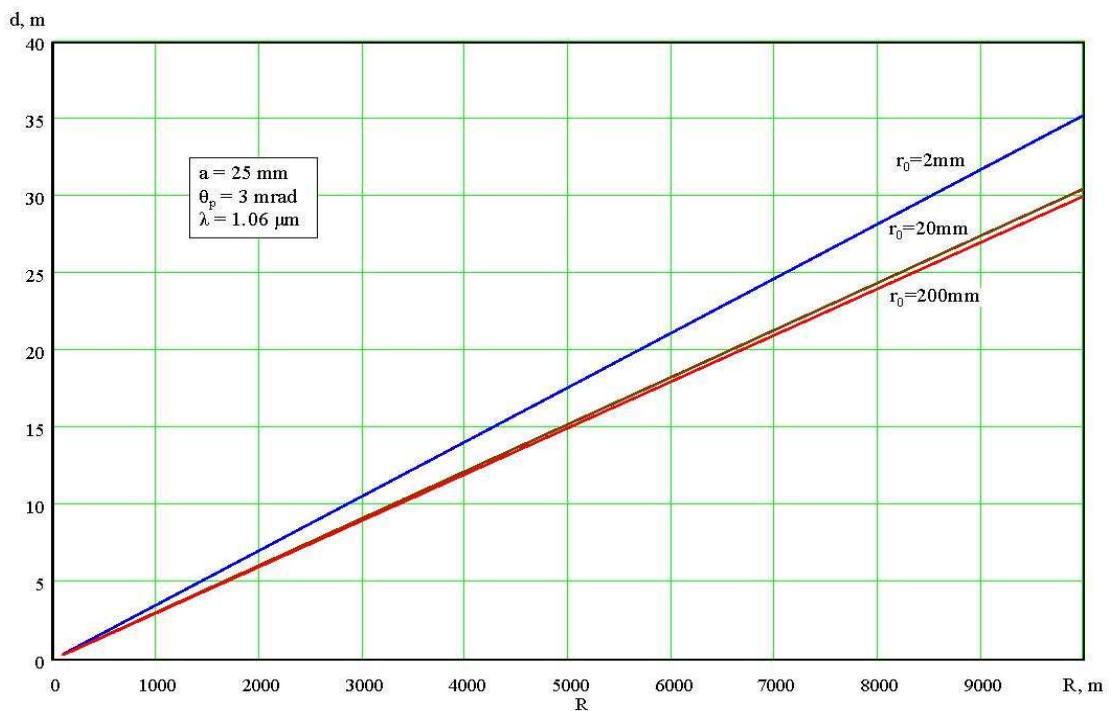
Figure 35 Laser beam diameter versus range for three different r_0 values

The results show that with reduction of coherence dimension (deterioration of a turbulence condition) the diameter of laser beam grows. At weak turbulence (big coherence dimension), beam diameter is defined actually only by initial divergence. Calculation of the laser beam expansion is carried out by the block of laser sensor model.

6.3.3 Fluctuations of Angle of Arrival

Fluctuations of angle of arrival (AOA) of radiation $\Delta\beta$, caused by atmospheric turbulence, are evaluated by the following expression [20]:

$$(\overline{\Delta\beta})^2 = 1.46 \cdot D^{-1/3} \cdot C_n^2 \cdot R \qquad (6.19)$$

Where D is the diameter of the receiving aperture, C_n^2 is the structural constant of refraction index, and R represent distance to the radiation source.

Using Mathcad, we plot dispersion of laser beam AOA against distance up to radiation source at three various values of aperture diameter (D_{rec1}=30mm, D_{rec2}=40mm, D_{rec3}=50mm). Results of these evaluations are presented in Figure 36, for weak turbulence, where as Figure 37 and Figure 38 present evaluations for medium turbulence and strong turbulence respectively.
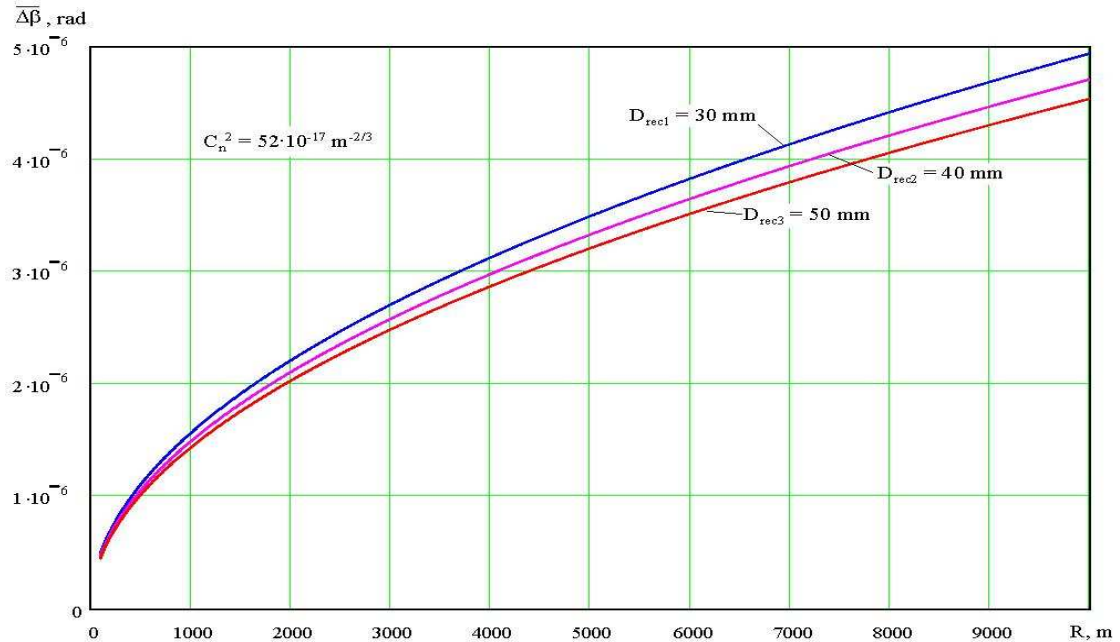

Figure 36 Laser beam AOA versus range at three values of aperture diameter for weak turbulence
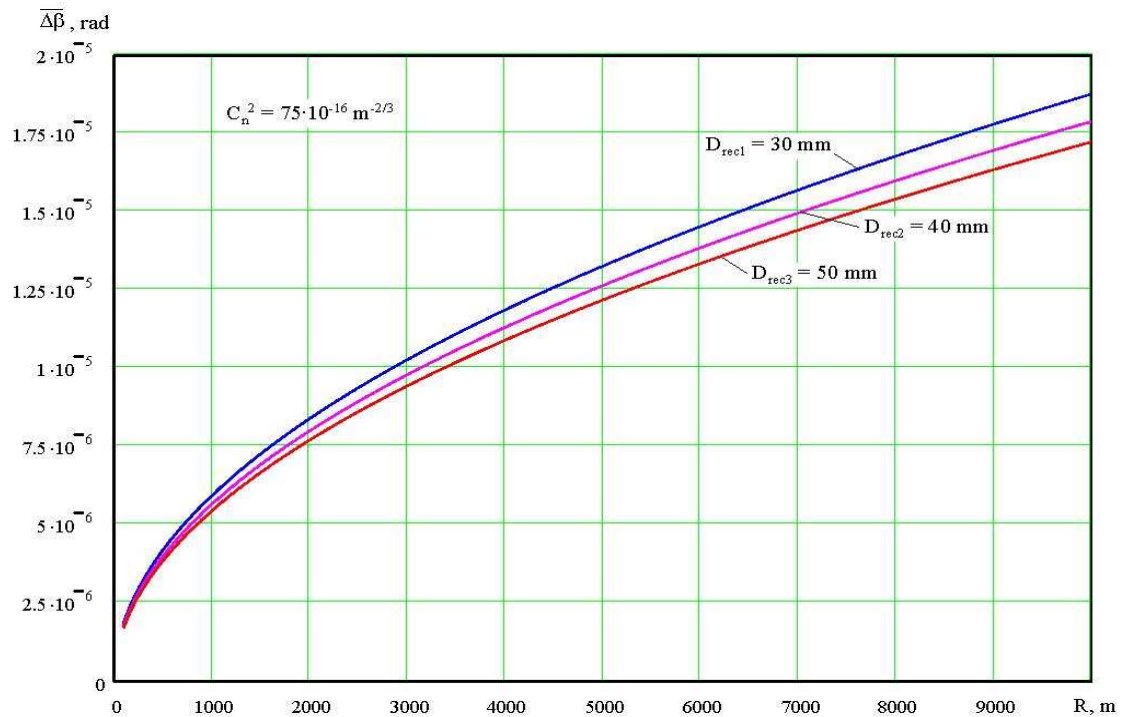
Figure 37 Laser beam AOA versus range at three values of aperture diameter for medium turbulence
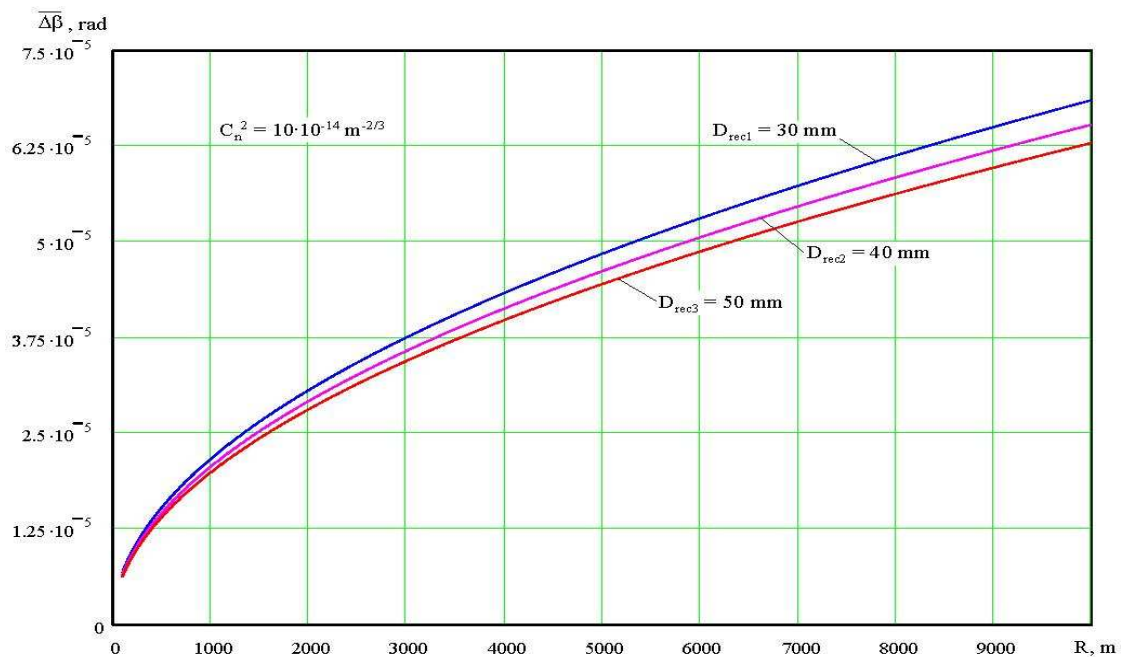
Figure 38 Laser beam AOA versus range at three values of aperture diameter for strong turbulence

Analysis of the results showed that with deterioration of turbulence level, the dispersion of arrival angle of radiation essentially grows. Also, increase in the diameter of the receiving object results in reduction in the arrival angle of radiation. From the graphs it is clear that for

real up to 10 kms, mean-square deviation of fluctuations of radiation arrival angle reaches values from units of angular seconds (in conditions of weak turbulence) up to tens of angular seconds (in conditions of strong turbulence).

Fluctuations of radiation angle of arrival appears on the receiving optical system in a linear deviation of formed image from the optical axis in the focal plane of the object. This deviation Δx can be evaluated by the following expression:

$$\Delta x = f_{ob} \cdot tg\,\overline{\Delta\beta} \approx f_{ob} \cdot \overline{\Delta\beta} \tag{6.20}$$

where Δx is the linear deviation of optical beam, f_{ob} is focal length of receiving objective and $\overline{\Delta\beta}$ is mean-square deviation of arrival angle of radiation.

To view the changes caused by a various turbulence levels on the angle of arrival, an evaluation has been done to investigate the dependence of linear deviation of the laser beam on focal plane from mean-square deviation of radiation arrival angle for three different values of focal lengths of the laser warning receiver ($f_{ob1} = 40$ mm; $f_{ob2} = 60$ mm; $f_{ob3} = 80$ mm). Results of investigations are shown in Figure 39.
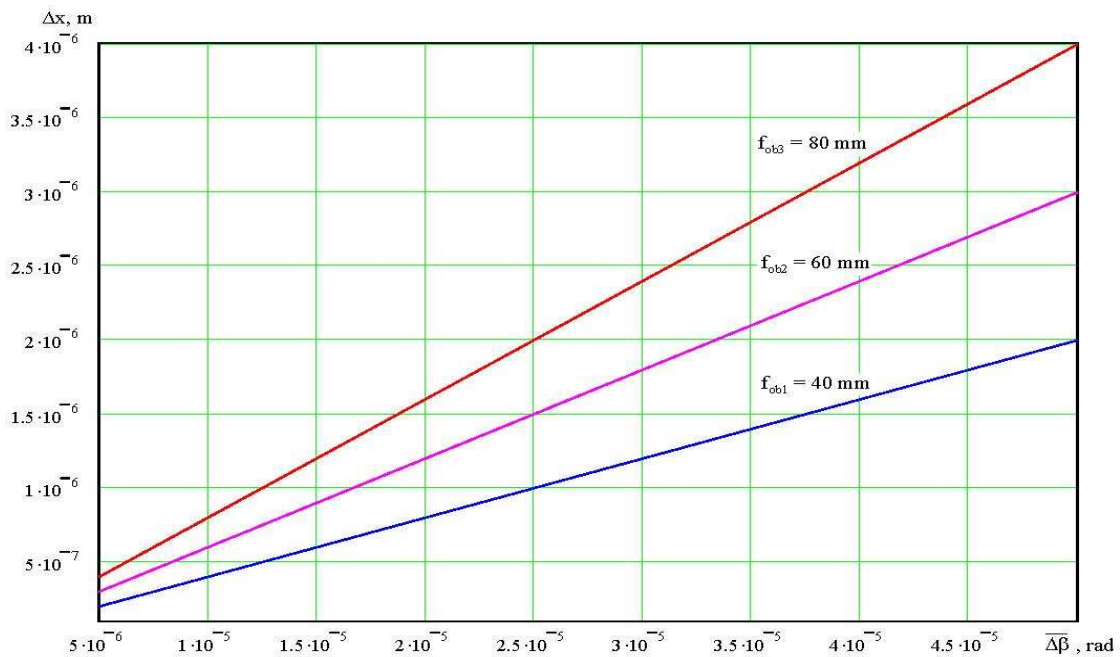
Figure 39 Deviation of laser beam versus AOA for three different focal lengths

Analysis shows that changes of beam linear deviation values, result in changes in mean-square deviation of arrival angle of radiation of micrometer (for weak turbulence) up to units and tens of micrometers (for strong turbulence). From the practical point of view, this range of deviation changes should be taken into account when choosing sensitive plate sizes of photodiodes and characteristics of receiving optical system for laser sensor.

6.3.4 Flicker

Essential influence on the functionality of the laser sensor is affected by the intensity fluctuations of the arrival optical signal. For homogeneous turbulence of the atmosphere and weak fluctuations, the dispersion of logarithm of radiation intensity is evaluated by expression [21]:

$$\sigma_0^2 = 1.23 C_n^2 k^{7/6} R^{11/6} , \qquad (6.21)$$

where,

σ_0^2 - dispersion of intensity logarithm for weak fluctuations

C_n^2 - structural constant of atmosphere refraction coefficient

$k = 2\pi/\lambda$ - wave number

λ - wavelength

R - distance to the radiation source

For strong fluctuations V.I.Tatarsky proposed an expression for evaluation of the logarithm of dispersion of radiation intensity logarithm [22]:

$$\sigma_I^2 = 1 - (1 + 6\sigma_0^2)^{-1/6} , \qquad (6.22)$$

where σ_I^2 represents the logarithm of dispersion of intensity at strong fluctuations.

Dispersion of intensity logarithm is estimated by expression [23]:

$$\sigma^2 = < \left[Ln(I) - < Ln(I) > \right]^2 > \ , \qquad\qquad (6.23)$$

where $Ln(I)$ is intensity logarithm while $< >$ indicates that we are taking the average.

Let us now investigate the dependence the logarithm of root mean square (RMS) radiation intensity for strong fluctuations (equation 22) from distance to the laser source for three different wavelengths ($\lambda_1=0.63\mu m$; $\lambda_2=1.06\mu m$; $\lambda_3=1.54\mu m$) at various turbulence numbers (types). Results of these evaluations are presented in Figure 40, for weak turbulence, where as Figure 41 and Figure 42 present evaluations for medium turbulence and strong turbulence respectively.
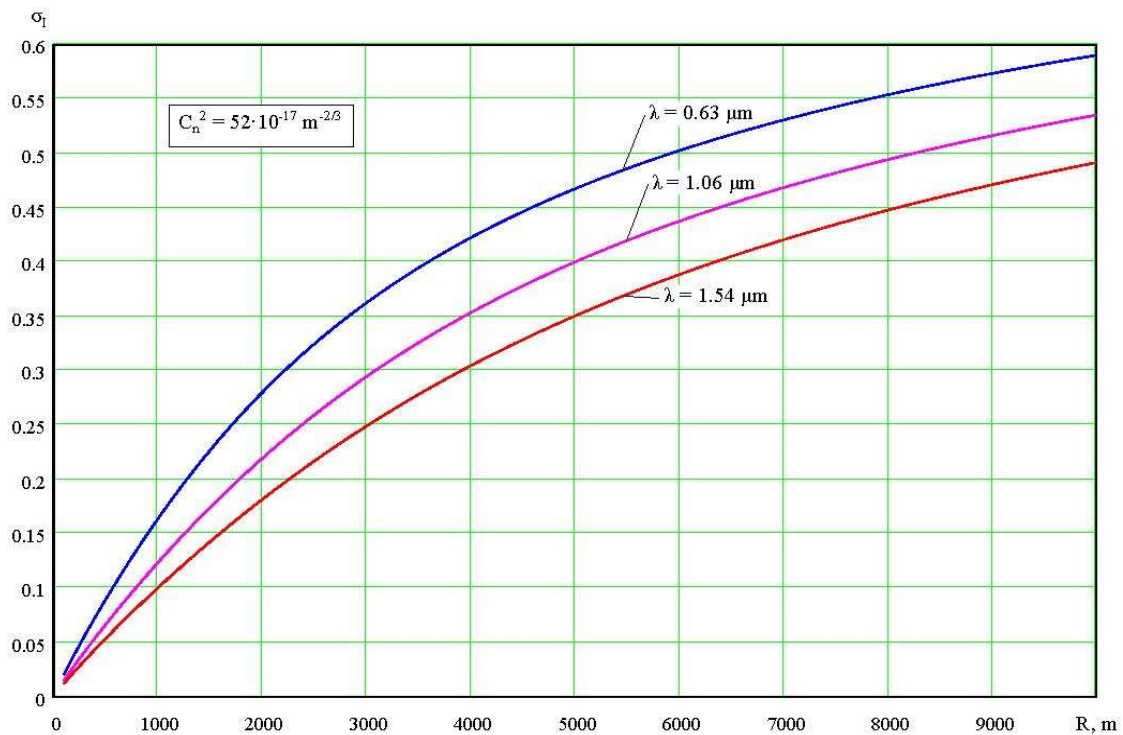

Figure 40 Radiation intensity versus range for weak turbulence at different wavelengths
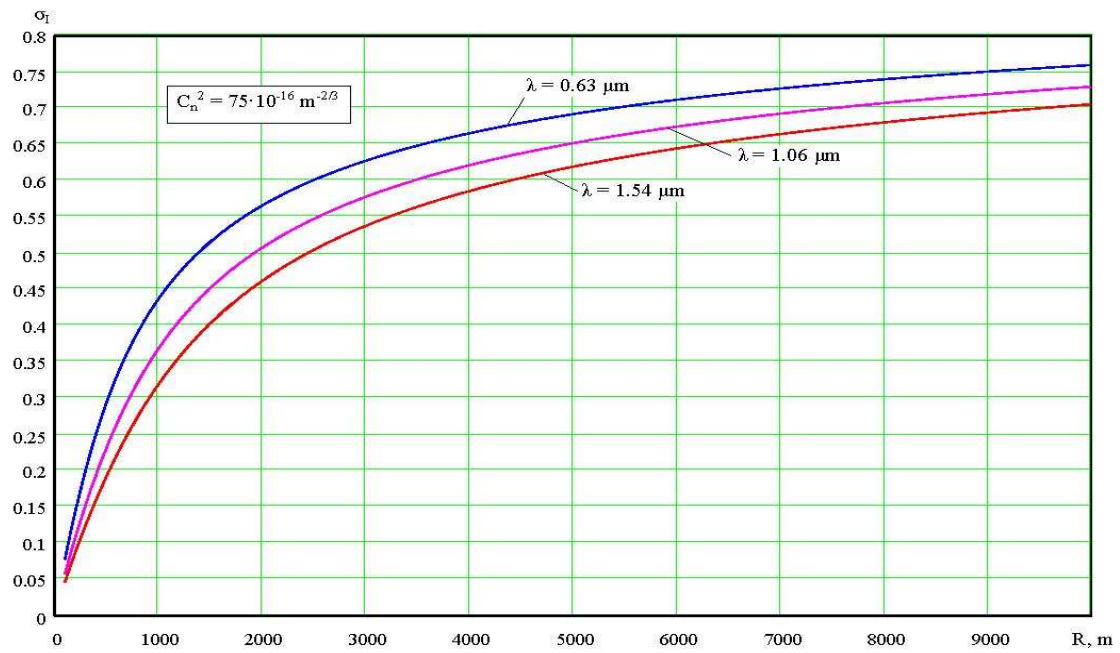
Figure 41 Radiation intensity versus range for medium turbulence at different wavelengths
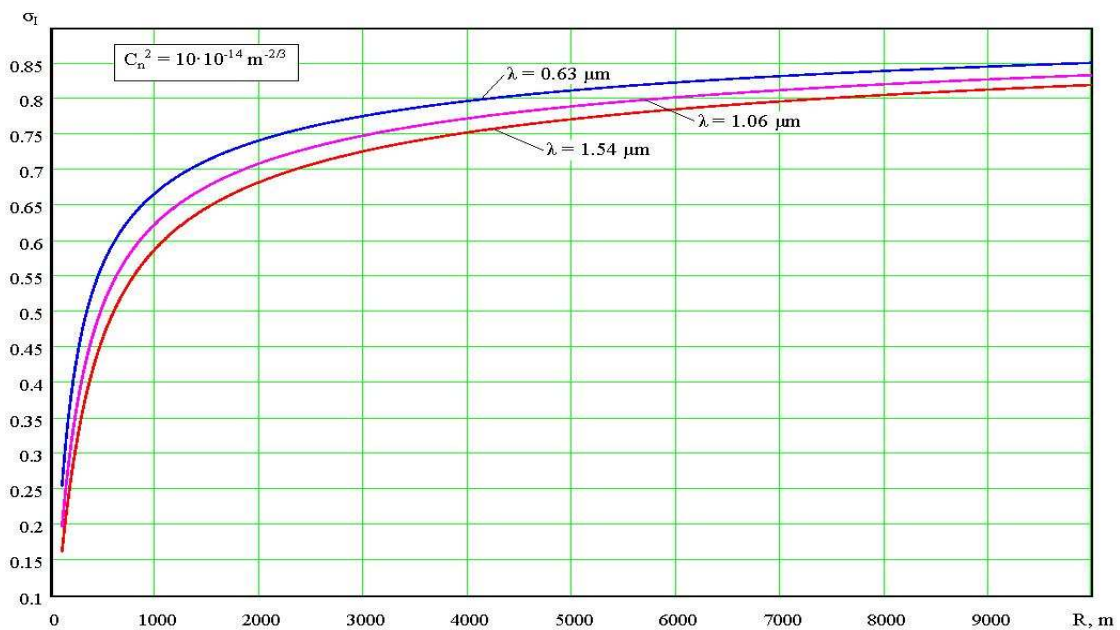
Figure 42 Radiation intensity versus range for strong turbulence at different wavelengths

These curves show that mean-square deviation of the logarithm of radiation intensity poorly depends on wavelength and essentially grows with increase in distance up to laser source and amplification of turbulence.

117

Fluctuations of laser radiation intensity cause flicker (scintillations) of the arrival optical signal. The frequency (spectrum) of flicker f_f is defined by velocity of moving optical heterogeneities (local velocity of wind) and the size of these heterogeneities:

$$f_f \approx \frac{V}{r_0},$$ (6.24)

where V is local velocity of wind in a ground layer of atmosphere and r_0 is size of optical heterogeneities (size of wave coherence).

At an average velocity of wind, V=5m/s, and optical heterogeneities sizes, r_0=5mm...5cm, flicker frequency reaches values from 100Hz up to 1kHz. By using expressions (6.2 to 6.24) in the laser sensor model, it is possible to take into account the influence of fluctuations of radiation intensity, caused by turbulence of the atmosphere, on functioning efficiency of the sensor.

6.3.5 Estimation of Influence Parameters

It was interesting to investigate the possibilities of increasing the detection range of the laser sensor by optimization of the parameters of the laser sensor model. First of all, let us see the maximum detection range that we can get with the current parameters of the laser sensor model for different atmospheric conditions and turbulence. Results are given in the Table 16.

Atmosphere condition	Turbulence		
	$C_n^2 \approx 52 \cdot 10^{-17}$ $m^{-2/3}$	$C_n^2 \approx 75 \cdot 10^{-16}$ $m^{-2/3}$	$C_n^2 \approx 10 \cdot 10^{-14}$ $m^{-2/3}$
Good	5500	4800	4300
Typical-1	5300	4700	4200
Typical-2	4200	3800	3500
Bad-1	2200	2100	2000
Bad-2	2100	2000	1900

Table 16 The changes in detection range at various atmospheric conditions and turbulence

(λ = 1.06 μm, $\Delta\lambda$ = 0.811...1.11 μm, sand sample - A,

receiving optical system: D=30mm, f=40mm)

These results show that the detection range essentially decreases with deterioration of atmospheric conditions and strengthening of turbulence.

To study the effect of receiving channel performances on the detection range, we tabulate results for three different values of receiving lens diameter (D=30mm, D=40mm, D=50mm). Results are given in the Table 17.

Atmosphere condition	Optical system		
	D=30mm, f=40mm	D=40mm, f=40mm	D=50mm, f=40mm
Good	5500	6300	6900
Typical-1	5300	6000	6700
Typical-2	4200	4600	4900
Bad-1	2200	2300	2500
Bad-2	2100	2200	2300

Table 17 Changes of detection range at various values of diameter receiving lens

($\lambda = 1.06$ μm, $\Delta\lambda = 0.811\ldots1.11$ μm, sand sample - A,

$C_n^2 = 52 \cdot 10^{-17}$ m$^{-2/3}$)

The results show that with increase of the receiving optical system diameter the detection range essentially increases, that is caused by the rise of received signal power.

Dependence of the maximal detection range on various values of a focal length (f=40mm, f=60mm, f=80mm) has also been investigated. Results are given in the Table 18.

Atmosphere condition	Optical system		
	D=30mm, f=40mm	D=30mm, f=60mm	D=30mm, f=80mm
Good	5500	6500	7300
Typical-1	5300	6300	7000
Typical-2	4200	4700	5100
Bad-1	2200	2300	2400
Bad-2	2100	2200	2200

Table 18 Changes of detection range at various values of a focal length

($\lambda = 1.06$ μm, $\Delta\lambda = 0.811\ldots1.11$ μm, sand sample - A,

$C_n^2 = 52 \cdot 10^{-17}$ m$^{-2/3}$)

The increase in focal length results in narrowing the field of view and accordingly, decrease of background level that causes an enhancement of sensitivity of the receiving channel.

Further evaluation has been carried out to observe the effect of the optical bandwidth on detection range. It has been carried out for various values of spectral ranges of:

- $\Delta\lambda_1 = 40$nm
- $\Delta\lambda_2 = 80$nm
- $\Delta\lambda_3 = 120$nm
-

The results of this evaluation are presented in Table 19.

Atmosphere condition	Pass bandwidths		
	$\Delta\lambda = 40$nm	$\Delta\lambda = 80$nm	$\Delta\lambda = 120$nm
Good	8500	7400	6900
Typical-1	8000	7100	6600
Typical-2	5500	5100	4800
Bad-1	2400	2400	2300
Bad-2	2200	2200	2200

Table 19 Changes of detection range at various values of the spectral bandwidths ($\lambda = 1.06$ μm, sand sample - A, $C_n^2 = 52 \cdot 10^{-17}$ m$^{-2/3}$, D=30mm, f=40mm)

Analysis of results testifies that with increase of spectral bandwidth detection range decreases. At the bad atmospheric conditions the detection range actually does not vary, that is caused by dominant effect of general attenuation of optical signal in atmosphere, instead of variations of background level.

The effect of photodiode parameters have been carried out using the following evaluation of detection range for various values of photodiode spectral response with $S_\lambda = 46.84$A/W, $S_\lambda = 19.77$A/W and $S_\lambda = 9$A/W.

This evaluation has been done with keeping the other parameters fixed. The results are given in Table 20.

Atmosphere condition	Spectral response		
	$\lambda=1.02\mu m$ $S_\lambda=46.84A/W$	$\lambda=1.06\mu m$ $S_\lambda=19.77A/W$	$\lambda=1.1\mu m$ $S_\lambda=9A/W$
Good	6600	5500	3800
Typical-1	6300	5300	3700
Typical-2	4700	4200	3200
Bad-1	2400	2200	1900
Bad-2	2300	2100	1800

Table 20 Changes of detection range at various spectral sensitivity of APD

(λ = 1.06 μm, $\Delta\lambda$ = 0.811…1.11 μm, D=30mm, f=40mm, sand sample - A, $C_n^2=52\cdot10^{-17}$ m$^{-2/3}$)

Analysis of results shows, that with increase of photodiode spectral response the detection range strongly increases. It is caused by increase of the signal/noise ratio in the reception channel.

The influence of the photodiode sensitive area size on the detection range has been observed for three different values of sensitive area size of the photodiode (l=200μm, l=500μm, l=800μm) and is given in Table 21.

Atmosphere condition	Detection area		
	l=200μm	l=500μm	l=800μm
Good	8000	5500	4500
Typical-1	7600	5300	4400
Typical-2	5400	4200	3600
Bad-1	2400	2200	2100
Bad-2	2200	2100	2000

Table 21 Changes of detection range at various values of photodiode sensitive area sizes

(λ = 1.06 μm, $\Delta\lambda$ = 0.811…1.11 μm, sand sample - A, $C_n^2=52\cdot10^{-17}$ m$^{-2/3}$)

Results shown that with increase in the size of the photodiode sensitive area the detection range is reduced. It is caused by the increase in noise level in the reception channel.

Observations in Table 20 are collected to investigate the dependence of detection range on the reception channel bandwidth. Results for three different values of a bandwidth ($\Delta f=30$MHz, $\Delta f=65$MHz, $\Delta f=100$MHz) are given in Table 22.

Atmosphere condition	Frequency band		
	$\Delta f = 30$MHz	$\Delta f = 65$MHz	$\Delta f = 100$MHz
Good	5600	4700	4200
Typical-1	5400	4600	4100
Typical-2	4200	3700	3400
Bad-1	2200	2000	1900
Bad-2	2100	1900	1800

Table 22 Change of detection range at various bandwidth values

($\lambda = 1.06$ μm, $\Delta\lambda = 0.811\ldots1.11$ μm, sand sample - A,

$C_n^2 = 52 \cdot 10^{-17}$ m$^{-2/3}$, D=30mm, f=40mm)

These observations show that with increase in bandwidth, the detection decreases. It is caused by increase of noise level of the reception channel.

6.4 Factors Impairing The Efficiency of The Laser Sensor

On the basis of the research results of the laser sensor model the factors reducing the detection range of the laser source radiation have been established. These factors are:

1. Significant attenuation of laser radiation in an atmosphere connected strongly to changes of weather conditions.

2. The influence of atmospheric turbulence can be seen in the expansion of the laser beam, strong fluctuations of its intensity and arrival angle.

3. Non-optimum choice of optical system parameters, diameter of aperture D and Focal length f, results in decrease in the level of useful signal and increase in the level of background radiation.

4. Non-optimum choice of spectral bandwidth of the optical filters causes an increase in the level of background radiation.

5. Discrepancy of the wavelength of the laser source to the maximum spectral sensitivity of the photodetectors results in a decrease of the level of signal in the receiving path.

6. Strong dependence of the photodetector amplification on the temperature in the case of using an Avalanche Photo Diode (APD).

7. Non-optimum choice of the size of sensitive area of the photodiode results in an increase of noise level.

8. Non-optimum choice of bandwidth of the amplification cascade results in distortion of the resulting signal or in increase of noise level.

9. Absence of measures on decreasing of noise in the receive channel.

10. Non-optimum choice of the threshold level of the comparator.

6.5 Requirements of Laser Sensor Parameters

On the basis of the analysis of the factors impairing efficiency of the laser sensor performance, the requirements of its key parameters have been developed and they allow us to increase the detection range of laser sources. These requirements are as follows:

1. Diameter of the aperture of receive optical system should be as large as possible (Table 17) with the purpose of maintaining the required maximal values of capacity of accepted the laser signal. Size restriction of the aperture will be connected only with weight and dimension restrictions of the optical system and its cost.

2. The focal length of the receiving lens should be chosen from the condition of maintaining of minimally possible field of view (Table 18) in order to decrease the level of background radiation. The increase of focal length will be limited by the dimensions of optical system and necessity of maintaining a sufficient light exposure of the image and required field of view of the sensor (typically 360° in azimuth) and hence may require more sensors.

3. The spectral bandwidth of the optical filters should be as smalll as possible (Table 19) in order to decrease the level of the background radiation and increase the detection range. However, it is limited by the quantity of fragmentation of the set spectral range

and the necessity of consideration of the temperature dependence of the wavelength of the laser radiation.

4. Spectral sensitivity of the photodiodes should be maximal (Table 20) at the wavelengths used by the laser radiation sources.

5. When using Avalanche Photo Diodes (APDs) it is necessary to establish a circuit for voltage control by the offset depending on the temperature or to apply a thermostatic switch with the purpose of stabilization of the APD multiplication factor.

6. The size of the photodiode sensitive area should be chosen as small as possible (Table 21) to decrease the noise level. However its reduction is limited by the sizes of the focal spot caused by the influence of atmospheric turbulence.

7. The bandwidth of the receiver channel should be coordinated with the width of the laser signal spectrum. With the absence of aprioristic data on the laser signal it should be minimized (Table 22) with the purpose of decreasing noise level, but should not result in distortion of the useful signal.

8. Parameters of electronic elements of the cascade amplifiers are chosen to maintain a minimum level of noise.

9. The amplification gain of the amplifier cascade should provide normal operation of collimator lens at low levels of optical signal.

10. The level of comparator starting threshold should be set taking into account all actual noises of the laser sensor, and maintenance of preset values of probabilities of correct detection and false alarm.

6.6 Quantification of Errors

Quantification of the errors in the model is inherently difficult, however, the scaling of results is probably accurate but the absolute values would need extensive field validation to justify the simplifications and any omissions of the model.

6.7 Conclusions

In this chapter of thesis, an estimation of the threshold sensitivity of the sensor is discussed and analyzed considering all the noise sources possible such as shot noise of the dark current, shot noise of the signal fluctuations, shot noise of the background radiation, and thermal noise of the electronic path. It was clear that for a reduction in background radiation, it is necessary to reduce the field of view of the sensor by increasing the focal length and reduction of the dimension of sensing area of photodetector.

Atmospheric turbulence was another issue discussed in this chapter to understand its effect on the output of the sensor and how to overcome any problems it posed. It results in fluctuation of phase longitudinally in the beam and also across the laser beam that reduces temporal and spatial coherence of the radiation. Fluctuations in laser beam angle of arrival are studied and it was clear that when atmospheric turbulence increased, the dispersion of arrival angle of radiation essentially grows.

Influence of laser sensor parameters on the performance is investigated. The results show that the detection range essentially decreases with deterioration of atmospheric conditions as turbulence strengthens.

Our study concluded with the factors impairing efficiency of laser sensor and the requirements to laser sensor parameters that must be considered to achieve a better performance especially in severe weather conditions.

Now it is time to introduce the missile seeker model. Chapter 7 represents a laser beam-riding missile seeker, which means that the seeker located at the rear of the missile to read the guidance commands from the firing post. Both, the laser warning receiver and the missile seeker will suffer from the same weather and atmospheric conditions since they are looking in the same direction.

6.8 References

[1] Introduction to Infrared and electro-optical systems, Ronald G. Friggers, Paul Cox, Timothy Edwards, Page 203.

[2] Introduction to Infrared and electro-optical systems, Ronald G. Friggers, Paul Cox, Timothy Edwards, Page 225.

[3] Optical Detection Theory for Laser Applications, George R. Osche, Page 136.

[4] Detection of Low-Level Optical Signals, Photodetectors, Focal Plane Arrays and Systems. M. A. Trishenkov, Page 27.

[5] Detection of Low-Level Optical Signals, Photodetectors, Focal Plane Arrays and Systems. M. A. Trishenkov, Page 307.

[6] Optical Detection Theory for Laser Applications, George R. Osche, Page 142.

[7] Optical Detection Theory for Laser Applications, George R. Osche, Page 140.

[8] The Infrred & Electro-Optical Systems Handbook, volume 7: countermeasure Systems by David H. Pollock, Page 121.

[9] Introduction to Infrared and electro-optical systems, Ronald G. Friggers, Paul Cox, Timothy Edwards, Page 146.

[10] Introduction to Infrared and electro-optical systems, Ronald G. Friggers, Paul Cox, Timothy Edwards, Page 146.

[11] Optical Detection Theory for Laser Application, George R. Osche, Page 138.

[12] Optical Detection Theory for Laser Applications, George R. Osche, Page 136.

[13] Tatarski, V., Wave Propagation in Turbulent Medium, New York: McGraw-Hill, 1961.

[14] Introduction to Infrared and electro-optical systems, Ronald G. Friggers, Paul Cox, Timothy Edwards, Page 140.

[15] Introduction to Infrared and electro-optical systems, Ronald G. Friggers, Paul Cox, Timothy Edwards, Page 140.

[16] Optical Detection Theory for Laser Application, George R. Osche, Page 185.

[17] Introduction to Infrared and electro-optical systems, Ronald G. Friggers, Paul Cox, Timothy Edwards, Page 141.

[18] Optical Detection Theory for Laser Application, George R. Osche, Page 200.

[19] Journal of Battlefield Technology, Vol 8, No1, March 2005. Kellaway & Richardson :Laser Analysis-Part 3. Page 30.

[20] Optical Detection Theory for Laser Application, George R. Osche, Page 200.

[21] Optical Detection Theory for Laser Application, George R. Osche, Page 201.

[22] Tatarski, V., Wave Propagation in Turbulent Medium, New York: McGraw-Hill, 1961.

[23] Tataroski, V., Wave Propagation in Turbulent Medium, New York: McGraw-Hill, 1961.

[24] Introduction to Infrared and electro-optical systems, Ronald G. Friggers, Paul Cox, Timothy Edwards, Page 153.

[25] Introduction to Infrared and electro-optical systems, Ronald G. Friggers, Paul Cox, Timothy Edwards, Page 170.

CHAPTER 7

Seeker Model

7.1 Seeker Applications

In modern warfare, laser-guided weapons play a significant role in ensuring each warhead deployed will only strike its intended target. Each laser-guided missile or bomb has a laser seeker that consists of an array of photodiodes. These photodiodes are sensitive to a predefined laser's optical wavelength. A high-intensity laser designator must acquire and lock onto the target, either from the air or from the ground. This is necessary to allow the missile or bomb to identify the target. Once the laser-guided weapon is launched, the laser seeker senses the laser beam reflected from the target, and the seeker's control system will then guide the missile straight to the target.

In general, the laser pulse width presented to the control system is very short [1]. The control system must be fast enough to reliably capture this laser pulse pattern to calculate the range to the target. The laser seeker is a device based on the direction of a sensitive receiver that detects the energy reflected from a laser designated target and defines the direction of the target relative to the receiver [2].

A laser designator device highlights a spot on the target with an encoded laser beam. This spot provides reference information to an incoming munition that allows it to make in-flight corrections to its trajectory. The use of an encoded signal reduces the threat of jamming as well as reducing interference in high-noise combat environments [3]. The primary limitation on this device is that it requires a line of sight to the target from both the munition and the shooter or designator.

'''Laser guidance''' is a technique of guiding a missile or other projectile or vehicle to a target by means of a laser beam. Some laser guided systems utilize beamriding guidance, but most operate similarly to semi-active radar homing (SARH) [4]. This technique is sometimes called '''SALH''', for '''Semi-Active Laser Homing'''. With this technique, a laser is kept pointed

at the target. This laser radiation bounces off the target and is scattered in all directions. The missile or bomb is launched or dropped somewhere near the target. When it is close enough some of the reflected laser energy from the target reaches it's laser seeker which notices the direction this energy is coming from and aims the projectile towards the source. As long as the projectile is in the right general area and the laser is kept aimed at the target, the projectile should be guided accurately to the target.

Note that laser guidance isn't useful against targets that don't reflect much laser energy, including those coated in special paint which absorbs laser energy. This is likely to be widely used by advanced military vehicles in order to make it harder to use laser rangefinders against them and harder to hit them with laser-guided munitions.

'''Beam-riding guidance''' leads a missile to its target by means of a radar or a laser beam (Appendix H)[5]. It is one of the simplest forms of radar or laser guidance. The main use of this kind of system is to destroy airplanes or tanks. First, an aiming station (possibly mounted in a vehicle) in the launching area directs a narrow radar or laser beam at the enemy aircraft or tank. Then, the missile is launched and at some point after launch is "gathered" by the radar or laser beam when it flies into it. From this stage onwards, the missile attempts to keep itself inside the beam, while the aiming station keeps the beam pointing at the target. The missile, controlled by a computer inside it, "rides" the beam to the target. The aiming station can also use the radar returns of the beam bouncing off the target to track it, or it can be tracked optically or by some other means.

Using a laser as a weapon itself places enormous demands on device physics and energy supply, but the fact that a laser beam can be precisely pointed and remains tightly compact ("coherent" in laser terminology) over a long range means that it could be used as a precise pointing device. A laser could be strapped to a telescope with crosshairs so that the beam could be focused to "illuminate" a particular target to "mark" or "designate" it. The fact that the laser also generates virtually monochromatic radiation also means that the light reflected off such a target could be easily detected by simple sensors through an optical filter. A guided weapon could be fitted with such a sensor, with the sensor linked to a feedback control mechanisms so that it would home in on an illuminated target. The seeker has an optical sensor, shielded by an optical filter that is transparent to laser light but blocks light of other wavelengths.

Though there are no tools to assist the planner, a very important consideration is the pulse repetition frequency code [6]. Laser designators use a pulse coding system to ensure that a specific seeker and designator combination work in harmony. The planner must be concerned with the limited number of codes available, their allocation, assignment, and characteristics.

Laser codes, depending on the equipment, are either three digits or four digits long. If it is a four digit code the first digit is always the numeral 1. The laser codes vary from 111-488 (Band 2) to 511-788 (Band 1) [7]. These numbers represent the nanoseconds of delay between the laser pulses. The smaller the number, the smaller the delay. The result is that band 2 pulse rates result in more laser energy striking and reflecting off the target, giving the seeker a better laser spot to guide on. As a result band 2 pulse rates are better for adverse conditions and when the mission has a high priority. If you throw in the fact that there are only six hundred and seventy-seven codes available (788-111=677) on any given day to U.S. forces, you soon see that priorities should be set for the distribution of these codes. This is where allocation and assignment becomes important. In a MAGTF the senior fire support coordination centre (FSCC) allocates different blocks of codes to artillery, air, and naval gunfire assets. The FSCC will also keep a block of codes for MAGTF special use. Fire support coordinators in subordinate units not only coordinate codes with adjacent units, they monitor missions and ensure proper code coordination between the delivery unit and the designator. Normally the delivery system will tell the designator which code to use. There may be occasions where a special code for that mission is assigned to the designator and delivery system from the block reserved by the MAGTF FSCC. All pulse repetition codes can be used for laser designation. However, the characteristics of band 2 codes make them more suitable when designating laser guided munitions.

Laser target designators are used to covertly point out a target for laser seeker equipped aircraft and for the laser designation of targets to provide semiactive guidance of free fall bombs or for the guidance of laser guided missiles. In such a system, pulses of laser energy of high peak power and short duration, e.g., a pulsed solid state laser such as Nd:YAG or Nd:Glass lasing material, are transmitted from the target designator to illuminate a target for tracking or guidance purposes [8]. In an area containing numerous targets, several laser designators may be operating simultaneously and the return energy may cause interference between friendly systems. Thus it becomes necessary for each system operating in one area to be capable of distinguishing the signal of one designator of that from another designator.

In addition, with the proven effectiveness of laser designator systems, it is likely that laser counter-measures will eventually be developed and become a serious threat to their continued success. It is thus of utmost importance that the system be relatively immune to at least those types of countermeasures such as PRF predicters and repeaters which could be presently available. In the event that the signal transmitted by a laser designator is encoded, the laser seeker receiving the energy must be able to rapidly detect the desired signal in the presence of any interfering signals. This requirement of speed in detecting the desired signal must, of course, be coupled with accuracy to insure reliability of the target seeker or tracking system.

7.2 Seeker Model Structure

The seeker model differs from Sensor Model only in the addition of the processing block which allocates the modulating frequency. The block generating this frequency has been developed on the basis of a matched filter with 5 delay lines. The seeker receives laser radiation with a known wavelength that allows us reduce the spectral bandwidth of the optical filter and to lower strongly the level of background radiation. A laser seeker is a device that detects the modulated laser radiation.

The seeker model has one channel for extracting the modulating frequency. Modulating frequencies can be various, but a frequency of 2 MHz was chosen to assure the quick working of the model. The seeker model is presented on Figure 43.
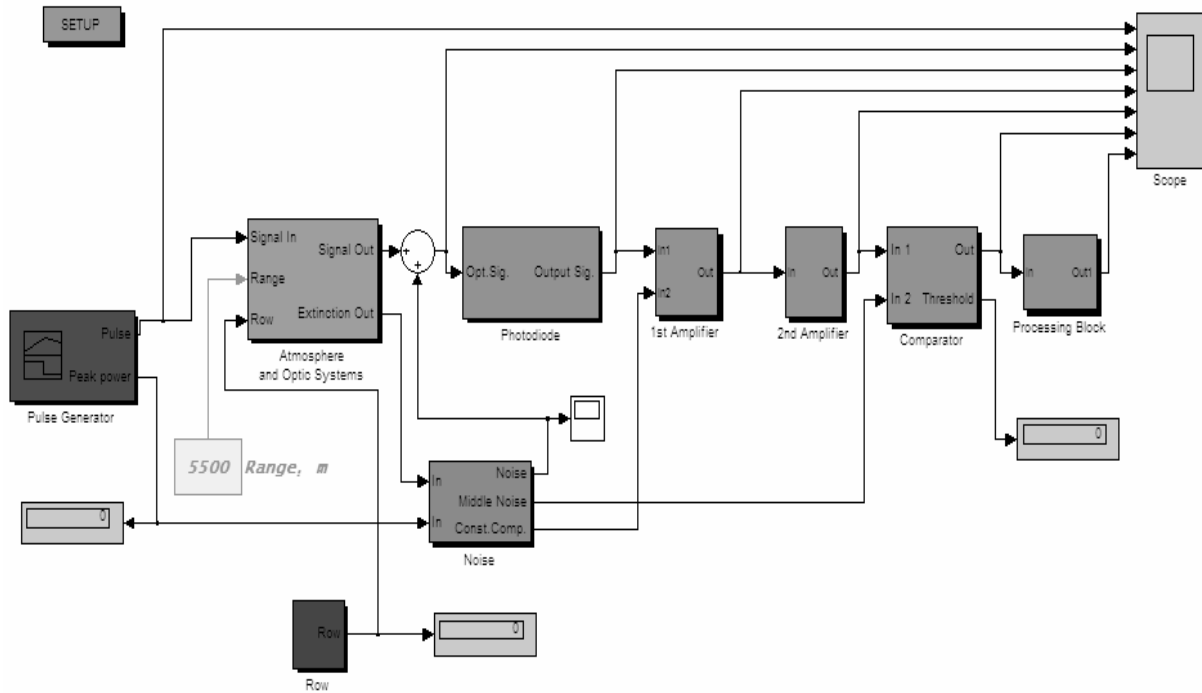
Figure 43 Seeker Model

The structure of the seeker model consists of:

1. Pulse Generator block forms rectangular pulses with the following parameters: Amplitude: 1, Period (sec)= 5e-7 (frequency - 2 MHz), Pulse Width (% of period)= 4, Phase delay (sec): 0.

$$S_1(t) = P \cdot S(t + T) \tag{7.1}$$

where,

$S_1(t)$ - output signal

P – laser power

t – current time

T – pulse period

S(t+T) - periodic rectangular pulses with parameters:

$$S(t+T) = 1, \text{if } t+T \leq \tau \tag{7.2}$$

$$S(t+T) = 0, \text{if } t+T > \tau \tag{7.3}$$

where τ is the pulse width.

2. Atmosphere and Optic Systems block simulates signal attenuation by the atmosphere and optics. The structure of this block is the same as in laser sensor.

3. Noise block simulates noise that affects the useful signal. The structure of the block is the same as in laser sensor.

4. Photodiode block simulates work of the photodiode, on reception of a signal. The structure of the block is similar to the block in the laser sensor.

5. The first amplifier block simulates work of the 1st Amplifier with gain factor 4. The structure of the block is same as in laser sensor.

6. The second amplifier block simulates the work of 2nd Amplifier with gain factor 20. The structure of the block is the same as in laser sensor.

7. The comparator block simulates the work of the comparator. Structure of the block is the same as in laser sensor:

$$U_c = A, \text{ if } U_{2A} > U_{thr} \tag{7.4}$$

$$U_c = 0, \text{ if } U_{2A} \leq U_{thr} \tag{7.5}$$

Where, U_c is the comparator output voltage and A represents the voltage amplitude.

The comparator block represents a subsystem that forms an output pulse only in the case of excess of input signal amplitude above a threshold level. It has two inputs. On one input the useful signal varies, and on another the threshold voltage varies. In the circuit to form the threshold voltage there is an input block of signal/noise value which provides the required level for the correct detection probability and false alarm rate. The subsystem consists of elementary blocks of Simulink.

8. The Processing block consists of:

- The matched filter adjusted to extract the pulse periodic signal with a repetition rate of 2 MHz and accumulation of six samples (the positive decision on the presence of the signal is taken as the simultaneous presence of signals on five of six outputs including

filter delay elements and repetition of the mentioned event not less than four times for all times of observation).

- The element of noise extraction taking the positive decision on the presence of noise on four of six outputs including filter delay elements simultaneously and repeats not less than 2 times for all times of observation.

- Logic element of decision-making "Controlled" or "Not controlled". The decision "Controlled" is taken at the presence of the signal of the intended frequency (2 MHz) on the matched filter output and the absence of a noise signal. Otherwise a decision "Not controlled" is taken.

"Controlled" – when $U_{proc} > 4 \cdot A$ (for ni>4) \hfill (7.6)

"Not Controlled" – when $U_{proc} \leq 4 \cdot A$ (for ni≥2) \hfill (7.7)

where ni is number of the pulses.

Modulated laser radiation in beam-riding represents periodic pulse signals with the known pulse repetition cycle T_1. For detection of such signals on a background of impulse noise or pulse signals with other periods of recurrence (T_2) the matched filter constructed on the basis of delay lines and the adder is used. Delay time in each line is T_1. The greater the quantity of delays lines, the greater the probability of correct detection of signals with period T_1. However, the circuit becomes complicated and processing time increases. Therefore, for practical reasons we have chosen only five delays lines (Figure 44).
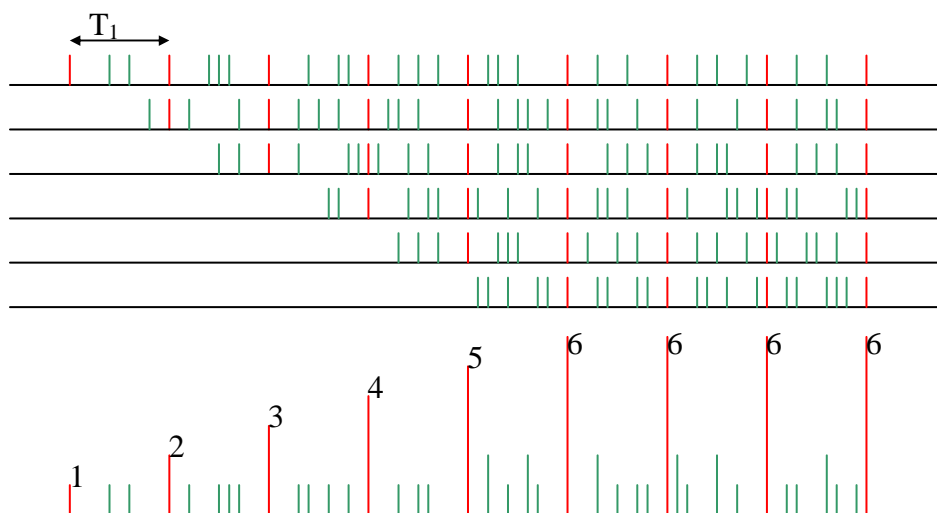
Figure 44 Processing block criteria of detection

134

Pulse signals with period T_1 after delay sum up in the adder and their amplitude increases six times. Random impulse noises and signals with other periods (T_2) practically do not sum up in the adder and their amplitude remains static. Random superposition of such pulses can take place at high enough noise density (the big pulse repetition frequency). This results in a decrease of the probability of correct detection.

For increasing the probability of correct detection of signals with period T_1, after the adder, there is a block realizing the following criteria of detection:

1. The signal with period T_1 is considered detected ("controlled") if the adder output presents not less than four signals with amplitudes 5 and 6, and amplitudes of random noise pulses do not exceed four pulses.

2. The signal with period T_1 is considered undetected ("not controlled") if the adder output presents not less than two noise pulses with amplitude 4 or in the case when the amplitude of the useful signal is less than a threshold level of the comparator.

7.3 Testing of Seeker Model

Some work has been carried out to test the seeker model performance. Dependences of the detection range on various seeker parameters and weather conditions were investigated. The same parameters used to investigate the LWS performance will b used to investigate the overall seeker performance has. However the range has increased as result of using of the narrow-band optical filter that has resulted in a decrease of background level.

Results of a study into the dependence of detection range on the change of weather conditions for various wavelengths and narrow-band optical filters are shown in Table 23.

Wavelength	Range, m				
	Good	Typical-1	Typical-2	Bad-1	Bad-2
$\lambda_1=0.63\mu m$	6900	6300	4000	2400	2200
$\lambda_2=1.06\mu m$	8800	8300	5600	2500	2300
$\lambda_3=1.54 \mu m$	11700	11300	8200	2700	2500

Table 23 Seeker controlled range versus various wavelengths at different weather

conditions

($\Delta\lambda$ = 40 nm, D=30mm, f=40mm, sand sample - A, $C_n^2=52\cdot10^{-17}$ m$^{-2/3}$)

These results show that by using the narrow-band optical filter, the detection range grows. The higher wavelengths gain longer detection ranges and with deterioration of weather conditions the range decreases.

Besides that, the overall seeker performance has been investigated for various values of modulating frequency. Results are given in Table 24.

Modulated frequency	Range, m				
	Good	Typical-1	Typical-2	Bad-1	Bad-2
$f_1=1.9MHz$	0	0	0	0	0
$f_2=2.0MHz$	8800	8300	5600	2500	2300
$f_2=2.1MHz$	0	0	0	0	0

Table 24 Seeker controlled range versus various modulated frequencies at different weather

conditions

(λ = 1.06 μm, $\Delta\lambda$ = 40 nm, D=30mm, f=40mm, sand sample - A,

$C_n^2=52\cdot10^{-17}$ m$^{-2/3}$)

Results testify that the seeker works only at corresponding value of modulating frequency to the frequency of the coordinated filter in the processing block. The seeker does not work for any other modulating frequencies.

This situation is illustrated on three oscilloscope graphs. In Figure 45, output signals of all blocks of the seeker model are recorded at a modulating frequency equal to 1.9 MHz. As

this frequency does not coincide with the frequency of the matched filter after the delay lines, signals develop during any moments of time and do not exceed the threshold criteria 7.6 and 7.7 above.
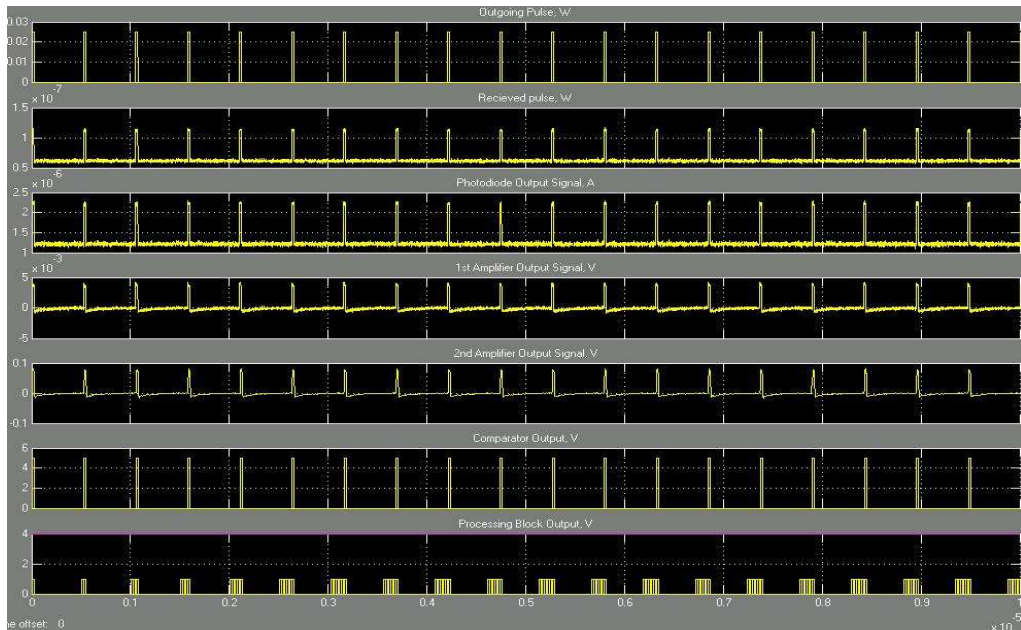
Figure 45 Seeker model output at 1.9 MHz

In Figure 46, output signals of blocks are reported at a modulating frequency of 2 MHz. In this case the matched filter is adjusted to this frequency and output signals according to criteria 7.6 are formed.
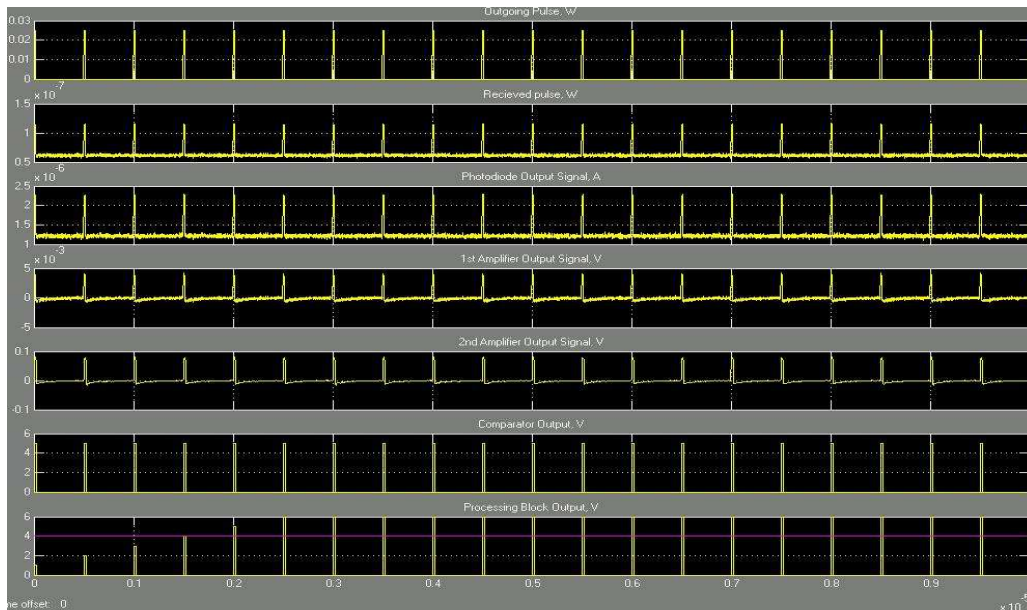
Figure 46 Seeker model output at 2 MHz

In Figure 47 output signals of blocks are given at a modulating frequency of 2.1 MHz. In this case the matched filter is not adjusted to this frequency and output signals do not exceed the threshold criteria.
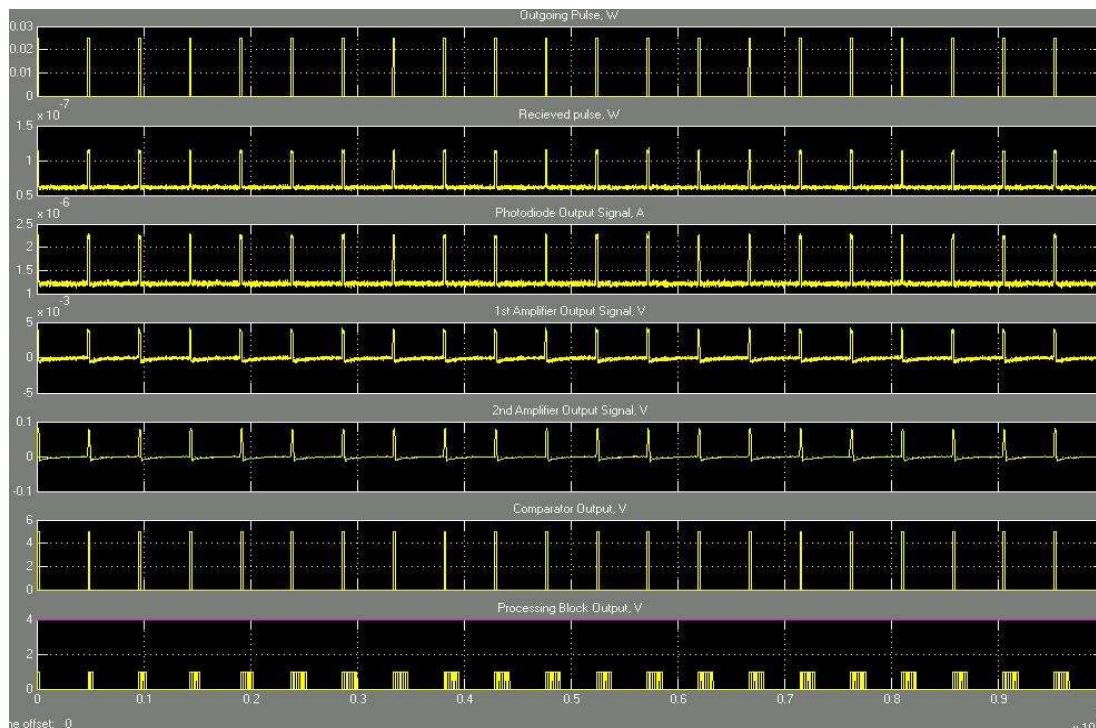
Figure 47 Seeker model output at 2.1 MHz

Studying the dependence of detection range on changes of seeker parameters and atmospheres have been carried out. In Table 25 results of detection range of the seeker with various turbulence levels are given.

	Range, m				
	Good	Typical-1	Typical-2	Bad-1	Bad-2
$C_{n1}^2=52\cdot10^{-17}$ $m^{-2/3}$	8800	8300	5600	2500	2300
$C_{n2}^2=75\cdot10^{-16}$ $m^{-2/3}$	7800	7500	5200	2300	2200
$C_{n3}^2=10\cdot10^{-14}$ $m^{-2/3}$	6900	6600	4800	2200	2100

Table 25 Changes of detection range at various turbulence strengths

(λ=1.06μm, $\Delta\lambda$ = 40 nm, D=30mm, f=40mm, sand sample - A)

Analyzing the above results, we can see that with deterioration of turbulence level and atmospheric conditions, the detection range is essentially reduced.

Research into the effect of the receiving channel performance has been carried out by evaluation of detection range for three different values of the diameter of the receiving lens (D=20mm, D=30mm, D=40mm). Results are submitted in the Table 26.

	Range, m				
	Good	Typical-1	Typical-2	Bad-1	Bad-2
D_1=20mm	7100	6800	4900	2200	2000
D_2=30mm	8800	8300	5600	2500	2300
D_3=40mm	10100	9500	6200	2600	2500

Table 26 Changes of detection range at various diameters of receiving lens

(λ=1.06μm, $\Delta\lambda$ = 40 nm, f=40mm, sand sample - A, C_n^2=52$\cdot$10^{-17} m$^{-2/3}$)

The analysis of results shows, that with increase of diameter of the receiving optical system, detection range essentially increases, which is caused by an increase of the received signal power.

Dependence of the maximal range of detection on various values of the focal length (f=30mm, f=40mm, f=50mm) have been then investigated. Results are shown in the Table 27.

	Range, m				
	Good	Typical-1	Typical-2	Bad-1	Bad-2
f_1=30mm	7800	7500	5200	2400	2200
f_2=40mm	8800	8300	5600	2500	2300
f_3=50mm	9500	9000	5900	2500	2300

Table 27 Changes of detection range at various focal lengths of receiving lens

(λ=1.06μm, $\Delta\lambda$ = 40 nm, D=30mm, sand sample - A, C_n^2=52$\cdot$10^{-17} m$^{-2/3}$)

As expected, the increase of focal length results in narrowing of field of view and accordingly decrease of background level that results in enhanced sensitivity of the receiving channel.

The influence of the photodiode sensitive area size on the detection range has also been investigated. Results for three different values of sensitive area of the photodiode (l=200 μm, l=500μm, l=800μm) are given in Table 28.

	Range, m				
	Good	Typical-1	Typical-2	Bad-1	Bad-2
l_1=0.2mm	12100	11200	6800	2500	2300
l_2=0.5mm	8800	8300	5600	2500	2300
l_3=0.8mm	7300	7000	5000	2400	2200

Table 28 Changes of detection range at various photodiode sensitive area sizes

(λ=1.06μm, $\Delta\lambda$ = 40 nm, D=30mm, f=40mm, sand sample - A, C_n^2=52·10^{-17} m$^{-2/3}$)

The analysis of the results shows that with increase in the size of photodiode sensitive area, the detection range is reduced. This is caused by the increase in noise level in the reception channel.

To investigate the dependence of detection range on the reception channel bandwidth, we present results for three different values of a bandwidth (Δf =30MHz, Δf =65MHz, Δf =100MHz), given in Table 29.

	Range, m				
	Good	Typical-1	Typical-2	Bad-1	Bad-2
Δf_1=30MHz	8800	8300	5600	2500	2300
Δf_2=65MHz	7400	7000	5000	2200	2100
Δf_3=100MHz	6600	6300	4600	2100	1900

Table 29 Changes of detection range at various bandwidths

(λ=1.06μm, $\Delta\lambda$ = 40 nm, D=30mm, f=40mm, sand sample - A, C_n^2=52·10^{-17} m$^{-2/3}$)

From the above table we can conclude that with increase in bandwidth, the detection range decreases. This is caused by an increase of noise level of the reception channel.

The effect of photodiode parameters have been carried out using the following evaluation of detection range for various values of photodiode spectral response: S_λ=46.84A/W,S_λ

=19.77A/W, S_λ =9A/W. This evaluation was done whilst keeping the other parameters fixed. The results are given in Table 30.

	Range, m				
	Good	Typical-1	Typical-2	Bad-1	Bad-2
λ=1.02μm (S_λ=46.84A/W)	10400	9700	6200	2700	2500
λ=1.06μm (S_λ=19.77A/W)	8800	8300	5600	2500	2300
λ=1.1μm (S_λ=9A/W)	5700	5600	4400	2100	1900

Table 30 Changes of detection range at various photodiode spectral responses

($\Delta\lambda$ = 40 nm, D=30mm, f=40mm, sand sample - A, C_n^2=52·10^{-17} m$^{-2/3}$)

Analysis of results has shown that with increase of the photodiode spectral response detection range is increased. It is caused by an increase of signal/noise ratio in the received channel. Also dependence of range on change of temperature has been investigated. Results of this study are submitted in Table 31.

	Range, m				
	Good	Typical-1	Typical-2	Bad-1	Bad-2
T_1=300K	8760	8280	5610	2310	2120
T_2=320K	8740	8260	5600	2300	2120
T_3=340K	8720	8250	5590	2290	2110

Table 31 Changes of detection range at various temperatures

(λ=1.06μm, $\Delta\lambda$ = 40 nm, D=30mm, f=40mm, Δf=30MHz, R_L=10^{3}Ohm,

sand sample - A, C_n^2=52·10^{-17} m$^{-2/3}$)

The analysis of results has shown that this dependence weak. It is caused by a dominating role of shot noise of the received channel within the APD photodiode.

7.4 Conclusions

The seeker model has been discussed theoretically and built as a model using Mathlab and Simulink codes. It has been tested for various weather conditions. In addition, investigation has been carried out to find the effect of other parameters on the performance of the seeker and its components.

Dependence of detection range on weather conditions for various wavelengths and narrow-band optical filters show that the detection range grows with a narrow-band optical filter because of decreasing the noise level entering the receiving path. It was clear that using higher wavelengths gives longer detection range and with deterioration of weather conditions it decreases. Moreover, it was clearly proven that the seeker works only at the specified modulated frequency.

The seeker detection range essentially reduced with the increase of turbulence level and deterioration in atmospheric conditions. Simulation results indicate that with the increase of receiving optical system diameter, detection range essentially increases that is caused by a rise of the quantity of received signal power. As expected, the increase of focal length results in narrowing of the field of view and accordingly leads to a decrease of background level that causes enhanced sensitivity of the receiving channel.

Simulation results show that with an increase in the size of the photodiode sensitive area and bandwidth the detection range is reduced. It is caused by the increase in noise level in the reception channel. Nevertheless, analysis of results proved that with an increase of the photodiode spectral response, the detection range is increased. It is caused by the increase of signal/noise ratio in the received channel. Finally, the performance of the seeker matched the expected results.

7.5 References

[1] Counter-measure Systems, Voulme 7, David H. Pollok, page 118.

[2] Internet. Laser Seeker (DOD, NATO). 2/12/2005.

[3] Internet. US Patent 5023888. Pulse code recognition method and system. 16/11/2005.

[4] Internet. Laser Guidance. Wikipedia article. 5/12/2005.

[5] Internet. Beam Riding. Wikipedia article. 25/11/2005.

[6] Internet. Pulse code (DOD). 25/11/2005.

[7] Internet. Laser Mythology. Global Security. Org. 10/12/2005.

[8] Internet. Laser Guided Bombs. Tactical Air Command Pamphlet 50-25. 10/12/2005.

CHAPTER 8

Development of Counter-measures Model

8.1 Principles of countermeasures

A counter-measure can be regarded as a system (usually for a military application) that is designed to prevent weapons from acquiring and/or destroying a target. Counter-measures are devices, techniques, or actions taken in order to undermine the operational effectiveness of enemy activities. These enemy activities depend on, or take advantage of, the technical and operational characteristics of components like electro-optical sensors and/or millimeterwave systems. Counter-measures also include all means to analyze enemy activity, determine the enemy's intention and exploit this knowledge to reduce enemy effectiveness [1].

These preventive techniques may also function by concealing sensory signatures of the target. In addition, they can also disrupt the target detection systems of the attacker. They can act against target acquisition systems that depend on electronic, thermal, infrared, optical, or radar technology. Moreover, counter-measures are most popularly associated with aircraft defence, examples include metallic foil chaff to disrupt radar detection, decoy flares to disrupt infrared, and electronic systems to disrupt other targeting and communications systems. However, land and sea-based forces can also use such measures with smoke-screens to disrupt laser ranging, infrared detection, laser weapons, and visual observation.

Counter-measures not only avoid detection and identification by an enemy sensor or weapon, but they are also thought to include means to reduce the effectiveness of their destructive systems. Electronic counter-measures (ECM) systems are one way to deal with the enemy threat. The subdivision of an ECM system involves: (a) threat warning and avoidance, (b) detection/finding, (c) target homing and tracking and (d) selection of the proper response to the incoming threat. Effective ECM may involve spot/barrage/sweep jamming, chaff and infrared flares, deception (creation of a false radar image) and the activation of radar decoys. High speed signal processing is critical in order to deal with the short response time successfully [2].

This subject closely revolves around classified information and this can be a major difficulty in studying counter-measures. Receivers determine the presence or absence of a contact. Detection sensors heavily depend on these receivers. Possessing the technical means to disrupt or deceive that receiver is, therefore, an advantage one would guard very closely, by keeping this information classified [2].

All Infra-red (IR) direct threat weapons require line of sight (LOS) to be established prior to launch and the in-flight missile must maintain LOS with the target heat source until impact (or detonation of the proximity fuse). IR missiles require the operator to visually detect the target and energize the seeker before the sensor acquires the target. The operator must track the target with the seeker docked to the LOS until can be determined that the IR sensor is tracking the target and not any background object (natural or man made objects to include vehicles, sun, or reflected energy from the sun off clouds, etc.). The IR sensor is also susceptible to atmospheric conditions (haze, humidity), the signature of the aircraft and its background, flares, decoys, and jamming. When an aircraft has been detected, targeted, locked-on, and the missile fired, it becomes essential for survival to defeat the incoming missile. Of course, except in the case of autonomously guided missiles, counter-measures against the ground (or hostile aircraft) tracking and command guidance system could still be effective [2].

IR guided missiles like shoulder-launched "fire and forget" types can be a real challenge. In most cases, such missiles require lock-on prior to launch; they do not have autonomous reacquisition capability[3]. Given an adequate hemispheric missile warning system , it is quite conceivable that the missile can be defeated in flight. One technique to defeat guidance elements is to use an RF weapon (directed from the aircraft under attack, or counter-launched). For optical or IR seekers that are obviously not "in-band" to the RF weapons, a "back-door" means of coupling the RF energy into the attacking missile must be used. Such back-door mechanisms exist; however, they are thought to be unpredictable and statistically diverse. The inaccuracy of these techniques differs from missile to missile within the same class and depends on the missile's maintenance history [4].

The following four factors and considered to be very important when counter-measures are developed for opto-electronic guidance systems of high-precision:

- Spectral range in which guidance systems is operating (visible, near infrared, middle wave infrared, long wave infrared)
- Principles of guidance (passive, active, semi-active)
- Placing of sensitive elements (in a front or rear part of the carrier)
- Duration of guidance process

In anti-tank systems using beam-riding guidance (semi-active), the missile itself corrects a movement trajectory to the target, being all the time inside (within) a laser beam. The laser beam is formed at the aiming station and goes on the target. The missile continuously receives the information on it's spatial position due to special modulation of a laser beam. This information is formed in the seeker that is located in rear part of a missile. Such guidance systems usually work in the near infrared spectrum (spectral range).

To cause the failure of guidance processes of missiles and reduction of fighting efficiency of similar anti-tank devices it is possible to use the following counter-measures:

- Smoke (aerosol) screens
- Active jamming
- Formation of decoys
- Destruction of anti-tank missiles in flight

Warning systems are essential for the counter-measure process [5]. This element of the self-protection suite determines threat presence, threat bearing, and, under certain conditions, degree of lethality. With this information the operator can take effective evasive action and activate counter-measures. Some systems automate this process.

The function of a warning system is to detect threats approaching the system and to alert the protected entity (nation, aircraft, ship, ground vehicle, soldiers) about a near-term danger. Thus, it differs in philosophy, and in the applied technologies, from reconnaissance and surveillance, which involve the longer term observation and characterization of potential

adversary, and from tracking and/or fire control, which involve detailed concentration on a detected threat. Typical warning scenarios involve a platform, or area, to be protected; an immediate danger; and an environment containing a variety of other (unimportant) objects/events that must be distinguished from the potential threat. Usually a warning device is continuously operative, has a wide field of regard, and covers a broad range of threat parameters.

The warning function involves continuous observation of the activities within its environment, detection/recognition of threats, detailed characterization of the threat, and alerting of its platform. Threat characterization must be of high reliability to avoid disturbing the platform with spurious alarms; also, it must be sufficient to enable the platform to initiate appropriate responsive actions. Once the warning system has alerted its platform to the impending threat, characterized it, and located it, the subsequent defensive action passes to other elements in the platform defensive/offensive suite.

8.2   Screening Systems

Smoke is a suspension in air (aerosol) of small particles resulting from incomplete combustion of a fuel. It is commonly an unwanted by-product of fires (including stoves and lamps) and fireplaces, but may also be used for pest control (cf. fumigation), communication (smoke signals), and defence (smoke-screen). Smoke particles are actually an aerosol (or mist) of solid particles or liquid droplets that are close to the ideal range of sizes for Mie scattering of the radiations (UV, VIS, IR). This effect has been likened to three-dimensional textured privacy glass, the smoke cloud does not obstruct an image, but thoroughly scrambles it [6].

Depending on particle size, smoke can be visible or invisible to the naked eye. A smoke-screen is a release of smoke in order to mask the movement or location of military units such as infantry, tanks or ships. It is most commonly deployed in a canister, usually as a grenade. The grenade releases a very dense cloud of smoke designed to fill the surrounding area even in light wind. Whereas smoke screens would originally have been used to hide movement from enemies' line of sight, modern technology means that they are now also available in new forms; they can screen in the infrared as well as visible spectrum of light to prevent detection

by infrared sensors or viewers, and are also available for vehicles is a superdense form used to prevent laser beams of enemy target designators or range finders on vehicles[6].

Use of smoke (aerosol) screens near the target allows a laser beam from a guidance system to be blocked and, thus, provide in conditions of the absence of direct visibility of the target failure of the guidance process of a missile. In this case, the laser warning system detects the threat laser system and automatically orients the turret in the direction of the threat. It then triggers the grenade launchers which create an off board smoke (aerosol) screen. The composition of this cloud is intended to screen the tank against laser designator and beam-riding threats and is also claimed to be sufficiently hot to seduce infra-red homing weapons away from the tank.

In a smoke (aerosol) screen the laser beam will have very strong attenuation due to the effects of scattering and absorption. Such attenuation can be described by expression [7]:

$$T_s = \exp[-(\alpha_{abs} + \alpha_{scat}) \cdot z], \tag{8.1}$$

where,

T_s - transmission factor of the smoke (aerosol) screen

α_{abs} - attenuation factor caused by absorption of laser radiation

α_{scat} - attenuation factor caused by scattering of laser radiation

z - depth of a cloud (screen) at the height of the laser beam

Expression (8.1) is used in counter-measure model for describing the influence of smoke (aerosol) screens on the efficiency of guidance process of a missile to the target. Values of parameters in expression (8.1) are taken from the specifications used in Grenade Systems.

8.3 Active jamming

Communications jamming is usually aimed at radio signals to disrupt control of a battle. A transmitter, tuned to the same frequency as the opponents receiving equipment and with the same type of modulation, can with enough power override any signal at the receiver. The most

common types of this form of signal jamming are: Random Noise; Random Pulse; Stepped Tones; Wobbler; Random Keyed Modulated CW; Tone; Rotary; Pulse; Spark; Recorded Sounds; Gulls; and Sweep-through. All of these can be divided into two groups obvious and subtle [8].

Obvious jamming is easy to detect as it can be heard on the receiving equipment. It is some type of noise such as stepped tones (bagpipes), random-keyed code, pulses, erratically warbling tones, and recorded sounds. The purpose of this type of jamming is to block out reception of transmitted signals and to cause a nuisance to the receiving operator[8].

Subtle jamming is that during which no sound is heard on the receiving equipment. The radio does not receive incoming signals yet everything seems superficially normal to the operator. These are often technical attacks on modern equipment. Radar jamming is the intentional emission of radio frequency signals to interfere with the operation of a radar by saturating its receiver with false information. There are two types of radar jamming: noise jamming and deception jamming [9].

A noise jamming system is designed to delay or deny target detection. Noise jamming attempts to mask the presence of targets by substantially adding to the level of thermal noise received by the radar. Noise jamming usually employs high power signals tuned to the same frequency of the radar. The most common techniques include barrage, spot, swept spot, cover pulse, and modulated noise jamming. Noise jamming is usually employed by stand-off jamming (SOJ) assets or escort jamming assets[9].

Deception jamming systems (also called repeat jammers) are designed to offer false information to a radar to deny specific information on either bearing, range, velocity, or a combination of these. A deception jammer receives the radar signal, modifies it and retransmits the altered signal back to the radar[9].

Initially, the challenge was simple: tune in to the fixed frequencies of the radar, and then start jamming on those frequencies. However, as radars became more sophisticated they used irregular noise superimposed on the radar signal to cloak it, and the signals were broken up into short bursts, and the frequencies used were changed rapidly and constantly.Radar

jamming for the purposes of defeating speed detection radar is simpler than for military application, although it is often illegal.

In anti-tank systems using beam-riding guidance, the seeker is located in rear parts of the missile. In this case the active optical jammer in the field of view of the seeker. The main task of the active jammer will consist in the formation of false signals in the control loop of anti-tank missiles with semi-automatic command systems of guiding. Thus the jamming represents modulated or noise-like radiation which generates false signals in the receiving path of the seeker. The jamming power at the input of the seeker optical system can be represented by the following expression (from geometry as in the laser sensor discussed in Chapter 3):

$$P_j(t) = P_{0j} \cdot \frac{B_D}{B_j} \cdot e^{-\alpha_j \cdot z_j} \cdot \frac{D^2}{\theta_j^2 \cdot z_j^2} \cdot F(t) \qquad (8.2)$$

where,

$P_j(t)$ - jamming power at the seeker input

P_{0j} - average power of jamming radiation

B_D – seeker bandwidth

B_j - bandwidth of a jamming radiation

α_j - attenuation factor of jamming radiation

z_j - distance from the jammer up to seeker

D - diameter of a receiving lens of seeker;

θ_j - divergence (the angular dimension) of jamming radiation;

$F(t)$ - modulation function of jamming radiation.

In case of using noise-like jamming:

$$F(t)=n(t), \qquad (8.3)$$

where $n(t)$ is gaussian, stationary white noise with parameters $\sigma_n^2=1$; $m_n=0$.
Its probability density is described by expression [10]:

$$p(n(t)) = \frac{1}{\sigma_n \cdot \sqrt{2\pi}} \cdot \exp(\frac{-(n - \overline{m}_n)^2}{2\sigma_n^2}) \,, \qquad (8.4)$$

where n is the current value of jamming and is:

$$n = n_j - \eta \,, \qquad (8.5)$$

$\eta = 0\ldots1$ representing the threshold that helps setting the required density of the jammer. Expressions 8.2-8.5 were used in the counter-measure model for imitation of the jammer influence on the operational capability of the system.

The process of jamming guidance systems, in which the seeker is placed in a rear part of a missile, is difficult enough. The most probable scenario in this case is jamming from on board of an airborne vehicle (helicopter, unmanned vehicle, etc.) after reception of a preliminary command on a radio channel about a threat from the warning system (laser warning system or other means) which is placed on the armoured vehicles.

Active infrared counter-measures, in contrast to off-board expendable decoys, are on-board systems that utilize an active radiator to augment the signal that the missile receives from the platform engines and other radiating body parts. The active radiator can be derived from numerous sources: lasers, arc lamps, incandescent lamps, or cavities heated by burning fuel. The active infrared counter-measure systems required modulation schemes to be applied to the output of the active radiating source to provide a time-varying signal at the missile seeker. This signal would then interact with the seeker reticle modulated signal. The result generates false guidance commands to the missile aerodynamic control surfaces.

8.4 Decoy

A decoy is usually a person, device or event meant as a distraction to conceal what an individual or a group might be looking for. Decoys have been used for centuries most notably in game hunting, but also in wartime and in committing or resolving crimes. The decoy in war may *e.g.* be a wooden fake tank, designed to be mistaken by bomber plane crews to be real, or a device that fools an automatic system such as a guided missile, by simulating some physical properties of a real target [11].

Expendable decoys, in contrast, generate a very high intensity radiation source resulting from a chemical or pyrotechnic reaction. The reaction usually involves the burning of magnesium powder in the presence of other constituents, which creates magnesium fluoride and magnesium oxide, providing very high signals in the CO_2 and H_2O bands in the mid-infrared spectrum. The high signals received by the seeker mask the defended platform's much lower radiated signals and the missile is successfully decoyed away from the target [12].

The decoy is ejected away from the defended platform by an explosive charge drawing the threat away. Flare decoys are the primary defense against heat-seeking missiles for many high-performance fighter aircraft in addition to helicopters and slower flying transport aircraft.

8.5   Destruction

Destruction of a rocket or a missile during its flight to a target is considered a failure of performing a fighting task which, at the same time, is considered to be a very successful counter-measure. After detection of the attacking missile, the command must be given to the assets responsible of dealing with such threat. In this case rigid requirements to the speed of systems are crucial. In the following sections, we present the counter-measures model and the tests carried out. Finally, conclusions will be drawn from the analysis of results.

8.6   GUI for Counter-measures Model

A GUI designed in Matlab facilitates the user to run the counter-measure model easily. Figure 48 shows the GUI layout.
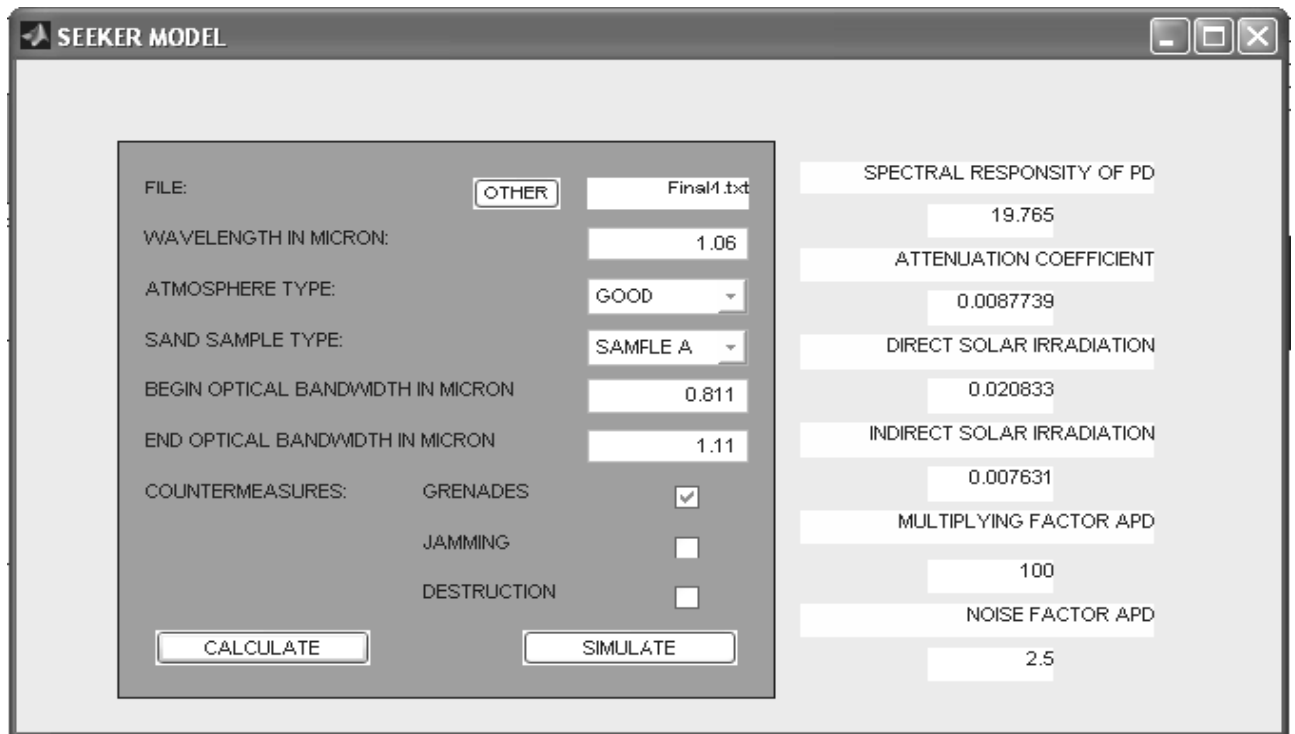
Figure 48 GUI layout for counter-measures model

It is similar to the GUI used in the laser sensor model, with the addition of three counter-measures. So, the user has the option to choose which counter-measure is selected for particular parameters being used for the model.

8.7   Testing of Counter-measures Model

On the basis of the analysis of possible variants of counter-measures, the seeker model with the counter-measures block has been developed. The model is shown in Figure 49. Three types of counter-measures have been used:

1. Grenade - smoke-screens
2. Jamming
3. Destruction

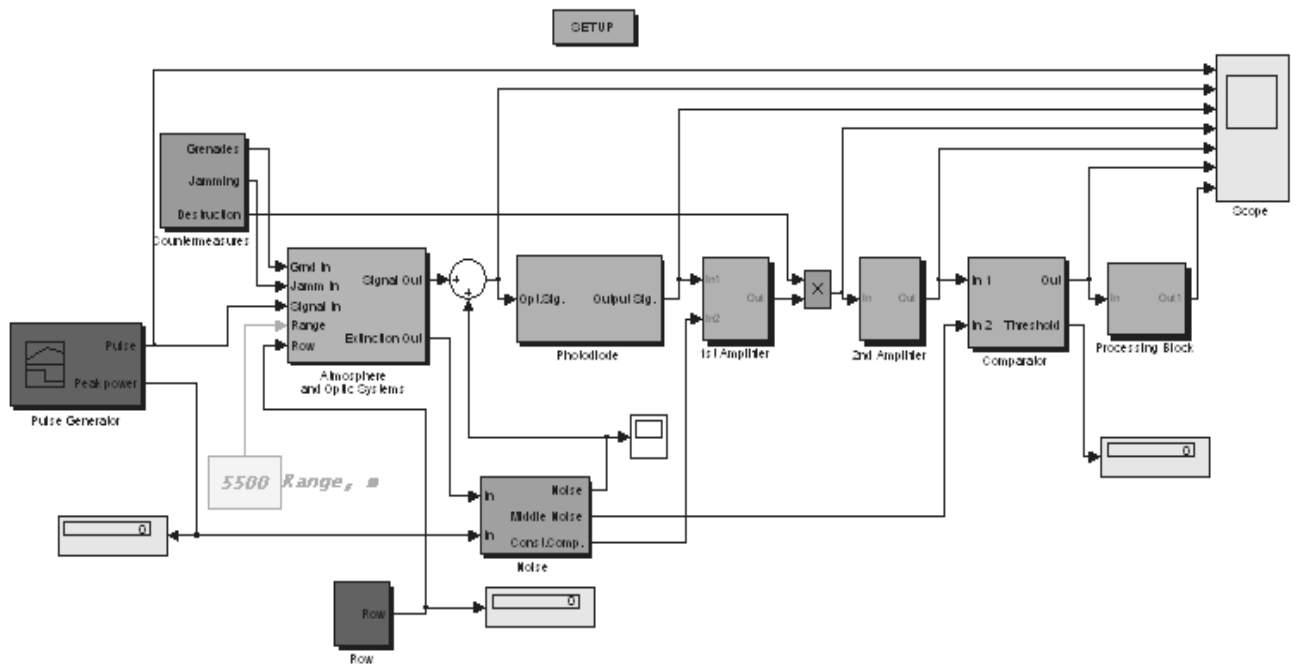Testing of the model for each type of counter-measures has been carried out.

Figure 49 Counter-measures model layout

The dependence of attenuation coefficient of laser radiation in a smoke-screen on the range up to the target, to ensure a failure of the guidance process, is shown in the results of Table 32.

R, m	α_{min}, m^{-1}
100	1.28
500	0.84
1000	0.65
1500	0.53
2000	0.45
2500	0.38
3000	0.33
3500	0.28
4000	0.24
4500	0.21
5000	0.18
5500	0.15

Table 32 Minimum attenuation coefficient required vs range for grenade counter-measure

($\lambda = 1.06$ μm, $\Delta\lambda = 40$ nm, D=30mm, f=40mm, sand sample - A,

$C_n^2 = 52 \cdot 10^{-17}$ m$^{-2/3}$)

154

Table 33 shows attenuation coefficients for various atmospheric conditions. It is the minimum attenuation coefficient that the smoke grenade must produce to effectively counter-measure the laser beam at the given range.

R, m	α_{min}, m^{-1}				
	Good	Typ-1	Typ-2	Bad-1	Bad-2
1000	0.65	0.65	0.65	0.6	0.58
1500	0.53	0.53	0.52	0.37	0.34
2000	0.45	0.45	0.42	0.18	0.13

Table 33 Minimum attenuation coefficient required vs range at diffirent weather conditions for grenade counter-measure

(λ = 1.06 μm, $\Delta\lambda$ = 40 nm, D=30mm, f=40mm, sand sample - A, C_n^2=52·10^{-17} m$^{-2/3}$)

Analysis of results shows that with increase in distance up to the target and deterioration of atmospheric conditions, the attenuation coefficient for laser radiation in the smoke-screen are reduced.

The influence of jamming on operational capability of the seeker has been investigated. Results are given in oscilloscope traces Figures 50, 51, and 52.
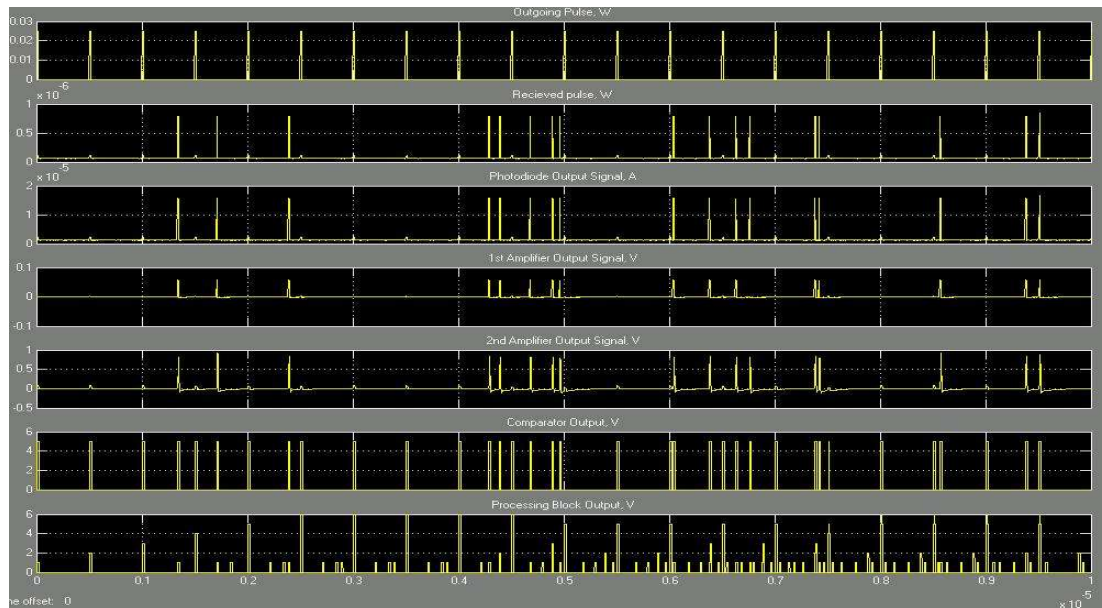
Figure 50 Output signals of seeker model with countermeasures at low density noise-like jamming ($\eta = 0.7$)

In Figure 50, output signals of the seeker model with countermeasures are shown with low density noise-like jamming ($\eta = 0.7$). In this case, the probability of occurrence of a false pulse at the output of the processing block is very low. Analysis of the oscilloscope output shows that with low density noise-like jamming, formation of a false pulse does not occur. In this case, the modulating frequency of interest is the only frequency detected and mode of steady control is maintained.
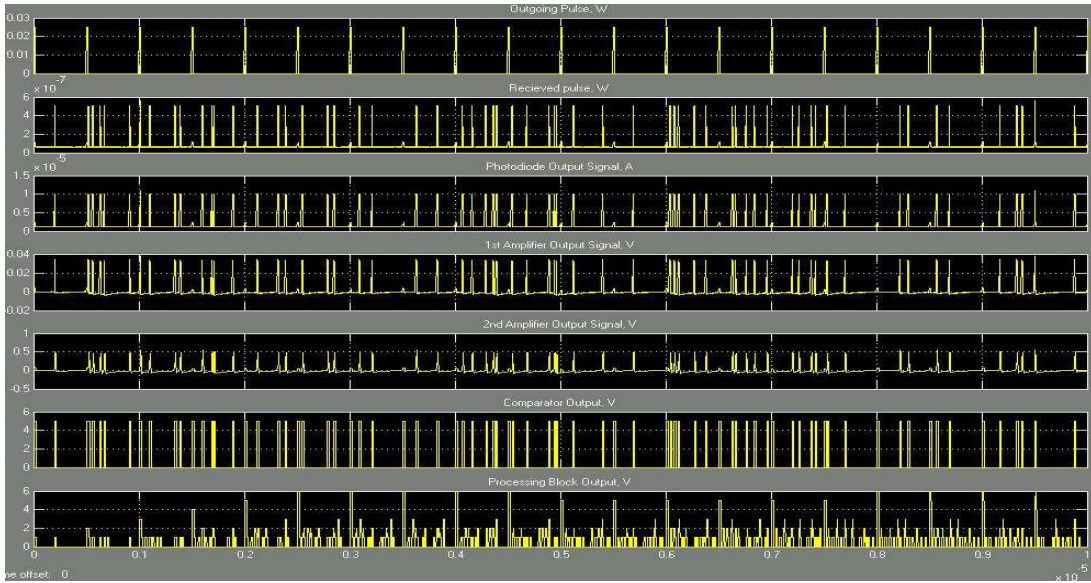
Figure 51 output signals of seeker model with countermeasures at the raised density noise-like jamming ($\eta = 0.5$)

In Figure 51, output signals of the seeker model with countermeasures are given at the raised density of noise-like jamming ($\eta = 0.5$).The oscilloscope output shows that with increase in density of noise-like jamming, there is superposition of the random pulses. In this case, formation of false signals does not occur because the random pulses do not exceed the established threshold.
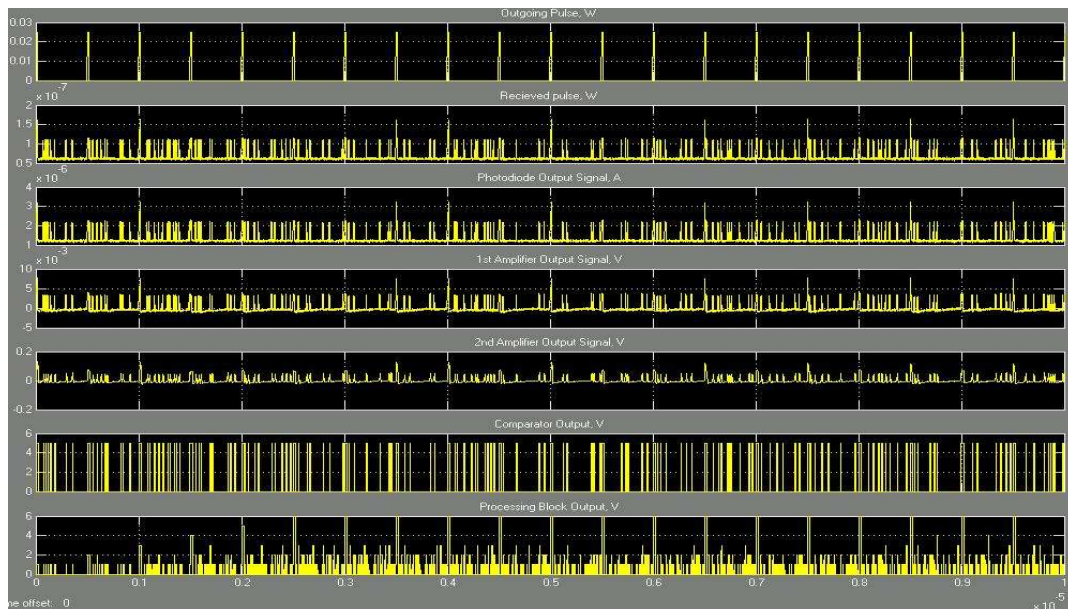

Figure 52 output signals of the seeker model with countermeasures at very high density noise-like jamming ($\eta = 0.3$)

In Figure 52, output signals of the seeker model with countermeasures are shown with very high density noise-like jamming ($\eta = 0.3$). In this case, the probability of occurrence of a false pulse at the output of processing block is high. This shows that with the increase in density of pulse random jamming, false signals are formed at the output of the matched filter. These signals enter in the control loop of a missile and result in errors (or failure) of the guidance process.

8.8 Conclusions

Results show that using of various types of counter-measures essentially influence the stability of the guidance process of anti-tank missiles. Applying of the smoke (aerosol) grenades as countermeasures for beam-riding systems is possible only on the basis of information on an irradiation from the laser warning receiver. The smoke (aerosol) screen should occur in a short time which is less than time of flight of a missile up to the target. The type of smoke (aerosol) grenades should be chosen for the required conditions of attenuation of the laser radiation (Table 31 and 32) and must cover the used spectral range of systems.

Using active jamming for the beam-riding systems is possible if the jammer is placed into the field of view of the missile seeker. Parameters of a jammer can be taken according to expressions 8.2-8.5. With increase in density of jamming, requirements for higher power of the jamming source are reduced. When using noise-like jamming with sufficient density, there is a superposition of the random pulses at the output of the matched filter. This leads to false signals in the control loop of missile those results in a failure of the guidance process.

8.9 References

1. http://en.wikipedia.org/wiki/Countermeasures. 11/11/2005.

2. http://www.fas.org/man/dod-101/navy/docs/fun/part11.htm. 11/11/2005.

3. http://www.globalsecurity.org/military/systems/aircraft/systems/ircm.htm. 25/10/2005.

4. http://www.globalsecurity.org/military/systems/aircraft/systems/ircm.htm. 25/10/2005.

5. http://www.globalsecurity.org/military/systems/aircraft/systems/ircm.htm. 25/10/2005.

6. The Infrared and Electro-Optical Systems Handbook. Volume 7. Countermeasure Systems. 1993, p.3-5.

7. http://en.wikipedia.org/wiki/Smoke-screen. 11/11/2005.

8. The Infrared and Electro-Optical Systems Handbook. Volume 7. Countermeasure Systems. 1993, p.370.

9. http://en.wikipedia.org/wiki/Jamming. 11/11/2005.

10. http://en.wikipedia.org/wiki/Radar Jamming. 12/11/2005.

11. Gregory R. Osche. Optical Detection Theory for Laser Applications. A John Wiley and Sons, Inc., Publication, 2002, p. 7.

12. http://en.wikipedia.org/wiki/Decoy. 12/11/2005.

13. http://www.fas.org/man/dod-101/navy/docs/fun/part11.htm. 11/11/2005.

CHAPTER 9

THESIS CONCLUSIONS AND RECOMMINDATIONS

9.1 Introduction

This thesis has described the research work preformed designing, developing, and testing a new laser sensor model, laser seeker, and counter-measures system using Matlab and Simulink software. It has examined the vulnerability of laser warning systems to guided weapons especially laser beam-riding missiles that use low power lasers in their guidance systems. The idea to do his project came as a result of the unexpected poor performance of a number of warning systems during field trials in the United Arab Emirates desert. The bad weather conditions, the high temperatures, and other factors were the reason to initiate this project. The goal was to help find a solution for these systems to do their job in protecting the tanks and armoured vehicle crews from such a threat.

The objective of this work was to study the reasons for the performance degradation of the laser warning systems in the weather conditions of United Arab Emirates and to develop and recommend optimization of their structure, characteristics and hence increase the overall performance. In addition, it covered the laser seekers used in beam-riding systems, their problems and evaluation of an opportunity of effective functioning in the severe weather conditions of United Arab Emirates. Moreover, developments of counter-measures, which can deceive laser beam-riding anti-tank missiles from destroying the armoured and personnel carriers were investigated.

For this purpose, mathematical models of the laser sensor, laser seeker and laser seeker with countermeasures have been developed. The laser sensor model is the base structure for the other two models which differ from it only by additional blocks of processing and counter-measures and in some of the parameters of each one of them.

The computer model has been developed to enable the assessment of all phases of a laser warning receiver and missile seeker. MATLAB & SIMULINK software have been used

to build the model. During this process experimentation and field trials have been carried out to verify the reliability of the model.

9.2 Conclusions

- The survivability of tanks and armoured vehicles is one of the most difficult challenges for military technology. The cycle of threat and counter-measures will never stop. The hard kill defensive aid has been proved as a successful system when it comes to protecting the crew and its capabilities. Soft kill is another system that should be considered as the future of counter-measure systems because of its relative simplicity and low cost compared to hard kill systems.

- For increase of efficiency for laser warning sensors with increase detection range, it is necessary to improve the sensitivity of the receiving channel and reduce the influence of various factors which were found as a result of research and development of the laser sensor.

- The model of the laser sensor is executed in a MATLAB program and represents the set of blocks combined by a unified algorithm of the laser sensor operation. These blocks realize mathematical transformations which adequately describe the physical processes occurring in each element of the model (Chapter 3).

- The structure of the laser sensor consists of:

1. Block of input signals describing the process of formation of the laser pulses with the required parameters.
2. Block of an atmosphere describing the attenuation of radiation while travelling through the atmosphere and its distortion caused by turbulence.
3. Block of noise describing the processes of formation of external and internal noises.
4. Block of the photodiode describing the transformation of an optical signal to an electric signal.
5. Block of 1st amplifier describing the process of amplification of a signal in the 1st cascade.

6. Block of 2nd amplifier describing the process of amplification of a signal in the 2nd cascade and its filtration in the limited pass band.

7. Block of the comparator describing the extraction and transformation of an analog signal to a digital signal.

- Such a structure of the model makes it possible to evaluate each factor and each elements influence on the sensor operation. Parameters of each element were selected from condition of their conformity to the real physical components. For evaluation of atmospheric conditions influence, LOWTRAN VII atmospheric computer code was used.

- The solar effect is an essential factor which has been considered in the model for these systems deployed in UAE desert. Three sand samples have been brought from the United Arab Emirates to study the reflectivity characteristics of these samples in various spectral ranges. These samples have been subject of an experiment to read the reflectivity of each one of them. Results of this study were used for evaluation of the reflective level part of the background radiation and the effect of that on the laser sensor performance.

- Testing of the model was carried out on the basis of atmospheric conditions typical for the United Arab Emirates and real characteristics of the components. Results of testing show good conformity of the model signals with output signals of real optoelectronic devices.

- The model runs as designed and detects the weak optical signal at 5.5 km (which is the maximum range for antitank missiles) or more since the maximum detected range obtained in the real trials was 4.5 km.

- The laser sensor model has been built and tested for different cases and weather conditions. The outputs of the model demonstrate it is behaving as predicted. The model is flexible and general enough to encompass all expected variations and can easily be updated with new or different data files.

- The analysis of output results testifies that the detection range essentially depends on atmospheric conditions, concrete performance of the receiving channel and the photo detector type. For the given characteristics of the laser sensor the maximal range of detection does not exceed 5.5km. With deterioration of atmospheric conditions the range of detection is essentially reduced and in the range from Good up to Bad-2, it reduces by a factor of 2.

- The type of sand as a reflecting surface for indirect solar irradiation has an influence on the detection range under good atmospheric conditions only. Under bad atmospheric conditions other factors dominate.

- The laser sensor was built as hardware and tested for various cases. A lot of parameters have been evaluated to see if we can match the output coming from the laser sensor model simulation. The experimental work divided into two parts, first without light source and second when adding the light source to see the effect of solar background on the output results just like in the simulation. First, a mathematical model of the experimental setup was introduced and discussed. It was important to define the dependence between value of transmission of optical attenuator filters, used to carry out the test, and values of the corresponding distances from laser source to the photoreceiving device. Then, and after creating the calibration curve, we read the output for various cases without the light source and ran the simulation model for the same setup. The results show that there are small differences between the two outputs and that can be explained as a result of the nonlinear operation of the amplifier. The same process has been repeated but with a light source to imitate the solar background. Comparison of experimental results with the model shows rather good correspondence.

- Dependence of the laser sources detection range on the change of key parameters of the sensor and weather conditions (Chapter 6) was investigated.

- The analysis of the received results has shown that the overall performance of the laser Sensor essentially depends upon:

   1. Status of the atmospheric conditions at the time of performance

2. Atmospheric turbulence level

3. Parameters of the optical model

4. Type and characteristics of the photodiode

5. Parameters of the amplification path

- An estimation of the threshold sensitivity of the sensor is discussed and analyzed considering all the noise sources possible such as shot noise of the dark current, shot noise of signal fluctuations, shot noise of the background radiation, and thermal noise of the electronic path. It was clear that for a reduction in background radiation, it is necessary to reduce the field of view of sensor by increasing the focal length and reduction of the dimension of the sensing area of photodetector.

- Atmospheric turbulence was another issue discussed in this thesis to understand its effect on the output of the sensor and how to overcome any problems it posed. It results in fluctuation of phase longitudinally in the beam and also across the laser beam that reduces temporal and spatial coherence of the radiation. Fluctuations in laser beam angle of arrival were studied and it was clear that when atmospheric turbulence increased, the dispersion of arrival angle of radiation essentially grows.

- Influence of laser sensor parameters on the performance was investigated. The results show that the detection range essentially decreases with deterioration of atmospheric conditions as turbulence strengthens.

- **Factors Impairing The Efficiency of The Laser Sensor**

On the basis of the research results of the laser sensor model the factors reducing the detection range of the laser sources radiation have been established. These factors are:

1. Significant attenuation of laser radiation in an atmosphere connected strongly to changes of weather conditions.

2. The influence of atmospheric turbulence can be seen in the expansion of laser beam, strong fluctuations of its intensity and arrival angle.

3. Non-optimum choice of optical system parameters, diameter of aperture D and Focal length f, results in decrease in the level of useful signal and increase in the level of background radiation.

4. Non-optimum choice of spectral bandwidth of the optical filters causes an increase in the level of background radiation.

5. Discrepancy of the wavelength of the laser source to the maximum spectral sensitivity of the photodetectors results in a decrease of the level of signal in the receiving path.

6. Strong dependence of the photodetector amplification on temperature in the case of using an Avalanche Photo Diode (APD).

7. Non-optimum choice of the size of sensitive area of the photodiode results in an increase of noise level.

8. Non-optimum choice of bandwidth of the amplification cascade results in distortion of the resulting signal or in increase of noise level.

9. Absence of measures of decreasing noise in the receive channel.

10. Non-optimum choice of the threshold level of the comparator.

- **Requirements of Laser Sensor Parameters**

On the basis of the analysis of the factors impairing efficiency of the laser sensor performance, the requirements of its key parameters have been developed and they allow us to increase the detection range of laser sources. These requirements are as follows:

1. Diameter of the aperture of receive optical system should be as large as possible (Table 17) with the purpose of maintaining the required maximal values that can be accepted the laser signal. Size restriction of the aperture will be connected only with weight and dimension restrictions of the optical system and its cost.

2. The focal length of the receiving lens should be chosen to maintain the minimal possible field of view (Table 18) in order to decrease the level of background radiation. The increase of focal length will be limited by the dimensions of optical system and necessity of maintaining sufficient light exposure of the image and required field of view of the sensor (typically 360° in azimuth) and hence may require more sensors.

3. The spectral bandwidth of the optical filters should be as small as possible (Table 19) in order to decrease the level of the background radiation and increase the detection

range. However, this is limited by the quantity of fragmentation of the set spectral range and the necessity of considering the temperature effect on the laser radiation.

4. Spectral sensitivity of the photodiodes should be maximal (Table 20) for the wavelengths used by the laser radiation sources.

5. When using Avalanche Photo Diodes (APDs) it is necessary to establish a circuit for voltage control of the offset depending on the temperature or to apply a thermostatic switch with the purpose of stabilizing the APD multiplication factor.

6. The size of the photodiode sensitive area is necessary to be kept as minimal as possible (Table 21) to decrease the noise level. However its reduction is limited by the size of the focal spot caused by the influence of atmospheric turbulence.

7. The bandwidth of the receiver channel should be coordinated with the width of the laser signal spectrum. With the absence of aprioristic data on the laser signal it should be minimized (Table 22) with the purpose of decreasing noise level, but should not result in distortion of the useful signal.

8. Parameters of electronic elements of the amplifier cascade are chosen to maintain a minimum level of noise.

9. The multiplication factor of the receiving channel has to be sufficient to provide a normal performance of the comparator at a low level of optical signal.

10. The level of comparator starting threshold should be set taking into account all actual noises of the laser sensor, and maintenance of preset values of probabilities of correct detection and false alarm.

- Comparing the evaluation of the laser sources detection range received in our model with field trials results, given in Table 15, it is possible to realize extreme ranges (up to 5,500 m in good weather conditions on 1.06 microns wavelength), that can be achieved by optimization of the parameters of the laser sensor.

166

- Table 15 shows the results of field trials carried out in summertime (May - August) in the United Arab Emirates desert by various companies - manufacturers (A, B, C, D) during 2001-2003. The best performances are received by company (A) which was 4.5 km for good weather conditions at 1. 06 microns wavelength. From Table 13, it is clear that with the deterioration of weather conditions the range of the laser source detection is essentially reduced.

- On the basis of the results of the testing of the laser sensor model in our research, the requirements of the parameters of the sensor receiver path have been developed (Chapter 7). These requirements can be used as recommendations by the companies or manufactures for providing high efficiency of combat application for the laser warning systems

- The seeker model has been discussed theoretically and built as a model using Mathlab and Simulink codes. It has been tested for various weather conditions. In addition, investigation has been carried out to see the effect of other parameters on the performance of the seeker and its components. Dependence of detection range on weather conditions for various wavelengths and narrow-band optical filters show that the detections range grows with the use of a narrow-band optical filter because of decreasing the noise level entering the receiving path. It was clear that using a higher wavelength gives longer detection range and with deterioration of weather conditions it decreases. Moreover, it was clearly proven that the seeker works only at the specified modulated frequency.

- The seeker detection range essentially reduced with the increase of turbulence level and deterioration in atmospheric conditions. Simulation results indicate that with the increase of receiving optical system diameter, detection range essentially increases that is caused by a rise of quantity of received signal power. As expected, the increase of focal length results in narrowing of the field of view and accordingly leads to a decrease of background level that causes enhanced sensitivity of the receiving channel.

- Simulation results show that with an increase in the size of the photodiode sensitive area and bandwidth the detection range is reduced. It is caused by the increase in noise level in the reception channel. Nevertheless, analysis of results proved that with an increase of the photodiode spectral response, the detection range is increased. It is caused by the increase of signal/noise ratio in the received channel. Finally, the performance of the seeker matched the expected results.

- Results of research in Chapter 8 show that applications of various types of counter-measures essentially have an influence on the stability of the guiding process of the anti-tank missiles. Application of the smoke (aerosol) grenades as countermeasures for beam-riding systems is possible only on the basis of the information on the irradiation from the laser warning receivers. The smoke (aerosol) screen should occur in a short time which is less than the time of flight of a missile up to the target. The type of smoke (aerosol) grenades should be chosen for the required conditions of attenuation of the laser radiation (Table 31 and 32) and must cover the used spectral range of the systems.

- Using active jamming for the beam-riding systems is possible if the jammer is placed into the field of view of the missile seeker. Parameters of a jammer can be taken according to expressions 8.2-8.5. Increasing the noise density creates random impulses at the output of the matched filter. Such impulses can exceed the preset threshold. This leads to false signals in the control loop of the missile and, as a result, a failure of the guiding process results.

- Decoys employ infra-red emitters to "mimic" those used by most semi-automatic missile systems to facilitate missile tracking. In this way, the enemy fire control system is made to issue erroneous flight correction commands to the missile, causing it to deviate from its intended target. Destruction of the threat missile can be achieved by eliminating the incoming missile with a high power laser beam or any other mean. For this purpose, it is very important to have a fast system of the notification means. High speed signal processing is critical to successfully dealing with the reduced response time.

9.3 Recommendations and Future Work

- Create a model to calculate the refractive index structure ($C_n^2=f(H\%;P;T^0)$), which makes the laser sensor model more dynamic and will allow to estimate of its importance as a parameter for the absolute measuring conditions.

- To carry out optimization of the aperture ratio (D/f) value for the receiving optical system for the concurrent providing of sufficient luminosity in a focal spot (small f) and narrow field of view (large f) and number of sensors and field of view.

- Develop an estimation model of transmission coefficient of the optical system combined with an optical filter.

- Develop a method of choosing the photodetectors with a maximal sensitivity and covering the required spectral range in a way of making the model more dynamic.

- Create an estimation model to find an optimum size of photodiode active region in order to provide minimum NEP and required size of the focal spot caused by influence of turbulent atmosphere and aberrations of the optical system.

- Create an estimation model to find the most appropriate value of multiplication factor ($M=f(T^0)$) of the avalanche photodiode (APD) at the change of ambient temperature. Develop estimation methods of their efficiency to provide the required size of displacement at the used temperature compensator.

- Develop an estimation model to find the best amplification factor and bandwidth of amplifying channel with the help of concrete parameters of transimpedance amplifier and subsequent cascades.

- Develop an estimation model to come up with the optimum value bandwidth (Δf) of receiving channel in order to find the minimum noise level (small Δf) and forming of the undistorted useful signal (large Δf).

- To carry out an estimation model of the comparator threshold level taking into account and providing the required values of probability of correct detection (D) and false alarm (F).

- Add new blocks into the laser sensor model taking into account the undirected laser radiation (reflected from other objects or surfaces) which hit the input of the laser sensor. Develop methods of noise-immunity for this case.

- Add new blocks into the laser sensor model which makes it possible to form signals with different types of modulation.

- Add new blocks into the laser seeker model to develop the signal processing, allowing the ability to select signals with the different types of modulation.
- Add a cooling system to the laser sensor model to reduce the temperature effects on the sensor performance.
- Develop an estimation model for counter-measures efficiency for the laser seeker.
- Create a user interface for the laser sensor model allowing the entry of all current parameters of atmospheric conditions of this locality.
- Choice of high –speed electronic components.

BIBLIOGRAPHY

BOOKS

"Arena Active Protection System". Armour. Vif2.ru/tank/EQP/arena.html.

ARMY NEWS, RUSSIA-Second Generation Protection System For Tanks.

Bertolotti, M, *"Masers and Lasers, an Historical Approach"*, Adam Hilger Ltd, Bristol: 1983.

Bromberg, J .L," *The Laser in America" 1950-1970*, MIT Press: 1991

Capt A Sacristan "Techniques To Counter Modern IR-Missile Technology", MSc Thesis, No. 4, MESE, 1990.

Cooke C.R. "Automatic laser tracking and ranging system". – Appl. Opt., 1972, v.11, No.2, p.277.

David H. Pollock, "The Infrared & Electro-Optical Systems Handbook", Volume 7, Countermeasures Systems.

Dereniak, E., and G. Boreman, *Infrared Detectors and Systems,* New York: Wiley, 1996.

Dr. Mark A. Richardson, "EO/IR Course Notes", GWSC/MESE, The Royal Military College of Science.

DTC(MA) System Study1, Module 4. The Military Applications of Radar, The Millimetric Wave Radar.

Flight Lieutenant JK Bradgate, "Retro-Reflective Detection For Enhanced Infra-Red Countermeasures", 2001.

Fried D.L. "Analysis of propagation lose factors for the ground based acquisition aid portion of the big altitude experiment". Rep. TR-001, Opt. St.: Consultants, 1970.

George R. Osche, "Optical Detection Theory for Laser Applications".

Gurevich A.S., Kon A.I. "Laser radiation in turbulent atmosphere". Moscow, Science, 1976, p. 277 .

Helston C.W. "Detection theory and quantum mechanics". Inform. Contr., 1968, No.3.

Karim Mohammad. "ELECTRO_OPTICAL DEVICES AND SYSTEMS", PWS_KENT

Kuriksha A.A. "Quantum optics and optical detection". Moscow, Soviet Radio, 1973, p. 183.

Lewicell W. "Radiation and noise in quantum electronics". Moscow, Science, 1972.

Maj J R Bright, "Laser Warning Receivers", MSc Thesis, No 2 MESE, 1988.Publishing Company. Boston, Massachusetts.

Malashin M.S., Kaminskiy R.P., Borisov Yu.V. "Fundamentals of laser systems engineering". Moscow, 1983.

Matveev I.N., Protopopov V.V., Troitskiy I.N., Ustinov N.D. "Laser Detection". Moscow, Mechanic Engineering, 1984.

Military Handbook, *Quantitative Description of Obscuration Factors for Electro-Optical and Millimetre Wave Systems Metric*, DOD-HDBK-178(ER), 1986.

Oliver B.M. "SNR in photoelectron mixing". Proc. IRE, 1961, v.49, No.12, p.160.

P Michon and J M Maesenellie, "A new design in the AFV Smart protection systems". 10th AFV attack and survivability symposium. 23 May 2001, Cranfield University, UK.

Ronald G. Driggers, Paul Cox, and Timothy Edwards. Introduction To Infrared and Electro-Optical Systems. Page 140

Stephen B. Alexander, *"Optical Communication Receiver Design"* (Bellingham, Washington USA: SPIE optical Engineering Press & London, UK: Institution of electrical Engineers, 1997), 49.

Tatarsky V., *Wave Propagation in Turbulent Medium*, New York: McGraw-Hill, 1961.

Tatarsky V.I. *Waves transmission in turbulent atmosphere*. M.: Nuka, 1967.

The Infrared & Electro-Optical Systems Handbook. Active Electro-Optical Systems, Volume 6.

The Infrared & Electro-Optical Systems Handbook. Active Electro-Optical Systems, Volume 7.

Zuev V.E. "Distribution of laser radiation in turbulent atmosphere". Moscow, Radio & Communication, 1981, p. 288.

JOURNALS

What's New in EO/IR Countermeasures: The industry responds to new-generation seekers.(electro-optical and infrafed; electronic warfare). Sherman, Kenneth B. Journal of Electronic Defense. November 01, 2001.

Directed Infrared Countermeasures – The Total Solution? By Salvatore Cezar Pais. Homeland Defense Journal Online.

Turkey Announces Major Helo EW Program.(Helicopter Electronic Warfare Suite)(Government Activity)(International Pages)(Brief Article) . Journal of Electronic Defense; July 01, 2001; Cakirozer, Utku.

Jane's International Defence Review. Jane's Electro-Optic Systems. Avitronics (Maritime) Naval Laser Warner System (NLWS). Date Posted: 25-Apr-2005.

Jane's International Defence Review Jane's Armour and Artillery Upgrades. Thales Land & Joint Systems LWD 3 laser warning system. Date Posted: 02-Aug-2005

ane's International Defence Review. Jane's Radar and Electronic Warfare Systems. Laser Warning System for Combat Vehicles (LWSCV). Date Posted: 02-Sep-2005

ane's International Defence Review. Jane's Electro-Optic Systems. Goodrich Model 218S Laser Warning Receiver System (LWRS). Date Posted: 11-Feb-2005

Jane's International Defence Review. Jane's Electro-Optic Systems. Goodrich AN/VVR-1 Laser Warning Receiver System (LWRS). Date Posted: 11-Feb-2005

Jane's International Defence Review. Jane's Electro-Optic Systems. BAE Systems LWR-98GV (2) Laser Warning Receiver. Date Posted: 11-Feb-2005

R M Ogorkieicz, " Future Tank Armour Revealed Developments in Electric and Explosive reactive armour", IDR Exclusive, p50-51, Janes international defence review, Vol 5, 1997.

William L. Janning, "Improving Laser Warning", Defence Electronic, April 1981. p90-94.

P J Hazeel. "Ceramic Armour", Journal of Battlefield Technology, Vol 2, No 1, March 1999.

Frank Colucci, " Countering The Laser Threat; Laser Warning and Protection Concepts emerge", Defence Helicopter World, October-November 1988, P18-22.

Dr. C. I. Coleman, "Laser Threat Warning; A Growing Need on the Modern Battlefield", International Defence Review 7/1986 P965-967.

APPENDIXES

APPENDIX A TRANSMITTANCE GRAPHS

Transmittance of a Good weather condition. Figure 53.
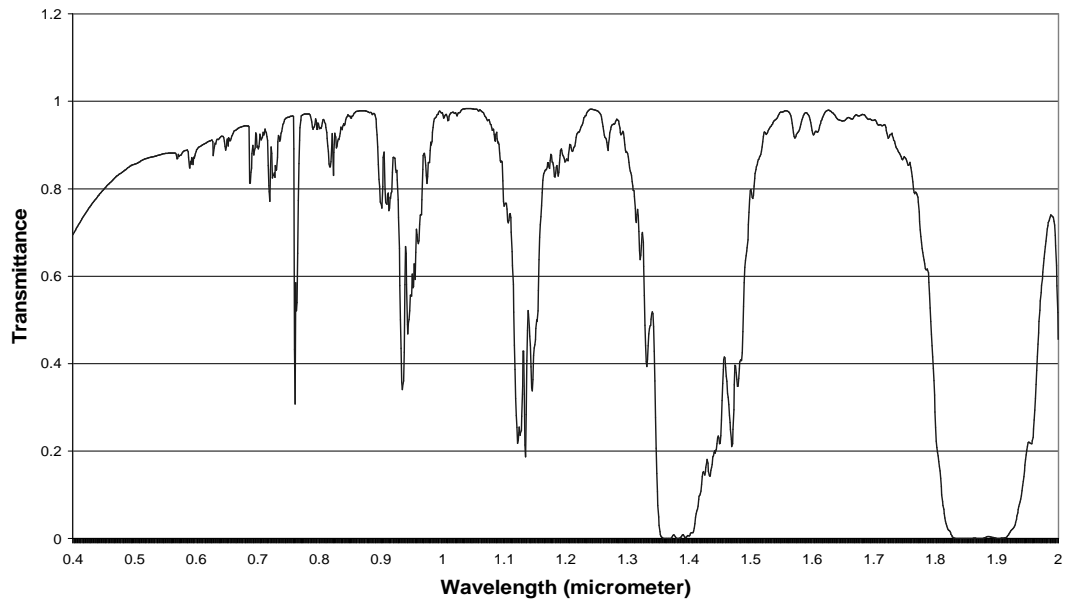
Figure 53 Transmittance of a Good weather condition
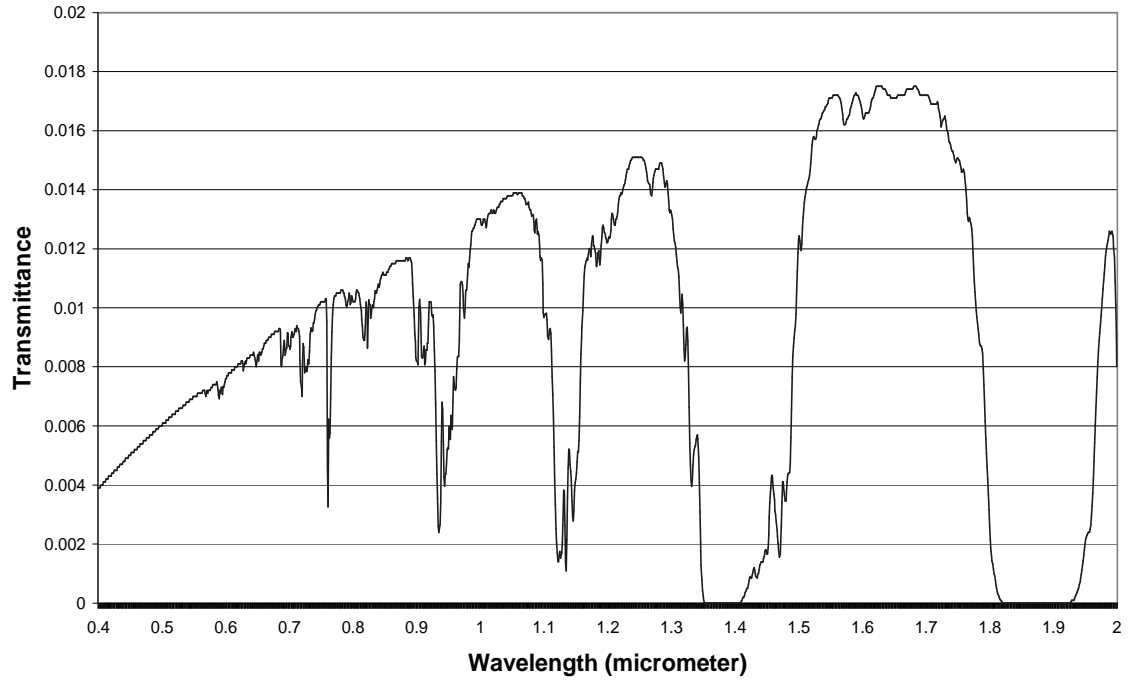
Transmittance of a Typical-I weather condition. Figure 54.
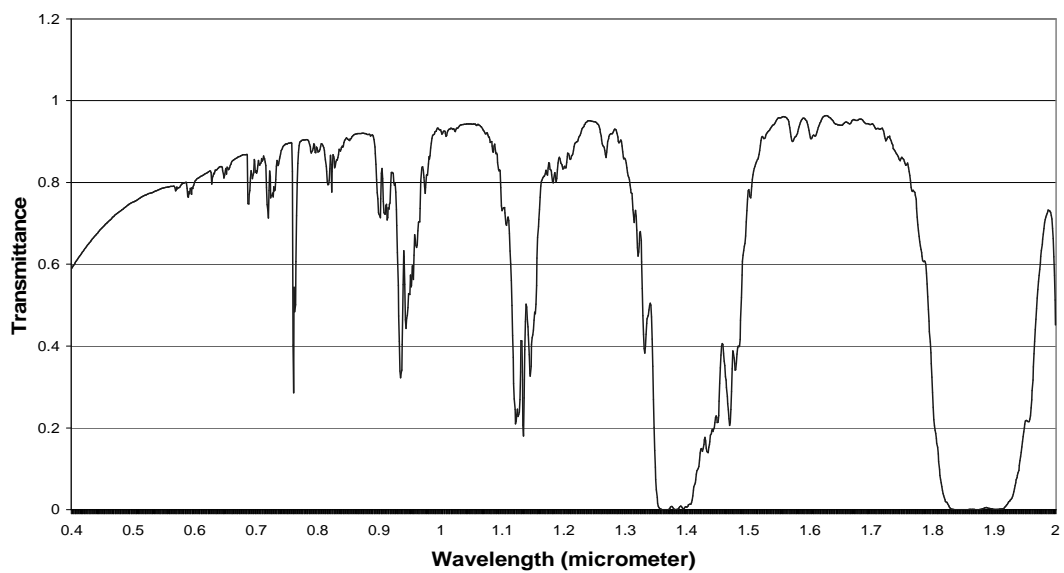
Figure 54 Transmittance of a typical-I weather condition

Transmittance of a Typical-II weather condition. Figure 55.
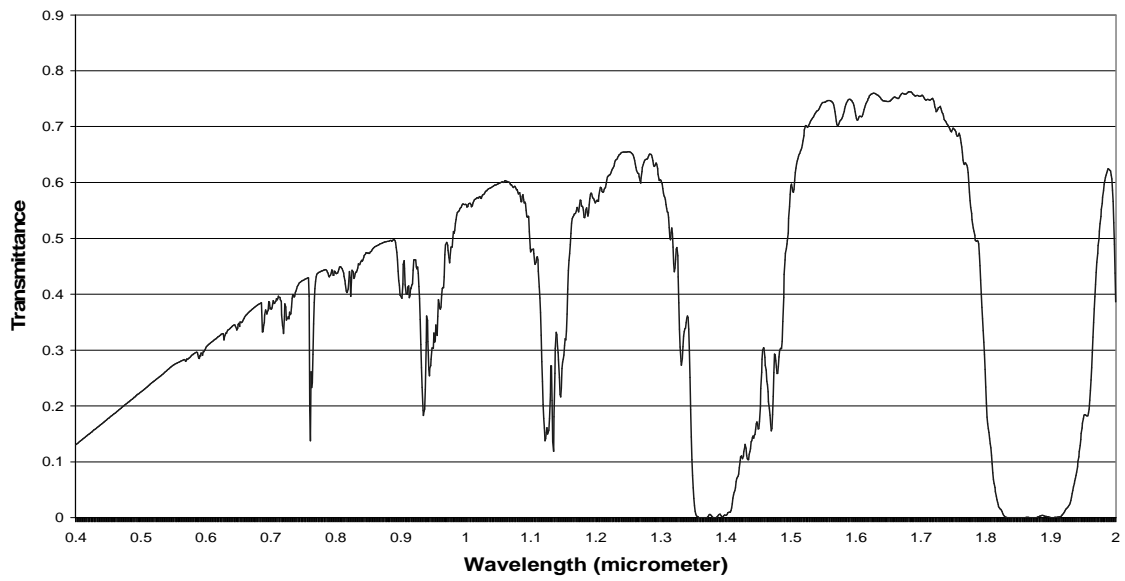
Figure 55 Transmittance of a typical-II weather condition

Transmittance of a Bad-I weather condition. Figure 56.
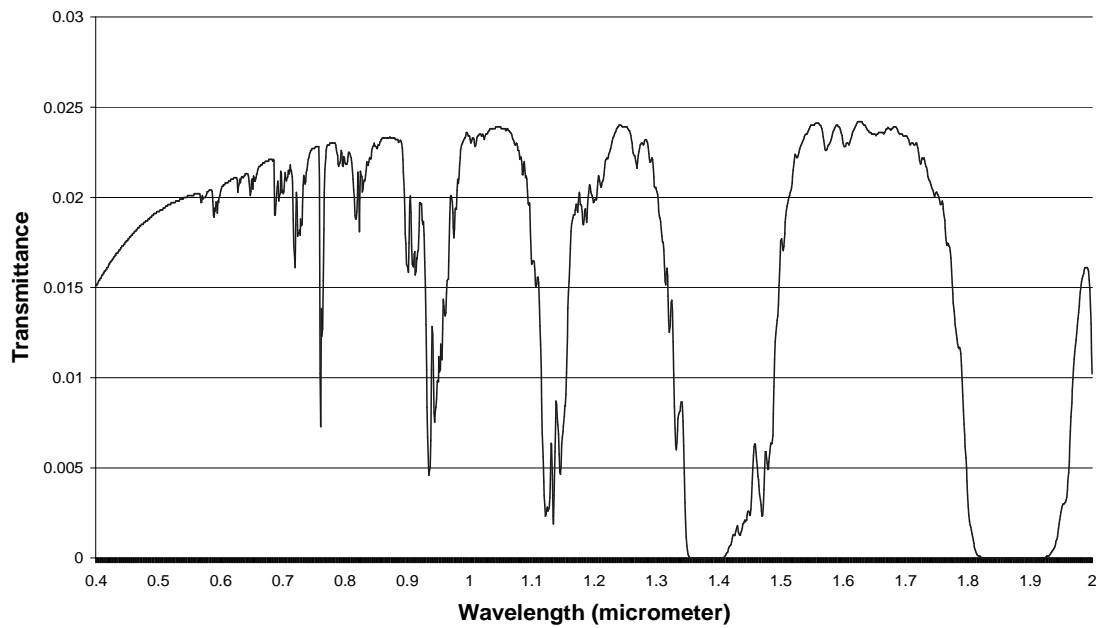
Figure 56 Transmittance of a bad-I weather condition

Transmittance of a Bad-II weather condition. Figure 57.

Figure 57 Transmittance of a bad-II weather condition

APPENDIX B Measuring the Reflectivity of Desert Sand Samples

Sample A, B, and C in Figure 58 corresponded to the sand types in UAE desert.

Figure 58 UAE sand samples

Figure 59 shows the result of the experiment. It gives the reflectivity in % of the incident light on the sample and from that we can know the behaviour of the sample in adding noise to the laser warning receiver for that range of the spectrum.
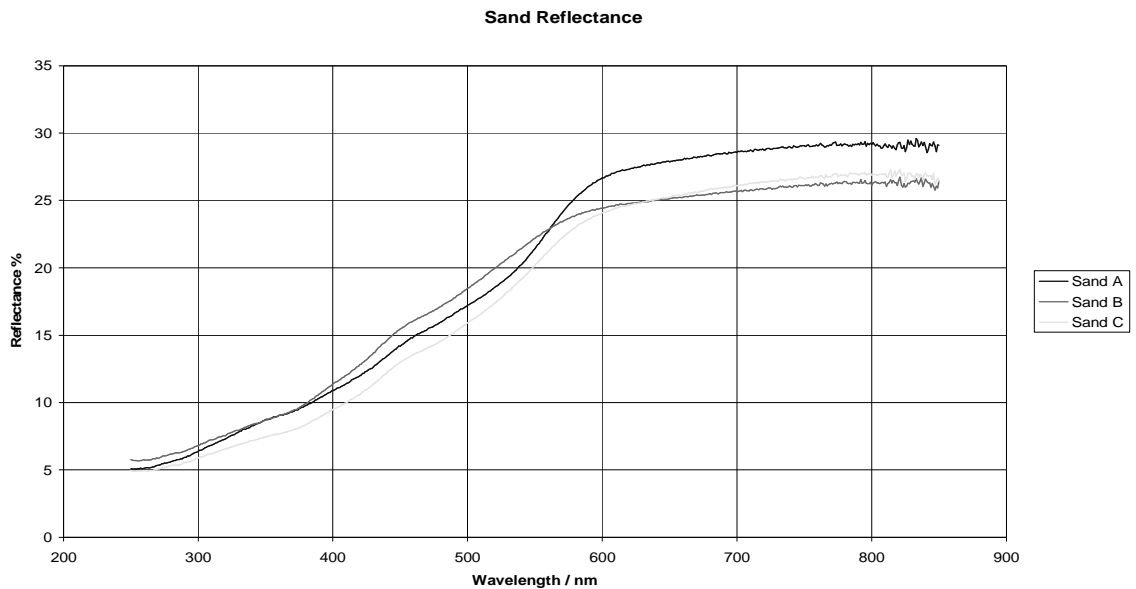
Figure 59 UAE sand reflectance

APPENDIX C Calculations of Laser Sensor Parameters

Calculation of parameters of Laser Sensor

(for distance - 5500 m, atmospheric conditions - Good, sand sample - A,

$C_n^2=52 \cdot 10^{-17}$ m$^{-2/3}$, $\lambda=1.06\mu$m and $\Delta\lambda=0.811\dots1.11\mu$m)

1.

$$\overline{P}_{in} = P_{out} \cdot T_a \cdot \frac{D_{ob}^2 \cdot \exp(-\sigma_I)}{\left(\theta_{div} + \dfrac{\lambda}{r_0}\right)^2 \cdot R^2} = 0.025 \cdot 0.9529 \cdot \frac{(0.03)^2 \cdot 0.66}{\left(3 \cdot 10^{-3} + 1.164 \cdot 10^{-5}\right)^2 \cdot (5500)^2} = 5.14 \cdot 10^{-8}$$

W - power of laser irradiation at the receiver input

2.

$$\overline{i}^2{}_{shot.n.s} = 2e\Delta f \overline{P}_{in}\varepsilon_\lambda MX = 2 \cdot 1.6 \cdot 10^{-19} \cdot 33 \cdot 10^6 \cdot 5.14 \cdot 10^{-8} \cdot 19.77 \cdot 100 \cdot 2.5 = 2.68 \cdot 10^{-15} \, \text{Å}$$

shot noise of signal

3.

$$\overline{i}^2{}_{shot.n.dc} = 2 \cdot e \cdot \Delta f \cdot \overline{I}_D \cdot M \cdot X = 2 \cdot 1.6 \cdot 10^{-19} \cdot 33 \cdot 10^6 \cdot 0.5 \cdot 10^{-9} \cdot 100 \cdot 2.5 = 1.32 \cdot 10^{-18}$$

A^2 - shot noise of dark current

4. $\overline{i}^2{}_{therm.n} = \dfrac{4 \cdot k \cdot T \cdot \Delta f}{R_L} = \dfrac{4 \cdot 1.38 \cdot 10^{-23} \cdot 328 \cdot 33 \cdot 10^6}{10^5} = 5.98 \cdot 10^{-18}$ A^2 - thermal noise of receiver

5. $\overline{P}_b = B(\lambda) \cdot S_D \cdot \Omega \cdot T_D = 1.197 \cdot 10^{-3} \cdot 7 \cdot 1.23 \cdot 10^{-4} \cdot 0.5 = 5.19 \cdot 10^{-7}$ W - power of background

6.

$\overline{i}^2{}_{shot.n.b} = 2 \cdot e \cdot \Delta f \cdot \overline{P}_b \cdot \varepsilon_\lambda \cdot M \cdot X = 2 \cdot 1.6 \cdot 10^{-19} \cdot 33 \cdot 10^6 \cdot 5.19 \cdot 10^{-7} \cdot 19.77 \cdot 100 \cdot 2.5 = 2.71 \cdot 10^{-14}$

A^2 - shot noise of background

7. $\overline{i}_{\sum noie} = \sqrt{\overline{i}^2{}_{shot.n.s} + \overline{i}^2{}_{shot.n.dc} + \overline{i}^2{}_{therm.n} + \overline{i}^2{}_{shot.n.b.}} =$

$= \sqrt{2.68 \cdot 10^{-15} + 1.32 \cdot 10^{-18} + 5.98 \cdot 10^{-18} + 2.71 \cdot 10^{-14}} = 1.72 \cdot 10^{-7}$ A - RMS total noise

8. $P_{thr} = \dfrac{\sqrt{\overline{i^2}_{\Sigma noise}}}{\varepsilon_\lambda} = \dfrac{1.72 \cdot 10^{-7}}{19.77} = 8.73 \cdot 10^{-9}$ W - threshold power of receiver

9. $P_{in\_PD} = P_{in} + P_b = 5.14 \cdot 10^{-8} + 5.19 \cdot 10^{-7} = 5.71 \cdot 10^{-7}$, W - power on receiver input

10. $U_{thr} = P_{thr} \cdot \varepsilon_\lambda \cdot R_L \cdot q \cdot k_1 \cdot k_2 = 8.73 \cdot 10^{-9} \cdot 19.77 \cdot 1000 \cdot 5 \cdot 4 \cdot 20 = 0.069$, V - threshold voltage for detection of signal with probability 0.9 (q – signal/noise)

11. $A_{signal.PD} = P_{in\_PD} \cdot \varepsilon = 5.71 \cdot 10^{-7} \cdot 19.77 = 1.13 \cdot 10^{-5}$, A - signal current in out photodiode

12.

$U_{signal.1Amp} = (A_{signal.PD} - P_b \cdot \varepsilon_\lambda) \cdot R_L \cdot k_1 = (1.13 \cdot 10^{-5} - 5.19 \cdot 10^{-7} \cdot 19.77) \cdot 1000 \cdot 4 = 4.06 \cdot 10^{-3}$,V

- signal voltage in out 1st amplifier

13. $U_{signal.2Amp} = U_{signal.1Amp} \cdot k_2 = 4.06 \cdot 10^{-3} \cdot 20 = 0.081$, V - signal voltage in out 2nd amplifier

14. $A_{noise.PD} = (P_{thr} + P_b) \cdot \varepsilon = (8.73 \cdot 10^{-9} + 5.19 \cdot 10^{-7}) \cdot 19.77 = 1.04 \cdot 10^{-5}$, A - noise current in out photodiode

15. $U_{noise.1Amp} = (A_{noise.PD} - P_b \cdot \varepsilon_\lambda) \cdot R_L \cdot k_1 = (1.04 \cdot 10^{-5} - 5.19 \cdot 10^{-7} \cdot 19.77) \cdot 1000 \cdot 4 = 6.9 \cdot 10^{-4}$,

V - noise voltage at the output of 1st amplifier

16. $A = \dfrac{P_{noise1}}{P_{noise2}} = \dfrac{\sqrt{B \cdot \Delta f_1}}{\sqrt{B \cdot \Delta f_2}} = \sqrt{\dfrac{\Delta f_1}{\Delta f_2}} = \sqrt{\dfrac{10^9}{30 \cdot 10^6}} = 5.774$ - degradation factor of spectral noise power

17. $U_{noise.2Amp} = U_{noise.1Amp} \cdot \dfrac{k_2}{A} = 6.9 \cdot 10^{-4} \cdot \dfrac{20}{5.774} = 2.39 \cdot 10^{-3}$, V - noise voltage at the output of 2nd amplifier

APPENDIX D   **The Amplifier Circuit**

Figure 60 shows the electronic circuit of the amplifier circuit.
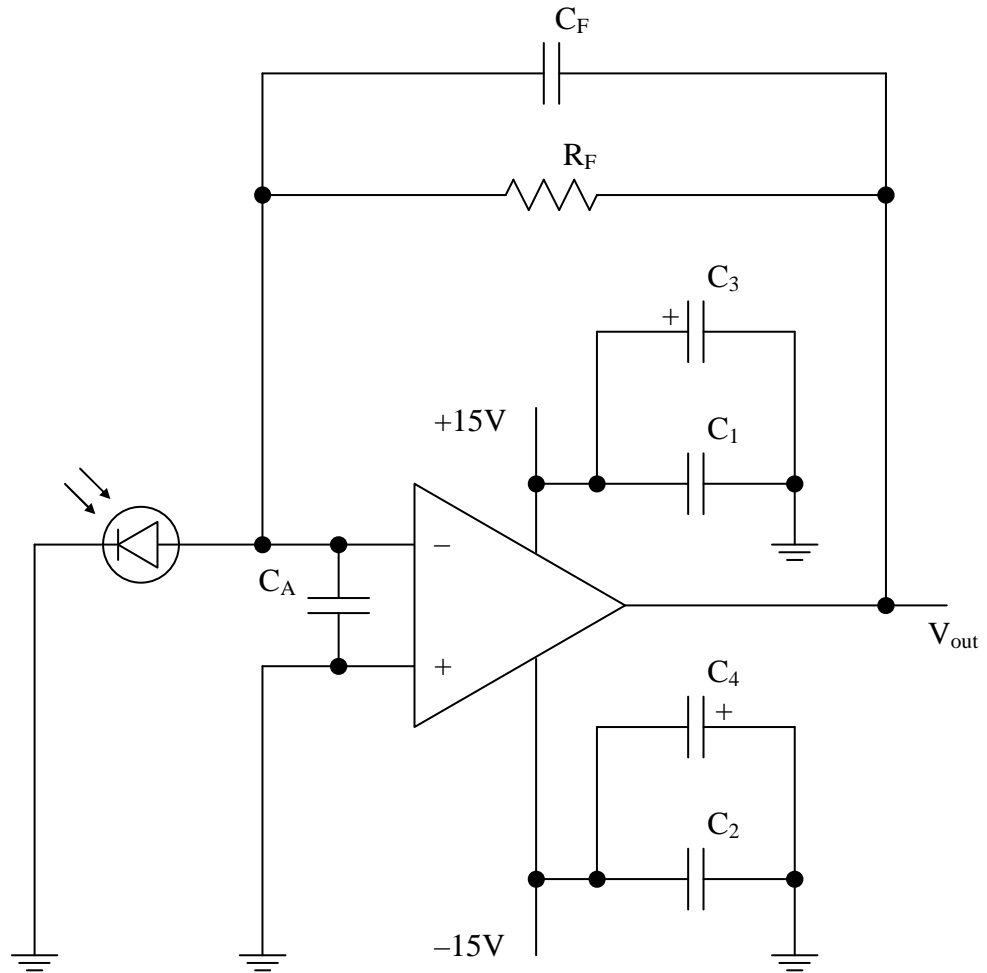
Figure 60 Amplifier circuit design

$C_1 = 0.1\ \mu F; C_2 = 0.1\ \mu F; C_3 = 47\ \mu F; C_4 = 47\ \mu F; C_F = 15\ pF; R_F = 1\ M\Omega;$

The bandwidth of amplifier calculated from formula:

$$\Delta f = \frac{1}{2 \cdot \pi \cdot R_F \cdot C_F} = \frac{1}{2 \cdot 3.14 \cdot 10^6 \cdot 15 \cdot 10^{-12}} = 10.6 \cdot 10^3,\ Hz$$

where, R_F is the feedback resistance and C_F - feedback capacity. The voltage on amplifier calculated from formula:

$$U_{out} = P_{in} \cdot \varepsilon_\lambda \cdot R_F$$

where, ε_λ is spectral responsivity of PD.

APPENDIX E Light Source Specifications

Definition:

Brightness of any source is the radiated power from 1 sm² of a surface in unit of a spatial angle and unit of a spectral range:

$$B = \frac{P_{opt}}{S \cdot \omega \cdot \Delta\lambda}\left[\frac{W}{sm^2 \cdot strad \cdot \mu m}\right]$$

Where,

$P_{opt} = P_{el} \cdot \eta$ is the optical power of the Light Source

P_{el} is electrical power of the Light Source (150W)

η - efficiency factor(50%)

$S = 2 \cdot \pi \cdot r \cdot l$ - area of the radiating surface filament heater

      r – radius of the filament heater(0.1 sm)

      l – length of the filament heater(3.0 sm)

$\omega = \pi$ - spatial angle (for Lambert radiators)

$\Delta\lambda$ - spectral range of the Light Source(0.4…2.4 μm)

Light Source Specs:

1.Wolfram Lamp.

2. P_{el}= 150 W – electrical power

3. $\eta = 0.5$ - efficiency factor

4. l =3.0 sm – length of filament heater

5. r = 0.1 sm – radius of filament heater

6. $\Delta\lambda = 2\mu m$ - spectral bandwidth

Brightness of Light Source:

$$B = \frac{P_{el} \cdot \eta}{\pi \cdot 2 \cdot \pi \cdot r \cdot l \cdot \Delta\lambda} = 6.33 \left[\frac{W}{sm^2 \cdot \mu m \cdot strad} \right]$$

In the model there is a block in which you can input the brightness value, which in or case is:

(B=6.33).

APPENDIX F Experimental Calculations (Without Light Source Noise)

Evaluations of a signal and RMS noise in the model (for distance 36.74 m corresponding to k_{nf}=2.4%) (without Light source noise)

1.

$$\overline{P}_{in} = P_{out} \cdot T_A \cdot \frac{\pi \cdot D_{os}{}^2/4}{(a+\theta \cdot R)^2} \cdot k_{bf} = 0.686 \cdot 10^{-3} \cdot 0.9985 \cdot \frac{3.14 \cdot (0.008)^2/4}{(0.0254 + 4.3 \cdot 10^{-3} \cdot 36.74)^2} = 6.14 \cdot 10^{-7},$$

W - power of laser irradiation at the receiver input

2. $\overline{i}^2_{shot.n.s} = 2 \cdot e \cdot \Delta f \cdot \overline{P}_{in} \cdot \varepsilon_\lambda = 2 \cdot 1.6 \cdot 10^{-19} \cdot 20 \cdot 10^3 \cdot 6.14 \cdot 10^{-7} \cdot 0.4 = 1.57 \cdot 10^{-21}$, A^2 - shot noise of signal

3. $\overline{i}^2_{shot.n.dc} = 2 \cdot e \cdot \Delta f \cdot \overline{I}_D = 2 \cdot 1.6 \cdot 10^{-19} \cdot 20 \cdot 10^3 \cdot 0.5 \cdot 10^{-9} = 3.2 \cdot 10^{-24}$, A^2 - shot noise of dark current

4. $\overline{i}^2_{therm.n} = \dfrac{4 \cdot k \cdot T \cdot \Delta f}{R_L} = \dfrac{4 \cdot 1.38 \cdot 10^{-23} \cdot 300 \cdot 20 \cdot 10^3}{10^6} = 3.31 \cdot 10^{-22}$, A^2 - thermal noise of receiver

5. $\overline{P}_b = B \cdot \Delta\lambda \cdot S_D \cdot \Omega \cdot T_D = 8.579 \cdot 10^{-5} \cdot 0.5027 \cdot 4.9 \cdot 10^{-4} \cdot 0.5 = 1.06 \cdot 10^{-8}$, W - power of background

6. $\overline{i}^2_{shot.n.b} = 2 \cdot e \cdot \Delta f \cdot \overline{P}_b \cdot \varepsilon_\lambda = 2 \cdot 1.6 \cdot 10^{-19} \cdot 20 \cdot 10^3 \cdot 1.06 \cdot 10^{-8} \cdot 0.4 = 2.71 \cdot 10^{-23}$, A^2 - shot noise of background

7. $\overline{i}_{\Sigma noie} = \sqrt{\overline{i}^2_{shot.n.s.} + \overline{i}^2_{shot.n.dc} + \overline{i}^2_{therm.n} + \overline{i}^2_{shot.n.b.}} =$

$= \sqrt{1.57 \cdot 10^{-21} + 3.2 \cdot 10^{-24} + 3.31 \cdot 10^{-22} + 2.71 \cdot 10^{-23}} = 4.398 \cdot 10^{-11}$, A - RMS total noise

8. $P_{thr} = \dfrac{\sqrt{\overline{i}_{\Sigma noie}}}{\varepsilon} = \dfrac{4.398 \cdot 10^{-11}}{0.4} = 1.099 \cdot 10^{-10}$, W - threshold power

9. $U_{thr} = P_{thr} \cdot \varepsilon \cdot R_F \cdot q = 1.099 \cdot 10^{-10} \cdot 0.4 \cdot 10^6 \cdot 5 = 2.199 \cdot 10^{-4}$, V - threshold voltage (q – signal/noise)

10. $I_{signal.PD} = \overline{P}_{in} \cdot \varepsilon = 6.14 \cdot 10^{-7} \cdot 0.4 = 2.46 \cdot 10^{-7}$, A - signal current at the output of the photodiode

11. $U_{signal.Amp} = I_{signal.PD} \cdot R_F = 2.46 \cdot 10^{-7} \cdot 10^6 = 0.246$, V - signal voltage at the output of the amplifier

12. $I_{noise.PD} = P_{thr} \cdot \varepsilon = 1.099 \cdot 10^{-10} \cdot 0.4 = 4.398 \cdot 10^{-11}$, A - noise current at the output of the photodiode

13. $U_{noise.Amp} = I_{noise.PD} \cdot R_F = 4.398 \cdot 10^{-11} \cdot 10^6 = 4.398 \cdot 10^{-5}$, V - noise voltage at the output of the amplifier

APPENDIX G Experimental Calculations (With Light Source Noise)

Estimation of RMS noise and constant component noise in model
(for distance 36.74 m corresponding to k_{nf}=2.4%)
(for d=1mm; d=5mm; f=40mm; f=100mm)
(with Light source noise)

1. $\overline{P}_{in} = P_{out} \cdot T_A \cdot \dfrac{\pi \cdot D_{os}{}^2/4}{(a + \theta \cdot R)^2} \cdot k_{bf} = 0.686 \cdot 10^{-3} \cdot 0.9985 \cdot \dfrac{3.14 \cdot (0.008)^2/4}{(0.0254 + 4.3 \cdot 10^{-3} \cdot 36.74)^2} = 6.14 \cdot 10^{-7}$,

W - power of laser irradiation at the receiver input

2. $\overline{i}^2{}_{shot.n.s} = 2 \cdot e \cdot \Delta f \cdot \overline{P}_{in} \cdot \varepsilon_\lambda = 2 \cdot 1.6 \cdot 10^{-19} \cdot 10.6 \cdot 10^3 \cdot 6.14 \cdot 10^{-7} \cdot 0.4 = 8.33 \cdot 10^{-22}$, A^2 - shot noise

of signal

3. $\overline{i}^2{}_{shot.n.dc} = 2 \cdot e \cdot \Delta f \cdot \overline{I}_D = 2 \cdot 1.6 \cdot 10^{-19} \cdot 10.6 \cdot 10^3 \cdot 0.5 \cdot 10^{-9} = 1.7 \cdot 10^{-24}$, A^2 - shot noise of dark

current

4. $\overline{i}^2{}_{therm.n} = \dfrac{4 \cdot k \cdot T \cdot \Delta f}{R_L} = \dfrac{4 \cdot 1.38 \cdot 10^{-23} \cdot 300 \cdot 10.6 \cdot 10^3}{10^6} = 1.76 \cdot 10^{-22}$, A^2 - thermal noise of

receiver

5.1. $\overline{P}_{b1} = B \cdot \Delta\lambda \cdot S_D \cdot \Omega_1 \cdot T_D = 6.33 \cdot 0.01 \cdot 0.5027 \cdot 7.85 \cdot 10^{-5} \cdot 0.5 = 1.25 \cdot 10^{-6}$, W - power of

background for d=1mm and f=100mm

5.2. $\overline{P}_{b2} = B \cdot \Delta\lambda \cdot S_D \cdot \Omega_2 \cdot T_D = 6.33 \cdot 0.01 \cdot 0.5027 \cdot 4.91 \cdot 10^{-4} \cdot 0.5 = 7.81 \cdot 10^{-6}$, W - power of

background for d=1mm and f=40mm

5.3. $\overline{P}_{b3} = B \cdot \Delta\lambda \cdot S_D \cdot \Omega_3 \cdot T_D = 6.33 \cdot 0.01 \cdot 0.5027 \cdot 1.96 \cdot 10^{-3} \cdot 0.5 = 3.13 \cdot 10^{-5}$, W - power of

background for d=5mm and f=100mm

5.4. $\overline{P}_{b4} = B \cdot \Delta\lambda \cdot S_D \cdot \Omega_4 \cdot T_D = 6.33 \cdot 0.01 \cdot 0.5027 \cdot 0.0132 \cdot 0.5 = 1.95 \cdot 10^{-4}$, W - power of background for d=5mm and f=40mm

6.1. $\overline{i}^2_{shot.n.b1} = 2 \cdot e \cdot \Delta f \cdot \overline{P}_{b1} \cdot \varepsilon_\lambda = 2 \cdot 1.6 \cdot 10^{-19} \cdot 10.6 \cdot 10^3 \cdot 1.25 \cdot 10^{-6} \cdot 0.4 = 1.7 \cdot 10^{-21}$, A^2 - shot noise of background for d=1mm and f=100mm

6.2. $\overline{i}^2_{shot.n.b2} = 2 \cdot e \cdot \Delta f \cdot \overline{P}_{b2} \cdot \varepsilon_\lambda = 2 \cdot 1.6 \cdot 10^{-19} \cdot 10.6 \cdot 10^3 \cdot 7.81 \cdot 10^{-6} \cdot 0.4 = 1.06 \cdot 10^{-20}$, A^2 - shot noise of background for d=1mm and f=40mm

6.3. $\overline{i}^2_{shot.n.b3} = 2 \cdot e \cdot \Delta f \cdot \overline{P}_{b3} \cdot \varepsilon_\lambda = 2 \cdot 1.6 \cdot 10^{-19} \cdot 10.6 \cdot 10^3 \cdot 3.13 \cdot 10^{-5} \cdot 0.4 = 4.24 \cdot 10^{-20}$, A^2 - shot noise of background for d=5mm and f=100mm

6.4. $\overline{i}^2_{shot.n.b4} = 2 \cdot e \cdot \Delta f \cdot \overline{P}_{b4} \cdot \varepsilon_\lambda = 2 \cdot 1.6 \cdot 10^{-19} \cdot 10.6 \cdot 10^3 \cdot 1.95 \cdot 10^{-4} \cdot 0.4 = 2.65 \cdot 10^{-19}$, A^2 - shot noise of background for d=5mm and f=40mm

7.1. $\overline{i}_{\sum noie1} = \sqrt{\overline{i}^2_{shot.n.s.} + \overline{i}^2_{shot.n.dc} + \overline{i}^2_{therm.n} + \overline{i}^2_{shot.n.b1}} =$

$= \sqrt{8.33 \cdot 10^{-22} + 1.7 \cdot 10^{-24} + 1.76 \cdot 10^{-22} + 1.7 \cdot 10^{-21}} = 5.2 \cdot 10^{-11}$, A - RMS total noise for d=1mm and f=100mm

7.2. $\overline{i}_{\sum noie2} = \sqrt{\overline{i}^2_{shot.n.s.} + \overline{i}^2_{shot.n.dc} + \overline{i}^2_{therm.n} + \overline{i}^2_{shot.n.b2}} =$

$= \sqrt{8.33 \cdot 10^{-22} + 1.7 \cdot 10^{-24} + 1.76 \cdot 10^{-22} + 1.06 \cdot 10^{-20}} = 1.08 \cdot 10^{-10}$, A - RMS total noise for d=1mm and f=40mm

7.3. $\overline{i}_{\sum noie3} = \sqrt{\overline{i}^2_{shot.n.s.} + \overline{i}^2_{shot.n.dc} + \overline{i}^2_{therm.n} + \overline{i}^2_{shot.n.b3}} =$

$= \sqrt{8.33 \cdot 10^{-22} + 1.7 \cdot 10^{-24} + 1.76 \cdot 10^{-22} + 4.24 \cdot 10^{-20}} = 2.08 \cdot 10^{-10}$, A - RMS total noise for d=5mm and f=100mm

7.4. $\overline{i}_{\sum noie4} = \sqrt{\overline{i}^2_{shot.n.s.} + \overline{i}^2_{shot.n.dc} + \overline{i}^2_{therm.n} + \overline{i}^2_{shot.n.b4}} =$

$= \sqrt{8.33 \cdot 10^{-22} + 1.7 \cdot 10^{-24} + 1.76 \cdot 10^{-22} + 2.65 \cdot 10^{-19}} = 5.16 \cdot 10^{-10}$, A - RMS total noise for d=5mm and f=40mm

8.1. $P_{thr1} = \dfrac{\sqrt{\overline{i_{\Sigma noise1}}}}{\varepsilon} = \dfrac{5.2 \cdot 10^{-11}}{0.4} = 1.3 \cdot 10^{-10}$, W - threshold power for d=1mm and f=100mm

8.2. $P_{thr2} = \dfrac{\sqrt{\overline{i_{\Sigma noise2}}}}{\varepsilon} = \dfrac{1.08 \cdot 10^{-10}}{0.4} = 2.69 \cdot 10^{-10}$, W - threshold power for d=1mm and f=40mm

8.3. $P_{thr3} = \dfrac{\sqrt{\overline{i_{\Sigma noise3}}}}{\varepsilon} = \dfrac{2.08 \cdot 10^{-10}}{0.4} = 5.2 \cdot 10^{-10}$, W - threshold power for d=5mm and f=100mm

8.4. $P_{thr4} = \dfrac{\sqrt{\overline{i_{\Sigma noise4}}}}{\varepsilon} = \dfrac{5.16 \cdot 10^{-10}}{0.4} = 1.29 \cdot 10^{-9}$, W - threshold power for d=5mm and f=40mm

9.1. $I_{noise.PD1} = P_{thr1} \cdot \varepsilon = 1.3 \cdot 10^{-10} \cdot 0.4 = 5.203 \cdot 10^{-11}$, A - noise current at the output of photodiode for d=1mm and f=100mm

9.2. $I_{noise.PD2} = P_{thr2} \cdot \varepsilon = 2.69 \cdot 10^{-10} \cdot 0.4 = 1.078 \cdot 10^{-10}$, A - noise current at the output of photodiode for d=1mm and f=40mm

9.3. $I_{noise.PD3} = P_{thr3} \cdot \varepsilon = 5.2 \cdot 10^{-10} \cdot 0.4 = 2.084 \cdot 10^{-10}$, A - noise current at the output of photodiode for d=5mm and f=100mm

9.4. $I_{noise.PD4} = P_{thr4} \cdot \varepsilon = 1.29 \cdot 10^{-10} \cdot 0.4 = 5.158 \cdot 10^{-10}$, A - noise current at the output of photodiode for d=5mm and f=40mm

10.1. $U_{noise.Amp1} = I_{noise.PD1} \cdot R_F = 5.203 \cdot 10^{-11} \cdot 10^6 = 5.203 \cdot 10^{-5}$, V - noise voltage at the output of the amplifier for d=1mm and f=100mm

10.2. $U_{noise.Amp2} = I_{noise.PD2} \cdot R_F = 1.078 \cdot 10^{-10} \cdot 10^6 = 1.078 \cdot 10^{-4}$, V - noise voltage at the output of the amplifier for d=1mm and f=40mm

10.3. $U_{noise.Amp3} = I_{noise.PD3} \cdot R_F = 2.084 \cdot 10^{-10} \cdot 10^6 = 2.084 \cdot 10^{-4}$, V - noise voltage at the output of the amplifier for d=5mm and f=100mm

10.4. $U_{noise.Amp4} = I_{noise.PD4} \cdot R_F = 5.158 \cdot 10^{-10} \cdot 10^6 = 5.158 \cdot 10^{-4}$, V - noise voltage at the output of the amplifier for d=5mm and f=40mm

11.1. $U_{c1} = \overline{P}_{b1} \cdot \varepsilon \cdot R_F = 1.25 \cdot 10^{-6} \cdot 0.4 \cdot 10^6 = 0.5$, V - voltage of constant component at the output of the amplifier for d=1mm and f=100mm

11.2. $U_{c2} = \overline{P}_{b2} \cdot \varepsilon \cdot R_F = 7.81 \cdot 10^{-6} \cdot 0.4 \cdot 10^6 = 3.125$, V - voltage of constant component at the output of the amplifier for d=1mm and f=40mm

11.3. $U_{c3} = \overline{P}_{b3} \cdot \varepsilon \cdot R_F = 3.13 \cdot 10^{-5} \cdot 0.4 \cdot 10^6 = 12.5$, V - voltage of constant component at the output of the amplifier for d=5mm and f=100mm

11.4. $U_{c4} = \overline{P}_{b4} \cdot \varepsilon \cdot R_F = 1.95 \cdot 10^{-4} \cdot 0.4 \cdot 10^6 = 87.125$, V - voltage of constant component at the output of the amplifier for d=5mm and f=40mm

APPENDIX H Guidance Methods

Figure 61 shows the guidance methods used nowadayas [1].

```
                            ┌─────────────┐
                            │  GUIDANCE   │
                            └──────┬──────┘
          ┌────────────────────────┼────────────────────────┐
  ┌───────────────┐        ┌───────────────┐        ┌───────────────┐
  │ Line of Sight │        │    Homing     │        │  Navigation   │
  └───────────────┘        └───────────────┘        └───────────────┘
     ┌───────────┐            ┌───────────┐            ┌───────────┐
     │   MCLOS   │            │  Passive  │            │  Inertial │
     └───────────┘            └───────────┘            └───────────┘
     ┌───────────┐            ┌───────────┐            ┌───────────┐
     │  SACLOS   │            │Semi Active│            │Natural Fix│
     └───────────┘            └───────────┘            └───────────┘
     ┌───────────┐            ┌───────────┐            ┌─────────────┐
     │   ACLOS   │            │  Active   │            │Artificial Fix│
     └───────────┘            └───────────┘            └─────────────┘
```
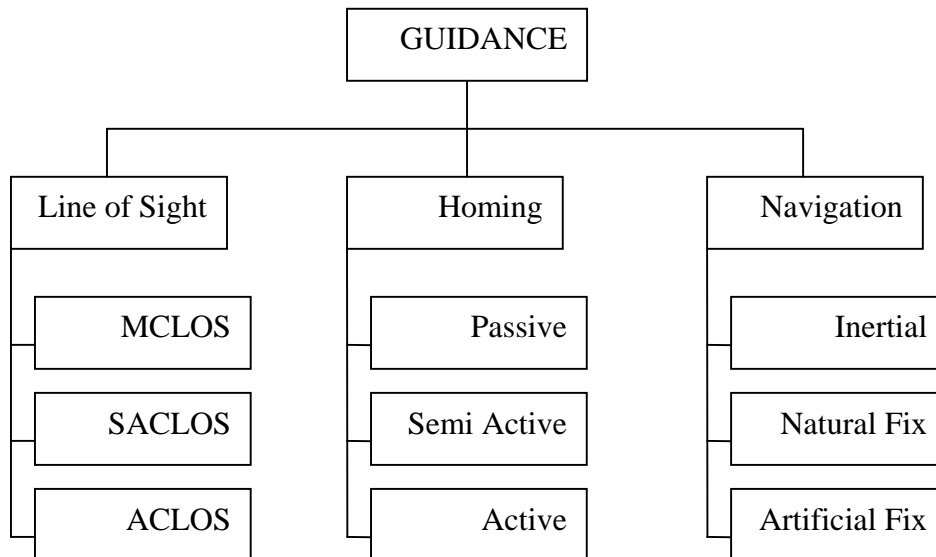
Figure 61 Guidance methods

H.1 Line of Sight Guidance (LOS)

For the purpose of this paper we will stick to the Line of sight guidance.

H.1.1 Manual Command to Line of Sight (MCLOS)
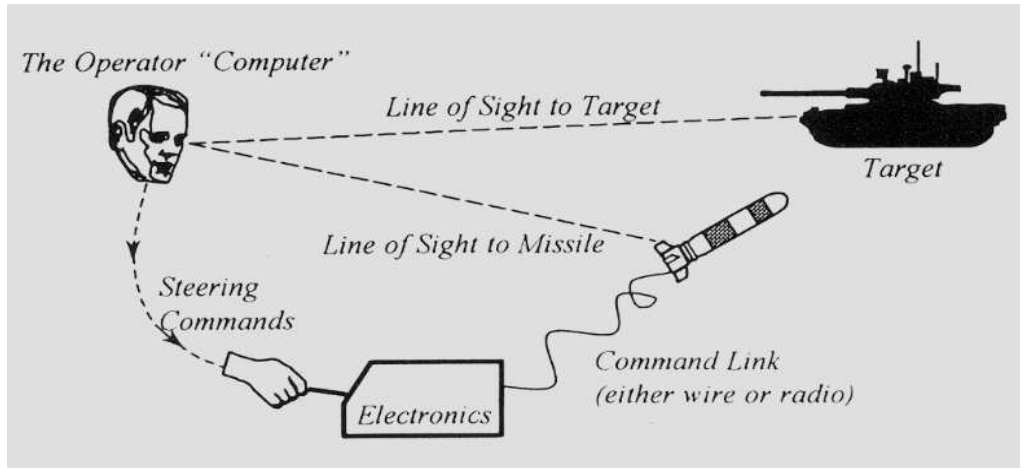
Figure 62 MCLOS

Figure 62 shows the principle of MCLOS. The human eye or fire post sensor observes the relative direction of the missile and the target, meanwhile, the brain of the operator works as the computer of the system. It is estimating the adjustment needed to get the missile on the line of sight with the target and keep tracking the target until the missile hits it.

The operator instructions are transferred to the missile through a command link which is usually a wire connected to the rear of the missile. This method of guidance is simple, cheap, and resistant to ECM but it also needs a highly trained operator.

H.1.2   Semi-automatic Command to Line of Sight (SACLOS)
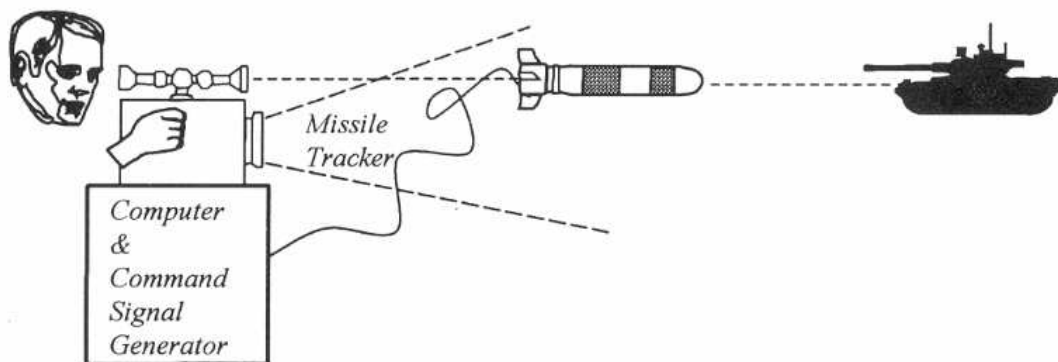
Figure 63 SACLOS

This system uses the human eye as well as the guidance computer to track targets. This is when a sighting camera is zeroed in and follows the target. Figure 63 describes the idea of the system. When the missile is launched, the automatic tracker detects any departure from the LOS - by the help of a flare on the back of the missile - and this is the error to be sent to the computer which will calculate the correct command to be sent to the missile as a coded instructions. So, the system determines what corrections are needed to get the missile to impact the target using a complicated algorithm based on dynamics. In order to protect the system, the beacon or the flare on the back of the missile is provided with a unique code. One advantage of SACLOS over MCLOS is less operator skill demanded. On the other hand, the SACLOS missile tracker maybe seduced by decoys that simulate the flare on the back of the missile [2].

H.1.3   Line of sight Beam Riding (LOSBR)
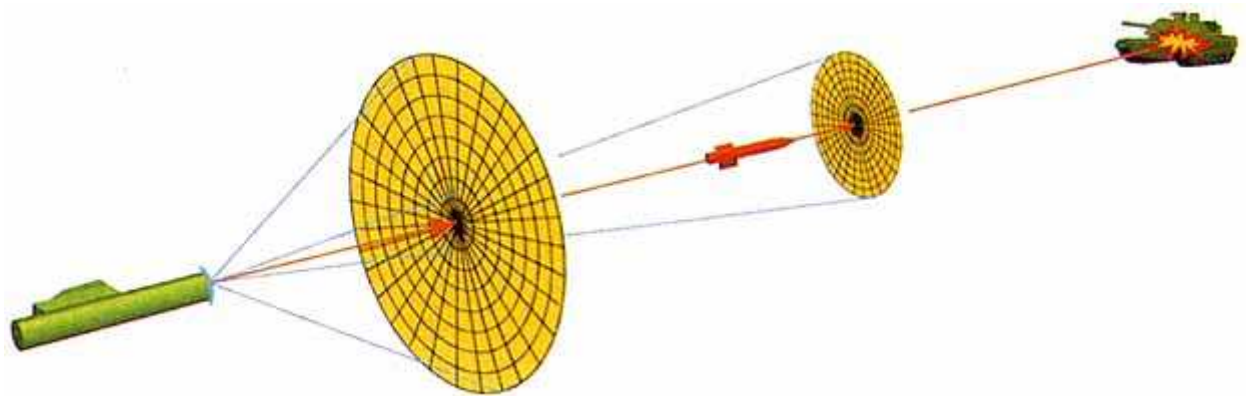
Figure 64 LOSBR

The riding beam is the essential part of the LOSBR system which is laid parallel to the LOS by the laser transmitter. The missile is steered to the centre of the scan pattern with the help of the gyro attached to it until it hits the target as shown in Figure 64 and 65. ATGW and low levels SAM (Surface to Air Missile) are the main form of LOSBR systems. One of the LOSBR features is its ability to guide more than one missile within the same beam. Moreover, this system is difficult to jam.
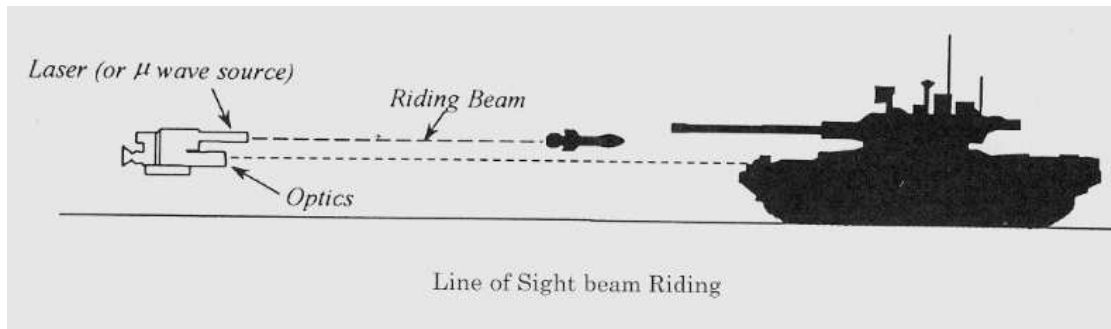
Figure 65 LOSBR

AS mentioned above, a great advantage of the beam riding technology is that the beam is more difficult to be detected by electronic countermeasures as the beam detector is at the rear of the missile. Semiconductor laser sample the first generation of beam riders. Pulsed GaAs semiconductor laser works in the near infrared part of the spectrum at 900 nm. Some of beamriding guidance nowadays use CO2 laser getting the benefit of its long wavelength. Add to that the capability of transmission through atmosphere with less losses. Turbulence is not a big problem, and CO2 laser has higher average power. All these advantages make CO2 laser one of the best in guidance especially during bad weather.

H.1.4 Automatic Command to Line of Sight (ACLOS)

ACLOS tracks both the target and the missile automatically with the help of guidance computer which calculates the target and position data. The computer then passes the coded command to the missile through the command link. This system uses different ways of tracking. One way for example is to track the target using radar while tracking the missile by IR. The other way is to use the same tracker (antenna or lens system) to track both target and missile at the same time, taking into consideration the importance of using range gating or Doppler shift velocity filtering to separate the signals for each one [3].

H.2 Homing Guidance

H.2.1 Active Homing

The target will be illuminated by a device carried within the missile itself. The signal transmitted from the missile will hit the target and reflected back to the missile receiver as shown in Figure 66. By this, the distance and speed of the target will be figured out and the guidance section will start do its calculation to intercept the target in the right point. Wings, fins, or Conrad control surfaces are mounted externally on the body of the missile and will be actuated by electric, gas generator power, hydraulic, or combinations of these to guide the missile to its target [4].
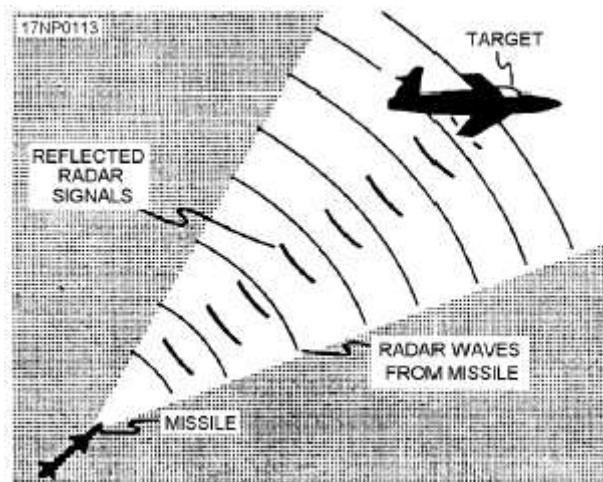
Figure 66 Active homing guidance

H.2.2 Semi-active Homing

An external source will illuminate the target and the missile receiver will receive the reflected signals. The guidance section will do the computing and sends the commands to the control system which start to work and actuate its parts to guide the missile to the intended target [5]. See Figure 67.
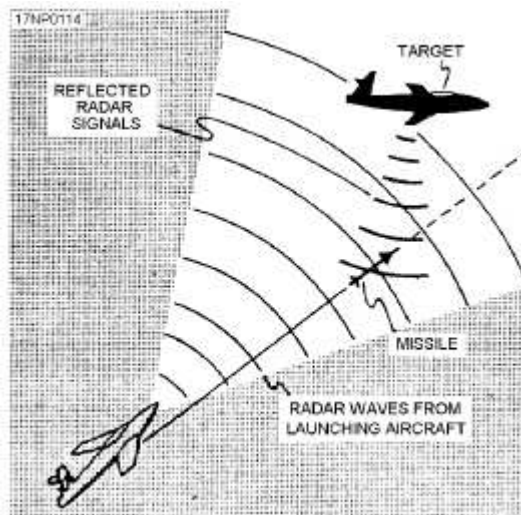
Figure 67 Semi-active homing guidance

H.2.3 Semi Active Laser Homing (SALH)

This guidance system homes on the reflected light from a laser designator. This system is very hard to fool and is very accurate. The only weaknesses is that the target must be within the line of sight of the director (no over the horizon targeting) and some targets with high tech sensors are capable of detecting when they are being targeted [6].

H.2.4 Passive Homing

The target will be the source of illumination in this type of guidance as can be seen from Figure 68. Infrared radiation or radar signals coming out of the target will be enough to guide a missile. The missile will receive the signals generated by the target and like in active and semi-active homing, the control section will guide the missile to the source of radiation [7].
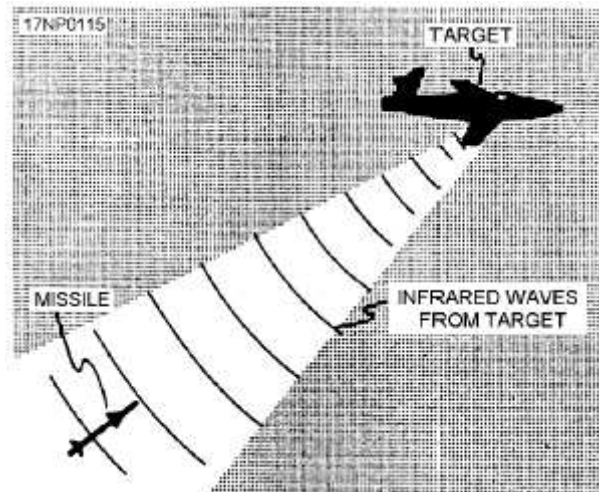
Figure 68 Passive homing guidance

H.3 Navigational Guidance Systems

In line of sight guidance and homing guidance the target will be in short distances where it can be seen with human eyes and sights. But what about targets on long distances and threat your forces. We need a guidance system to hit targets with high accuracy far away from the launching point. The only way is to have some form of navigational guidance must be used. Accuracy at long distances is achieved only after exacting and comprehensive calculations of the flight path have been made. The equations used to control the missile flight about the three axes, pitch, roll, and yaw contains specific factors designed to adjust the movement of the missile. There are three navigational systems that may be used for long-range missile guidance are inertial, celestial, and terrestrial [8].

H.3.1 Preset Guidance

The term preset completely describes this method of guidance. Before the missile is launched, all the information relative to target location and the required missile trajectory must be calculated. The data is then locked into the guidance system so the missile will fly at correct altitude and speed. Also programmed into the system are the data required for the missile to start its terminal phase of flight and dive on the target. One disadvantage of preset guidance is that once the missile is launched, its trajectory cannot be changed. Therefore, preset guidance is really only used against large stationary targets, such as cities [9].

H.3.2 Inertial guidance

Inertia is the simplest principle for guidance. The missile which use this type of guidance, will receives programmed information prior to launch. Despite the fact that there is no electromagnetic contact between the launching point and the missile after the launch, the missile is capable to correct its path with the aid of accelerometers that are mounted on a gyro-stabilized platform. All in-flight accelerations are continuously measured by this arrangement, and the missile attitude control generates corresponding correction signals to maintain the proper trajectory. The use of inertial guidance takes much of the guesswork out of long-range missile delivery. The unpredictable outside forces working on the missile are continuously sensed by the accelerometers. The generated solution enables the missile to continuously correct its flight path. The inertial method has proved far more reliable than any other long-range guidance method developed to date [10].

H.3.3 Celestial Reference

Celestial guidance system uses stars or other celestial bodies as known references (or fixes) in determining a flight path. This guidance method is rather complex and cumbersome. However, celestial guidance is quite accurate for the longer ranged missiles [11].

H.3.4 Terrestrial guidance

Terrestrial guidance is also a complicated arrangement. Instead of celestial bodies as reference points, this guidance system uses map or picture images of the terrain which it flies over as a reference. Terrestrial and celestial guidance systems are obviously better suited for large, long-range land targets [12].

H.4 References

[1] GUIDED WEAPONS, Fourth Edition. J F Rouse. Page 88.
[2] GUIDED WEAPONS, Fourth Edition. J F Rouse. Page 91.
[3] GUIDED WEAPONS, Fourth Edition. J F Rouse. Page 92.
[4] http://www.aerospaceweb.org/question/weapons/q0187.shtml. 2/6/2004.
[5] http://www.aerospaceweb.org/question/weapons/q0187.shtml. 2/6/2004.
[6]ttp://en.wikipedia.org/wiki/Laser_guidance. 25/5/2004.
[7]tp://www.aerospaceweb.org/question/weapons/q0187.shtml. 2/6/2004.
[8 http://www.ordnance.org/missile_components.htm. 27/5/2004.
[9]http://www.ordnance.org/missile_components.htm. 27/5/2004.
 [10 http://en.wikipedia.org/wiki/Inertial_guidance. 25/5/2004.
[11]http://www.aerospaceweb.org/question/weapons/q0187.shtml. 2/6/2004.
[12 http://www.ordnance.org/missile_components.htm. 27/5/2004.
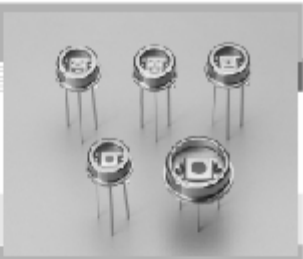
APPENDIX I Photodoides Specifications

PHOTODIODE

Si APD
S8890 series
Long wavelength type APD

Features
- High sensitivity
- High gain
- Low terminal capacitance

Applications
- YAG laser detection
- Long wavelength light detection

■ General ratings / Absolute maximum ratings

Type No.	Dimensional outline/Window material [1]	Package	Effective active area size [2] (mm)	Effective active area (mm²)	Absolute maximum ratings — Operating temperature Topr (°C)	Storage temperature Tstg (°C)
S8890-02	ΦK	TO-5	φ0.2	0.03	-20 to +85	-55 to +125
S8890-05			φ0.5	0.19		
S8890-10			φ1.0	0.78		
S8890-15			φ1.5	1.77		
S8890-30	ΦK	TO-8	φ3.0	7.0		

■ Electrical and optical characteristics (Typ. Ta=25 °C, unless otherwise noted)

Type No.	Spectral response range λ (nm)	Peak [3] sensitivity wavelength λp (nm)	Breakdown voltage VBR Io=100 μA Typ. (V)	Breakdown voltage VBR Io=100 μA Max. (V)	Temp. coefficient of VBR (V/°C)	Dark [3] current Io Typ. (nA)	Dark [3] current Io Max. (nA)	Terminal [3] capacitance Ct (pF)	Cut-off [3] frequency fc RL=50Ω (MHz)	Excess [3] noise figure x λ=800 nm	Gain M λ=800 nm
S8890-02	400 to 1100	940	500	800	2.5	0.2	2	0.2	280	0.3	100
S8890-05						1.5	15	0.5	240		
S8890-10						5.0	50	1.5	230		
S8890-15						10.0	100	2.5	220		
S8890-30						15.0	150	8.0	220		

*1: K: borosilicate glass
*2: Area in which a typical gain can be obtained.
*3: Values measured at a gain listed in the characteristics table.

SOLID STATE DIVISION

HAMAMATSU

1

200

■ Spectral response
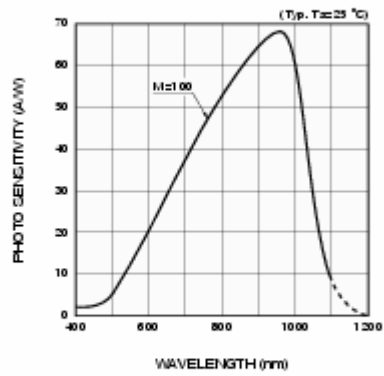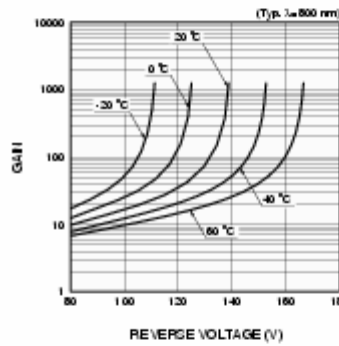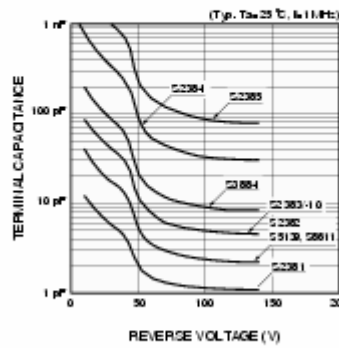

■ Dark current vs. reverse voltage
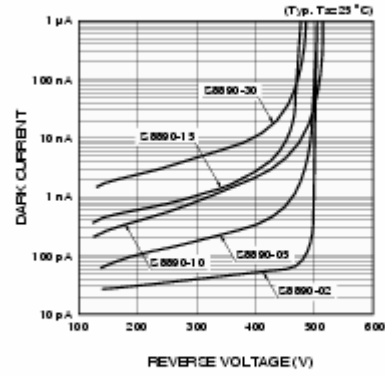
■ Gain vs. reverse voltage

■ Terminal capacitance vs. reverse voltage

2

■ Dimensional outline (unit: mm)

S8890-02/-05/-10/-15

TYPE No.	A
S8890-02	φ0.2
S8890-05	φ0.5
S8890-10	φ1.0
S8890-15	φ1.5

S8890-30

3
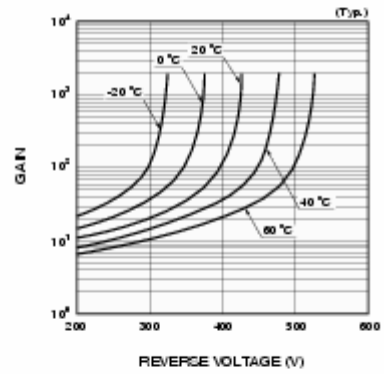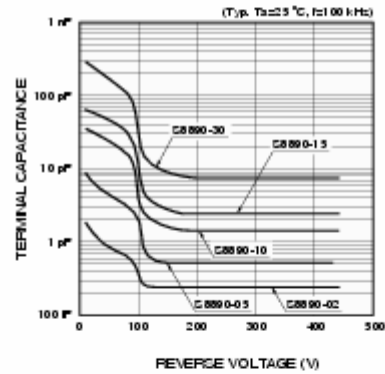
Si APD
S2381 to S2385, S5139, S8611, S3884

Low bias operation, for 800 nm band
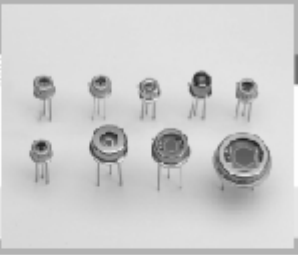
Features

- Stable operation at low bias
- High-speed response
- High sensitivity and low noise

Applications

- Spatial light transmission
- Rangefinder

■ General ratings / Absolute maximum ratings

Type No.	Dimensional outline/ Window material [1]	Package	Active area [2] size (mm)	Effective active area (mm²)	Absolute maximum ratings	
					Operating temperature Topr (°C)	Storage temperature Tstg (°C)
S2381	⌀/K	TO-18	⌀0.2	0.03	−20 to +85	−55 to +125
S2382						
S5139	⌀/L		⌀0.5	0.19		
S8611	⌀/L					
S2383	⌀/K		⌀1.0	0.78		
S2383-10 [3]						
S3884	⌀/K	TO-5	⌀1.5	1.77		
S2384	⌀/K		⌀3.0	7.0		
S2385	⌀/K	TO-8	⌀5.0	19.6		

■ Electrical and optical characteristics (Typ. Ta=25 °C, unless otherwise noted)

Type No.	Spectral response range λ (nm)	Peak [4] sensitivity wavelength λp (nm)	Photo sensitivity S M=1 λ=800 nm (A/W)	Quantum efficiency QE M=1 λ=800 nm (%)	Breakdown voltage VBR to=100 µA		Temp. coefficient of VBR (V/°C)	Dark current [4] ID		Cut-off [4] frequency fc RL=50 Ω (MHz)	Terminal [4] capacitance Ct (pF)	Excess Noise figure [4] x λ=800 nm	Gain M λ=800 nm
					Typ. (V)	Max. (V)		Typ. (nA)	Max. (nA)				
S2381	400 to 1000	800	0.5	75	150	200	0.65	0.05	0.5	1000	1.5	0.3	100
S2382								0.1	1	900	3		
S5139													
S8611													
S2383								0.2	2	600	6		
S2383-10 [3]													
S3884								0.5	5	400	10		
S2384								1	10	120	40		60
S2385								3	30	40	95		40

[1]: Window material K: borosilicate glass, L: lens type borosilicate glass
[2]: Active area in which a typical gain can be obtained
[3]: This is a variant of S2383 in which the device chip is light-shielded by aluminum coating except for the active area
[4]: Measured under conditions that the device is operated at the gain listed in the specification table

Note) Three ranks of breakdown voltage are available for S2381, S2382, S5139, S8611, S2383 and S3884. These are designated by a suffix number as follows.
- -01: 80 to 120 V
- -02: 120 to 160 V
- -03: 160 to 200 V

SOLID STATE DIVISION
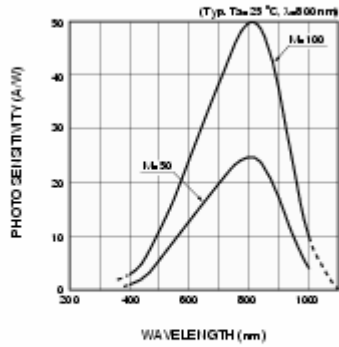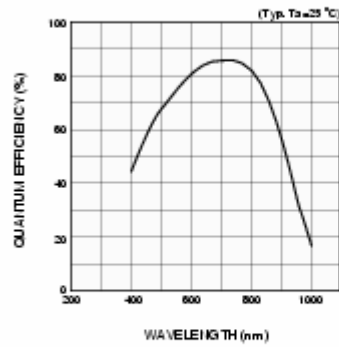
HAMAMATSU

1

■ Spectral response

(Typ. Ta=25 °C, λ=800 nm)

PHOTO SENSITIVITY (A/W) vs WAVELENGTH (nm)

M=100
M=50

■ Quantum efficiency vs. wavelength

(Typ. Ta=25 °C)

QUANTUM EFFICIENCY (%) vs WAVELENGTH (nm)

■ Dark current vs. reverse voltage

(Typ. Ta=25°C)

DARK CURRENT vs REVERSE VOLTAGE (V)

S2384
S3884
S2383-10
S2381
S2382, S5139, S8611

■ Gain vs. reverse voltage

(Typ. λ=800 nm)

GAIN vs REVERSE VOLTAGE (V)

20 °C
0 °C
-20 °C
-40 °C
60 °C

■ Terminal capacitance vs. reverse voltage

(Typ. Ta=25 °C, f=1 MHz)

TERMINAL CAPACITANCE vs REVERSE VOLTAGE (V)

S2384
S2385
S3884
S2383-10
S2382
S5139, S8611
S2381

■ Excess noise factor vs. gain

(Typ. Ta=25 °C, f=10 kHz, B=1 Hz)

EXCESS NOISE FACTOR vs GAIN

λ=650 nm
λ=800 nm

2

204
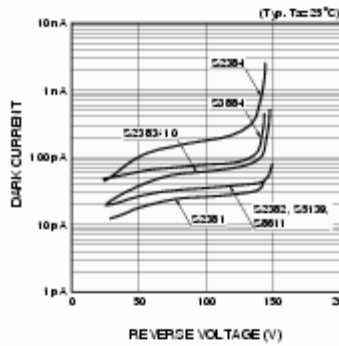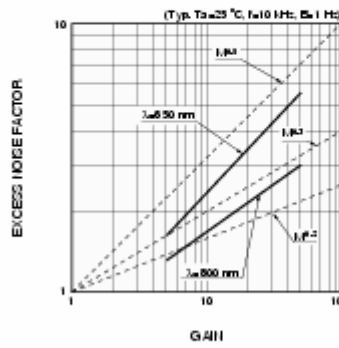
■ Dimensional outlines (unit: mm)

① S2381, S2082, S2383/-10

② S5139

③ S8611

④ S3884

⑤ S2084

The glass window may extend a minimum of 0.5 mm beyond the upper surface of the cap.

⑥ S2385

3
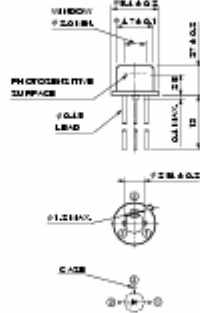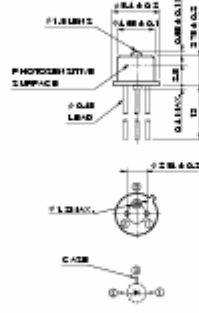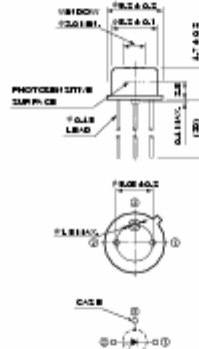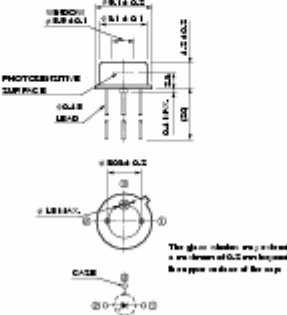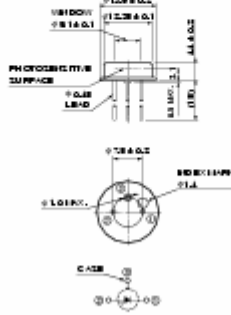
TE-cooled type APD S4315 series						
Parameter	Symbol	Condition	S4315	S4315-01	S4315-02	Unit
APD	-		S2381	S2382	S2383	-
Effective active area *5	-		φ0.2	φ0.5	φ1.0	mm
Spectral response range	λ		400 to 1000			nm
Peak sensitivity wavelength	λp	M=100	800			nm
Cooling temperature	ΔT		35			°C
Package	-		TO-8			-

*5 : Active area in which a typical gain can be obtained.
We welcome your request for active areas different from those listed above.

■ Cooling characteristic of TE-cooler
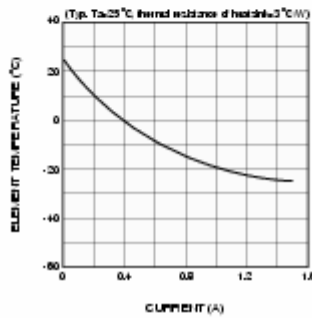
■ Current vs. voltage characteristic of TE-cooler
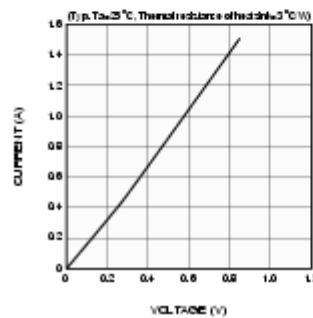
■ Thermistor temperature characteristic

■ Dimensional outline (unit: mm)

① DETECTOR (ANODE)
② DETECTOR (CATHODE)
③ COOLER (-)
④ COOLER (+)
⑤⑥ THERMISTOR

4

InGaAs Avalanche Photodiode

C30733E/C30644E/C30645E

Description

EG&G's C30644, C30645 and C30733 series high speed InGaAs/InP avalanche photodiodes. Their structure provides fast response and high quantum efficiency in the spectral range between approximately 1100nm and 1700nm. The APDs are optimized for use in fiber-optic communication systems, OTDRs, and range finders with 1300 to 1550nm wavelength ranges. The photodiodes are available on a ceramic carrier for use in hybrid applications. The C30644 and C30645 are also offered in the D2, D11 and D12 outlines.

Quality & Reliability

EG&G Optoelectronics Canada is committed to supplying the highest quality product to our customer. We are certified to meet ISO-9001 and are designed to meet Bellcore quality specification TA-NWT-00983. All devices undergo extended burn-in and periodic process qualification programs to assure high reliability.

Features

* Spectral response (1100 to 1700nm)
* High responsivity
* Bandwidth to 2.5 GHz
* Low dark current and noise

Applications

* OC-12, OC-48 receiver modules
* OTDR
* Range finding

EG&G
OPTOELECTRONICS

Specifications (at M = 10 @ 25)

PARAMETER	C30733			C30644			C30645			UNITS
	MIN	TYP	MAX	MIN	TYP	MAX	MIN	TYP	MAX	
Active Diameter		30			50			80		μm
Breakdown Voltage		60			60			60		Volts
Gain[3] (M)		10			10			10		
Temperature coefficient of V_r for constant gain		0.15			0.20			0.20		V/°C
Quantum Efficiency[3]										
1300 nm		85		75	85			85		%
1550 nm		75		65	75			75		%
Responsivity										
1300 nm	7.9	8.9		7.9	8.9		7.9	8.9		A/W
1550 nm	8.1	9.4		8.1	9.4		8.1	9.4		A/W
Total Dark Current (M = 10)		<1			5	10		10	25	nA
K_{eff}		0.45			0.45	0.55		0.45		
Noise Current (M = 10)		<0.1			0.15	0.25		0.25	1.0	$pA/Hz^{1/2}$
Capacitance (M = 10) ECER		0.26			0.6	0.8		1.5		pF
Frequency Response (3db) M = 10		3000			2000			1000		MHz

NOTES:

1. A specific voltage, V, is supplied with each device. When the photodiode is operated at this voltage (at 23 °C), the device will meet the electrical characteristic limits shown above. The voltage value will be within the range of 40 to 90 volts.

2. The voltage dependence of the gain, for gains above about 4, is given approximately by the following empirical formula: $M = 50 / (V_b - V)$.

3. Gain and quantum efficiency are not directly measurable quantities. The numbers quoted are estimated typical values. Gain, quantum efficiency and responsivity are related by the following: $R = \eta \lambda M / 1.24$ where λ is the wavelength in units of μm, η is the quantum efficiency, M is gain.

4. The detector noise current / $Hz^{1/2}$ is given by the following expression:

    $$in = (2q\,(Is + IbM^2F))^{1/2}$$

    where: $F = k_{eff}M + (1 - k_{eff})(2 - 1/M)$ and I_s and I_b are the unmultiplied and multiplied portions of the dark current, respectively. The total dark current is given by: $It = I_s + I_b M$.

    However, since both I_s and I_b are somewhat voltage dependent, and M is not directly measurable (see Note 3), it is not usually possible to determine both I_s and I_b unambiguously. Since system performance depends on noise current and responsivity, these measurable quantities are the ones which have been specified.

5. Most devices can be operated at gains up to about 30 or more, but with values of noise current correspondingly higher, as indicated by the discussion in Note 4 above.
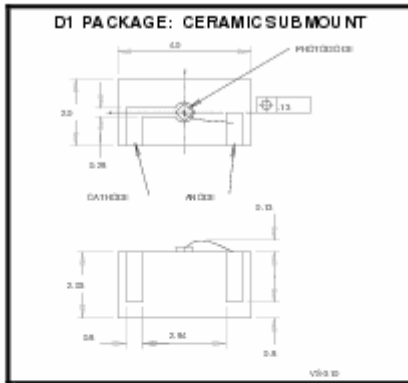
Figure 1: ECER Package: A low capacitance ceramic block for hybrid assemblies.
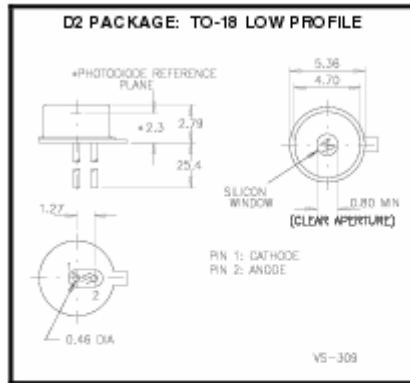

Figure 2 TO-18 Package, with low-profile silicon window cap for reduced window-chip distance. Available only for the C30644.
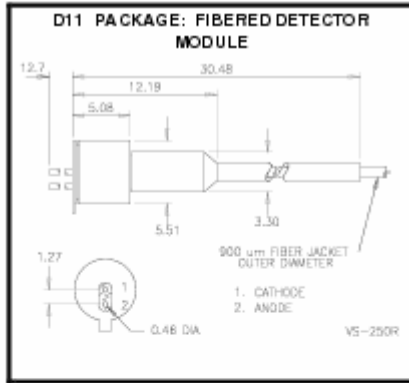

Figure 3: EQC package with integral fiber optic pigtail. Available only for the C30644.
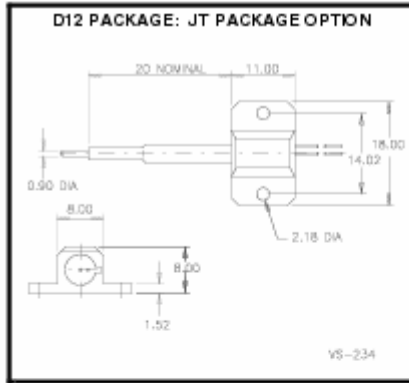

Figure 4: Mounting bracket package. Available only for the C30644.

Absolute Maximum Ratings, Forward Current, I_F:

Standard TO-18 Package	5mA
Ceramic Package	5mA
Pigtailed Package	5mA

Total Power Dissipation, PT:

Standard TO-18 Package	20mW
Ceramic Package	20mW
Pigtailed Package	20mW

Ambient Temp/Storage:

Standard TO-18 package	-60 to +125°C
Ceramic Package	-60 to +125°C
Pigtailed Package	-60 to +125°C
Operating TA:	
Standard TO-18 package	-20 to +70°C
Ceramic Package	-20 to +70°C
Pigtailed Package	-20 to +70°C
Soldering (10S) Tsd:	
Standard TO-18 package	250°C
Ceramic Package	250°C
Pigtailed Package	250°C

Typical Spectral Responsivity vs Wavelength (nm), Gain = 10, Temp. = 20°C

Typical Responsivity @ M=10
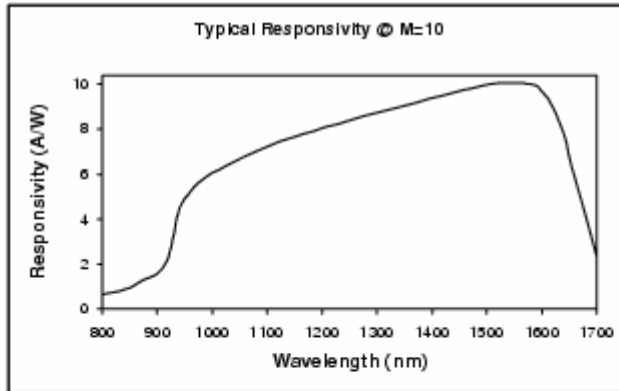
EG&G welcomes inquiries about special types. We would be pleased to discuss the requirements
of your application and the feasibility of designing a type specifically suited to your needs.

$\bigtriangleup$ *EG&G* is a registered trademark of EG&G, Inc.

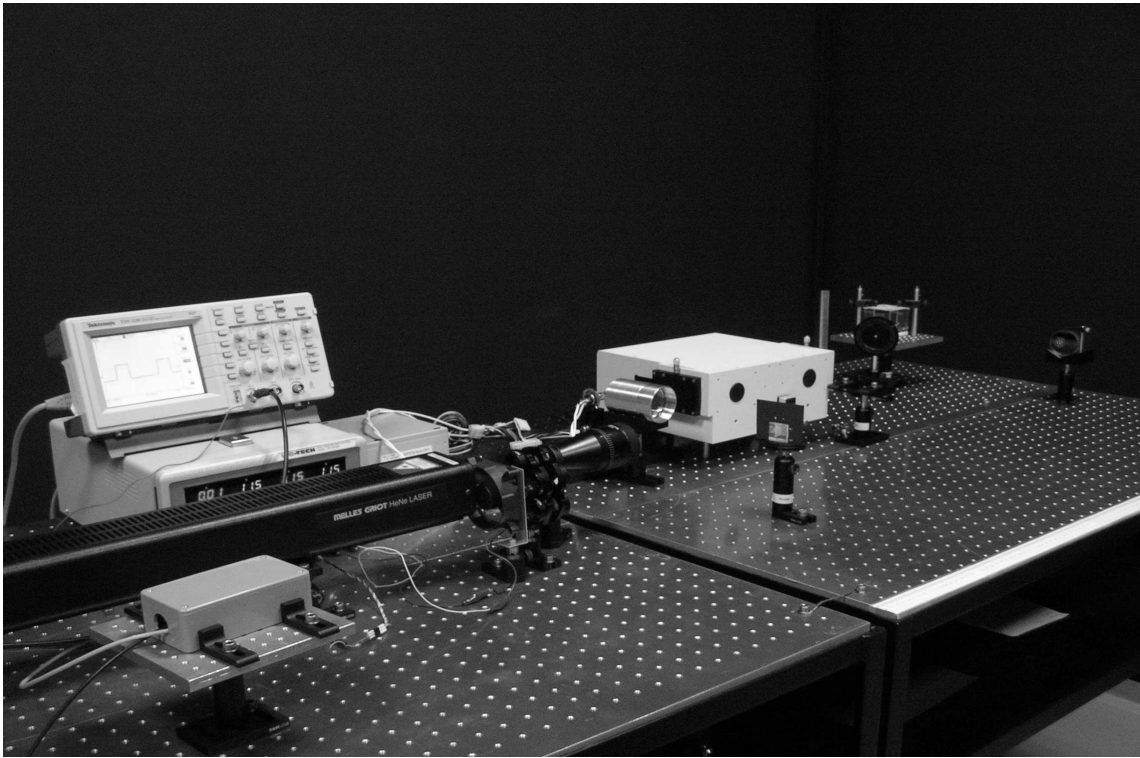**APPENDIX J**   **Lab Experiment Set Up Pictures**
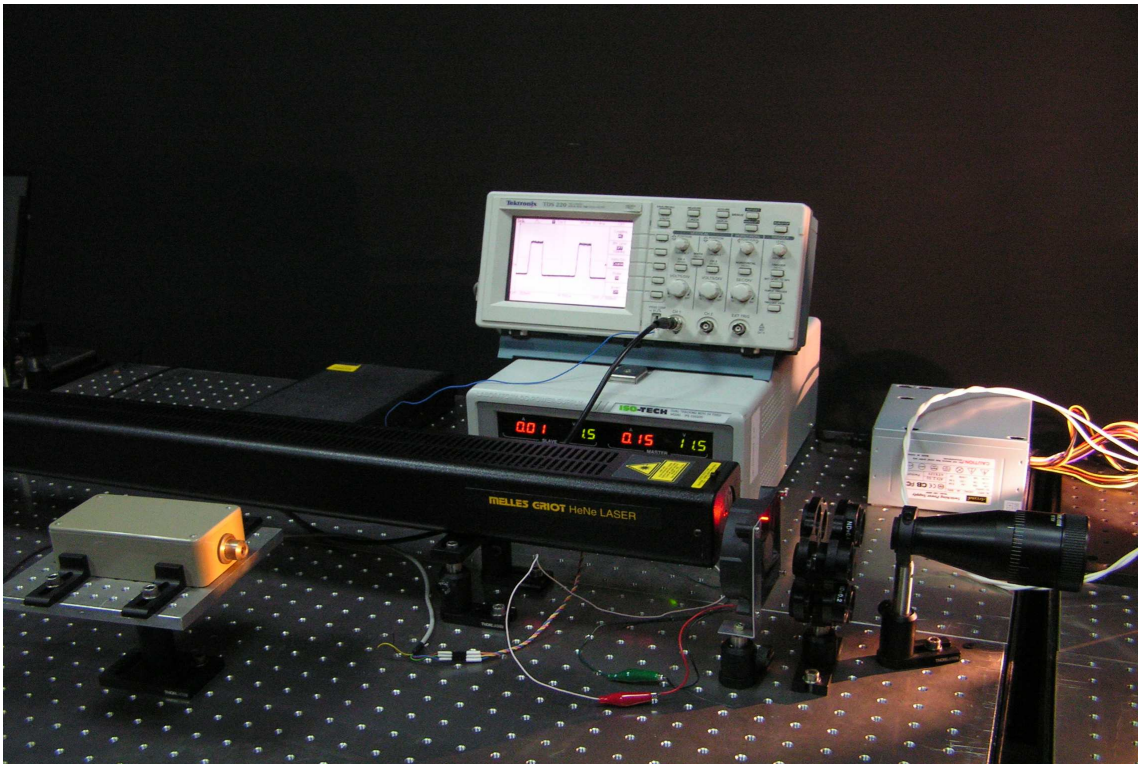

Figure 69 Experiment setup picture

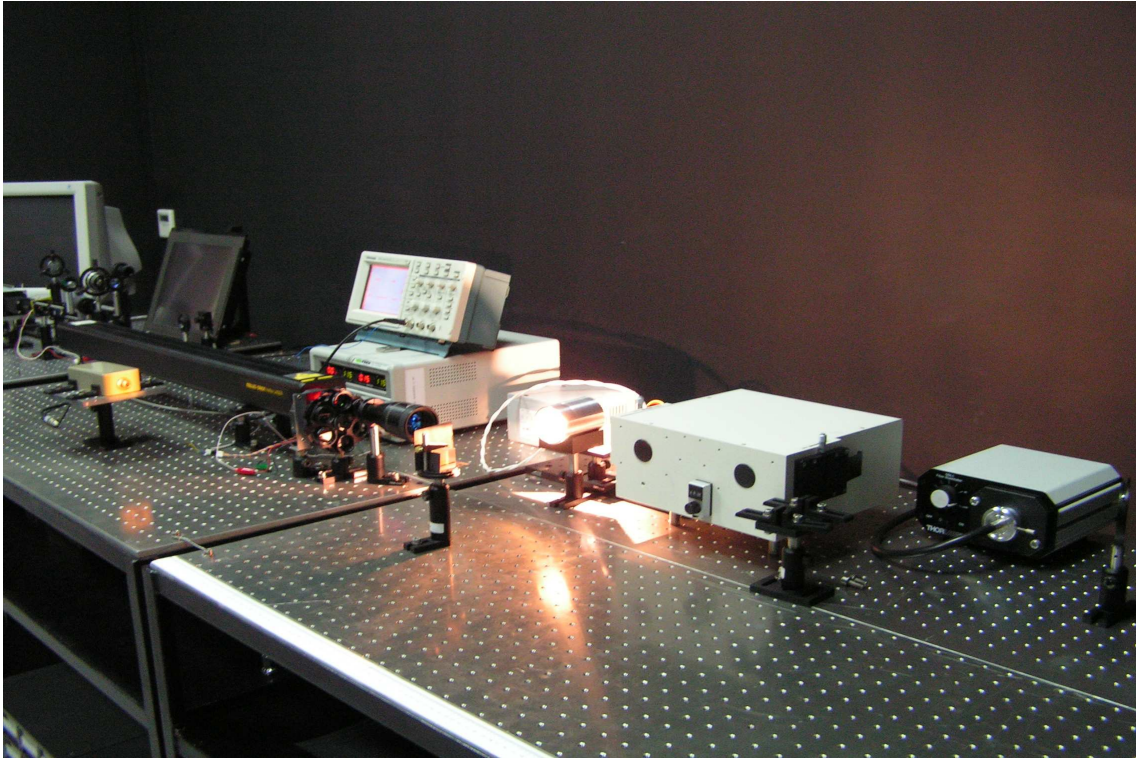**Figure 70 Experiment setup picture**

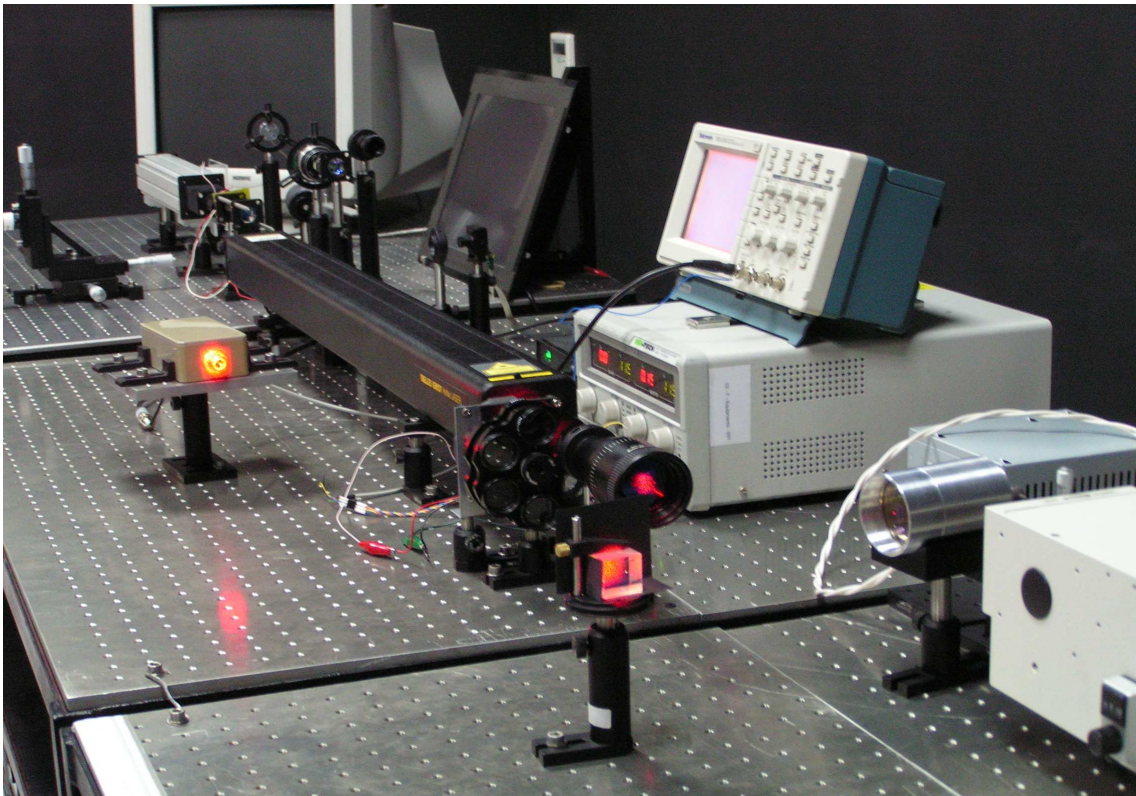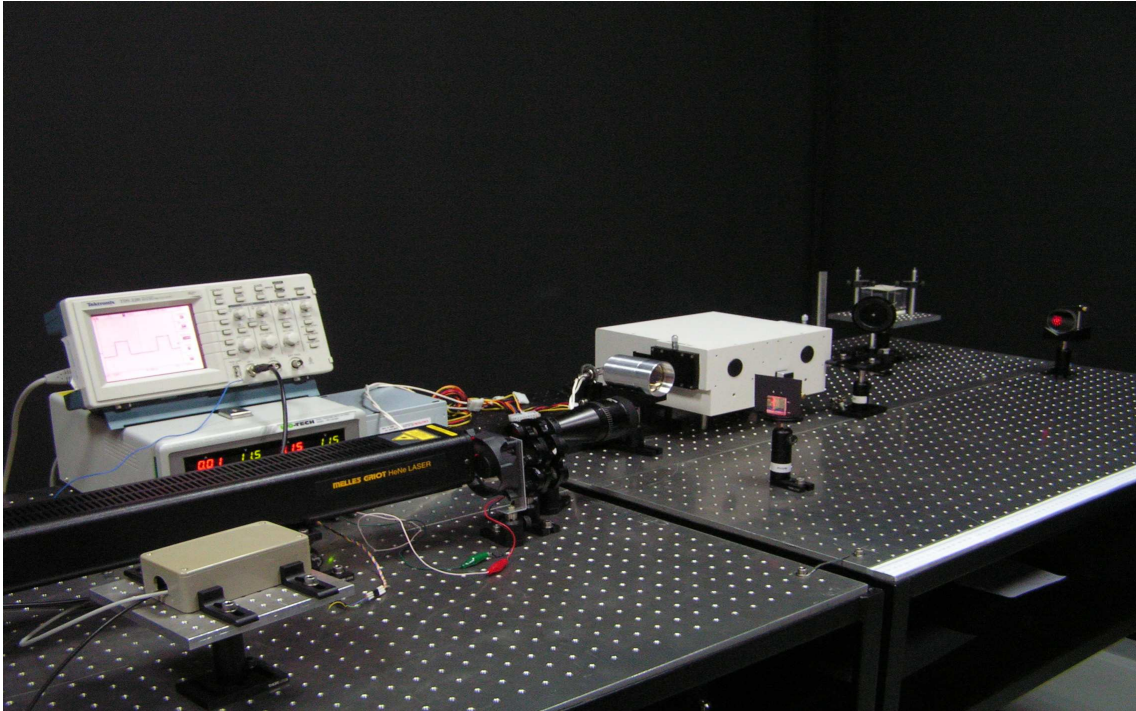**Figure 71 Experiment setup picture**

Figure 72 Experiment setup picture

Figure 73 Experiment setup picture